SISSA
Scuola
Internazionale
Superiore di
Studi Avanzati

Neuroscience Area – PhD course in

Neurobiology

Surface-embedded mechanical and chemical cues modulate neuronal mechanoadaptation in primary hippocampal networks

Candidate:

Francesca Zummo

Advisor:

Prof. Laura Ballerini

Co-advisor:

Dr. Denis Scaini

Academic Year 2020-21

Table of contents

Abstract

The possibility of external modulation of neuronal electrical behavior is becoming increasingly valuable and captivating for modern (neuro)medical research. Indeed, exogenous neuromodulation could open to the development of innovative technological tools that, in the field of neuro-engineering, concretize in advanced implantable devices (e.g., active and passive neurostimulators), neuro-prosthesis (e.g., neuro-regenerative scaffolds or synthetic ganglia) or neural interfaces (e.g., brain-machine interfaces). In this framework, there is a rising expectation about the critical role that mechano-chemical artificial cues could play in triggering or temper neuronal activity. This belief is mainly supported by the natural role recognized to extracellular matrix (ECM) physicochemical properties (e.g., stiffness, micro- nano-topography and/or chemical composition) in governing different cellular processes as well as inducing physiological or pathological evolution in tissues. In reason of that, a deeper investigation of the impact of external mechanical and chemical stimuli in regulating neuronal behavior represents a critical necessity in the attempt to govern neuronal behavior in a controlled way.

Therefore, in this study, I exploited functional substrates that aim to recapitulate in a *in vitro* model the complexity of ECM-mediated mechanochemical cues. Indeed, I studied the effect they have on primary murine neuronal cultures through a multidisciplinary approach.

In the first study, I evaluated the impact of substrate stiffness on primary hippocampal cultures. Specifically, nerve cells were let to develop for 9-10 days-in-vitro interfaced with polyacrylamide (PAA) hydrogels characterized by different “physiological” stiffnesses (Young’s elastic modulus E in the range 1–50 kPa). I investigated the impact of PAA-coupling on neuronal network development and morphology via immunofluorescence experiments, and on its functional aspects exploiting electrophysiological techniques. I focused, in particular, on how the synaptic activity of neuronal cells changes in relation to environmental stiffness. Surprisingly, a drastic reduction in spontaneous network activity was detected when cells were cultured on soft substrates. By treating hippocampal

cultures with specific compounds, we hypothesized that this electro-mechanical adaptation is ultimately associated with an altered homeostasis of plasma-membrane cholesterol in interfaced cells.

In a second investigation, I mimicked the contribution of external chemical cues making use of substrates endowing chemical functionalities. For the purpose of the study, I let rat hippocampal neuronal networks develop above glass control, single-layer graphene, and carboxyl-modified graphene substrates. In this case, the morphological and functional network adaptation was also evaluated through immunofluorescence and electrophysiology experiments, respectively. Furthermore, the study has taken advantage of advanced nano-microscopy techniques (i.e., Atomic Force Microscopy, and Total Internal Reflection Microscopy) to investigate the different surface chemistry's impact on focal adhesions organization and neuronal cell stiffness. My results demonstrated that, compared to glass controls, pristine graphene and functionalized graphene substrates induce an opposite effect on the spontaneous electrical activity of interfaced cells: an enhancement in the first case, a reduction in the latter.

Finally, in the attempt to evaluate the synergic contribution of ECM mechanical and chemical cues, primary hippocampal neurons were grown on three-dimensional carbon nanotubes (CNTs) foams where specific chemical functionalizations were introduced with the intent to modify substrate stiffness and introduce neuronal-specific responses in the interfaced network. In these preliminary experiments, I evaluated the neuronal network morphology uncovering a significantly different adaptation induced by pristine and functionalized CNTs foams in the form of cell distribution, elongation and orientation. Furthermore, from a functional point of view, I monitored neuronal functionality in terms of spontaneous calcium oscillations. I highlighted an increased calcium activity in cells developed above the stiffer functionalized CNTs compared to the pristine ones.

1. Introduction

1.1 Cellular Mechanobiology

1.1.1 Overview

Mechanobiology is a rapidly growing field that combines different disciplines ranging from cell biology to biophysics, bioengineering and material science (Jansen et al., 2015).

Traditionally, researchers focused their efforts in studying the role of chemical and molecular cues in regulating cell biology, for long neglecting biomechanical cues of the extracellular environment and their role in regulating biological processes. More recently, mechanical forces have been increasingly investigated in biology and their relevance recognized in, for example, governing cellular development, in promoting cell function in physiology or cell dysfunction in pathology (Franze et al., 2013). It is now largely accepted that cells are subjected to a wide range of mechanical forces in their native environment, and they continuously sense and respond to such mechanical stimuli. These forces were described to influence several cellular processes, such as differentiation, migration, morphogenesis, fluid homeostasis, ion channels gating, plasma membrane viscoelasticity, and gene expression (Tyler, 2018). Up to now, the majority of studies tackling mechanical forces in biology focused on two major classes of biomechanics: intrinsically force-generating or force-reactive biological systems, such as the cardiac and muscular systems, the skeletal system, and the vascular system (Blair & Pruitt, 2020; Mullender et al., 2004). On the other hand, there are many speculations and few certainties regarding the nervous systems, especially the central nervous system (CNS), historically considered a passive, neither mechano-active nor responsive, tissue. In modern neurobiology, the role of mechanical cues in regulating CNS functionality, for example in shaping neuronal morphology and pattern of interconnections, begins to be unravel. In the attempt to move through this new and intriguing aspect of neurobiology we have recently observed the convergence of neuroscience and mechanobiology research fields, giving rise to a new cross-subdiscipline, the neuro-mechanobiology, whose aim is to understand how the mechanical events modulate/affect brain

functions, both at cellular and tissue levels. Researchers involved in this novel interdisciplinary area recognized that various mechanical events take place within the whole nervous system. For instance, the peripheral nervous system (PNS) receives continuously mechanical cues that are collected by sensory receptors. Touch receptors, dubbed low-threshold mechanoreceptors (LTMRs), constitute an explicative example of sensory neurons able to sense and respond to mechanical stimulations (Abraira & Ginty, 2013). The mechano-transduction, that is the conversion of mechanical stimulus in electrical signal and, consequently, biological response, was well described in this type of neurons and channel proteins involved in mechano-sensation have been identified. These channels mainly belong to the degenerin/epithelial sodium, acid-sensing, transient receptor potential, mechanosensitive potassium, and piezo families (Chalfie, 2009; Cobo et al., 2020). Mechanical cues induce modifications in cell properties leading to the activation of membrane-embedded, mechanically-gated, ion channels. In particular, three different triggering mechanisms have been identified: i) modifications of cell membrane tensional state in the close vicinity of the channels; ii) changes in the strain of extracellular matrix and/or cytoskeleton constituents directly interacting with the extra- or intra-cytoplasmic domains of membrane ion channels, respectively; iii) coupling of secondary mechanosensory proteins to the ion channels (Lumpkin & Caterina, 2007; Matthews et al., 2006).

However, differently from the PNS where cell mechanics and involved processes have been deeply investigated and progressively elucidated, it is still mainly unclear how mechanical stimuli collected or generated by neuronal and glial cells within the central nervous system (CNS) can affect network functionality and which molecular mechanisms may be involved in governing the overall process.

The CNS is continuously subjected to mechanical cues. These stimuli may originate from the environment, external to the body, such as in the case of accidental bumps or therapeutic stimulation through ultrasound waves, they can be associated to body processes, as muscular activity, breathing or heart beating, or they can be intrinsic in cerebral parenchyma and be generated directly by nervous cells or by the mechanical properties (stiffness) of the extracellular matrix (ECM).

This thesis work aims at investigating the latter aspect, focusing the our attention to the impact that ECM stiffness could have on the morphology and electrical activity of neuronal cells and networks.

All cells exert forces directly on neighbour cells or on the surrounding ECM microenvironment while, simultaneously, they are themselves subjected to external forces or detect ECM stiffness. In general, these forces are distinguished in passive and active forces. For instance, the rigidity of the extracellular matrix or of a cell-supporting substrate are stimuli belonging to the first category, and are characterized by the absence of any motion during the interaction (at least at large time and dimensional scales). As a consequence of that, a stiffening or softening of the extracellular environment is sensed by cells and modulates their functionality (Dupont et al., 2011). On the other hand, cells can influence the behavior of neighbouring cells mechanically interacting with them by push/pulling or extending processes to touch and trigger a mechanical response. In this case, the mechanical cue is associated to the macroscopical motion of (at least) one of the subjects in interaction. In addition, other subtle mechanical events characterize cells and, in particular, neurons. For instance, it was observed that the propagation of an action potential (AP) in the squid giant axon determines a mechanical force associated to an instantaneous local "swelling" of axon's membrane. This rapid mechanical deformation propagates along the axon concurrently to the electrochemically originated and sustained AP (Iwasa & Tasaki, 1980). Besides, also the continuous motility of the neuronal arborization, the pruning of dendritic spines during development, or the synaptogenetic phenomena regulating nervous system plasticity seems to be, at least in part, regulated by a complex net of mechanical cues orchestrated by the neuronal cells (Kilinc, 2018).

Things become even more complicated if we consider that a cell could itself changes its mechanical properties in response to external static or dynamic stimuli. It can undergo, for example, a tension/rigidity adjustment of its cellular plasma membrane by modifying membrane composition in terms of proteins and lipids impacting, in this way, the opening kinetic of ion channels and, consequently, the electrical activity of neurons (Tyler, 2018). The cell membrane can readjust also as a consequence of cell cytoskeleton rearrangements, in the form of stress fibers formation following

the presence of an extracellular environment with high stiffness, or in response to external direct forces (Solon et al., 2007).

The picture appearing so far is complex, and is partially summarized by the molecular processes shown in Figure 1, where the extra- and intracellular key players involved in the mechanosensing process are recapitulated. Cells perceive mechanical stimuli through diverse mechanosensitive elements located at the plasma cell membrane level or part of cytoskeleton components or machinery. These mechanosensitive molecules include integrins and focal adhesion complexes, stretch-activated ion channels, G protein coupled-receptors, growth factor receptors, mechano-activated kinases all involved in the different mechano-transduction pathways simultaneously guaranteeing correct cell tensional homeostasis. The mechanical signals, collected by the focal adhesions (FAs), macromolecular structures including integrin receptors and numerous proteins (J. C. Kuo, 2014), are transferred to cell cytoskeleton and associated proteins and transmitted within the cell until they reach the cell nucleus, where the transcription of genes responsible for mechanical responses will be activated (Alonso & Goldmann, 2016; Martinac, 2014).

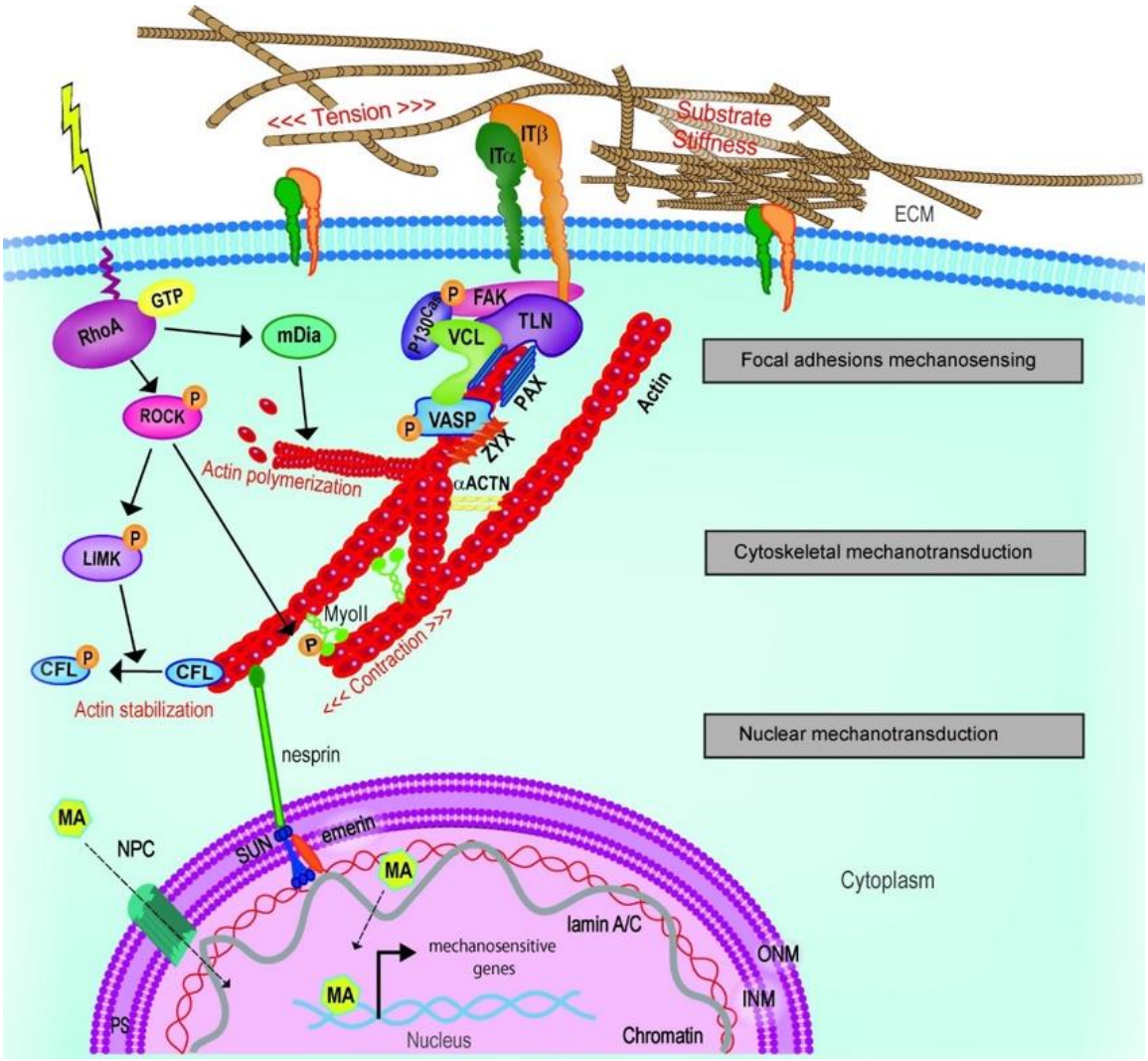

Figure 1: Cell key players in mechanosensing. *Extracellular physical stimuli, such as tension or substrate stiffness, are perceived by FAs at the cell-ECM interface; the signals are propagated by the cytoskeleton, that rearranges its stress fibers and contractility, and transferred to the nucleus where mechanosensitive genes are activated by mechanoactuators (MA). MA can be shuttling mechanotransducers or mechanosensitive transcription factors. ACTN, actinin; CFL, cofilin; FAK, focal adhesion kinase; INM, inner nuclear membrane; IT, integrin; LIMK, LIM kinase; mDia, Diaphanous-related formin-1; MyoII, myosin II; NPC, nuclear pore complex; ONM, outer nuclear membrane; PAX, paxillin; PS, perinuclear space; ROCK, Rho-associated protein kinase; TLN, talin; VASP, vasodilator-stimulated phosphoprotein; ZYX, zyxin. Adapted from* (Nardone et al., 2017).

The next paragraphs will highlight the main mechanisms contributing to the biomechanics of some cellular and extracellular components, focusing in particular on neuronal related aspects and implications.

1.1.2 The plasma membrane and its mechanical properties

The cellular plasma membrane has the fundamental role to protect and separate the intracellular environment from the extracellular one. It is an heterogenous bilayer structure mainly constituted by phospholipids, proteins, and cholesterol behaving as a viscoelastic non-Newtonian fluid. This phospholipid bilayer enfolding all eukaryotic cells, including neurons and glial cells, is a dynamic structure subject to continuous rearrangements across different time and length scales. Mechanical forces acting on cells influence lipid bilayers giving rise to deformations in terms of compression, expansion and bending. These deformations are all described by specific moduli: compression (K_C), stretching (K_A), bending (K_B), and expansion of the membrane (K_S). Higher values indicate greater resistance to a specific deformation force, lower values point out, instead, ease of deformation.

Many exogenous factors, as osmolarity, protein inclusion, and protein conformational changes can induce stress and deformations in cellular membranes and modulate their elasticity (Tyler, 2018).

The tension/rigidity state of a cellular membrane is primarily regulated by its composition in terms of proteins and lipids. In particular, it is well known that cholesterol can modulate the mechanical properties of the plasma membrane (Al-Rekabi & Contera, 2018; Needham & Nunn, 1990). Regarding cells of the CNS, it has been demonstrated that a different percentage of cholesterol in neuronal plasma membrane could alter their synaptic functions and ion channels activity. In their work, Wasser R. and colleagues demonstrated that the cholesterol plays a crucial role in regulating neuronal behavior; specifically it has an opposite effect on spontaneous and evoked neurotransmission. The researchers observed that, in hippocampal cultures, its removal from plasma membrane by exploiting methyl-β-cyclodextrin (MβCD), a compound able to sequester cholesterol, leads on the one hand to an increase in terms of spontaneous activity, on the other to a reduction of evoked responses (Wasser et al., 2007).

By the fact that cholesterol seems to have such a relevant impact on the electrical activity of neurons, it is worth noting the importance of investigating if and how mechanical stimuli, active or passive,

may alter cholesterol levels in cell plasma membranes. A similar effect will associate external mechanical cues to intracellular adaptation through a mechanosensing process.

The question now is whether passive mechanical cues, such as substrate stiffness, can affect plasma membranes cholesterol content altering membrane tension and ion channels conformations, or not. It is well known that ion channels are sensitive to mechanical perturbations in plasma membrane. Mechanical changes in phospholipid bilayer can affect not only mechanosensitive channels, such as transient receptor potential (TRP) or piezo proteins, but also voltage gated channels (VGCs) which are responsible for neuronal excitability (Tyler, 2012).

Neurons could express voltage-gated ion channels sensitive also to mechanical cues and, consequently, to transient changes in plasma membrane tension. An example is constituted by KV channels (voltage-gated potassium channels) that respond to small physiologically relevant mechanical perturbations of the lipid bilayer, shifting the channel activation curve and increasing in the maximum open probability (Schmidt et al., 2012). Mechanical cues can induce changes to KV channels activity and let these channels behave as incidental neuronal mechano-transducers. Similarly, also other voltage-gated ion channels known to regulate neuronal signalling and plasticity, such as sodium and calcium channels, could alter their behavior as function of membrane tensional state, acting as secondary mechanosensors.

In a study performed in 2004 by Lundbaeck J. and co-workers, it was shown how the functionality of sodium channels could be modulated by the elasticity of the plasma membrane. Furthermore, it highlighted that a depletion of cholesterol, that changes bilayer stiffness, gives rise to a shift in sodium channels inactivation toward hyperpolarization potentials (Lundbæk et al., 2004).

However, it is also crucial to highlight that the cell membrane is not a self-standing system but, instead, is supported by and linked to the underneath cytoskeleton. As a consequence of that, the viscoelastic properties of the plasma membrane are affected and affect the cellular cytoskeleton, that exerts tension through its fibers and to which the membrane is anchored (Jerusalem et al., 2019).

1.1.3 The role of the cytoskeleton in cell mechanosensing

All eukaryotic cells, including those constituting the nervous system, are endowed with a cytoskeleton (CSK), playing a crucial role in cell functionality. The CSK spatially organizes the cell cytoplasm compartments, permits the correct anchoring of intracellular organelles, regulates vesicles trafficking and provides cell's ability to move and change shape, or to support external mechanical stresses, eventually interfacing cells to the external environment (Hohmann & Dehghani, 2019; Zampieri et al., 2014). CSK complex three-dimensional network is composed of four types of filaments: microtubules (MTs), actin microfilaments, intermediate filaments (IFs) and septins (Fletcher & Mullins, 2010; Mostowy & Cossart, 2012). Specifically, microtubules are mainly involved in the transport of organelles and proteins (Dent & Baas, 2014); actin microfilaments are involved in cell motility, contractility and endo- eso-cytosis processes. Unlike microtubules and actin polymers, IFs are not polarized structures and have mainly structural and mechanical function. Their protein constituents strongly differ among different cell types as, for example, neurofilaments for neurons, and glial fibrillar acid protein (GFAP) for astrocytes (the most abundant glial cells) (Fletcher & Mullins, 2010). Septins, a recently discovered component of CSK, belong to a family of GTP-binding proteins. Septins assemble in not polar filaments within ring-like structures and act as scaffold for protein recruitment and as diffusion barriers for subcellular compartmentalization in numerous biological processes (Mostowy & Cossart, 2012).

Besides aforementioned roles, the CSK is also crucially involved in cellular mechanosensing: its actin constituent is responsible for the generation of forces via the activation of the actomyosin contractility (Burridge & Wittchen, 2013).

This mechanism (as summarized in figure 1), together with integrin and FAs complexes activation, plays a key role in ECM/substrate stiffness mechanosensing. Specifically, at membrane level, integrin receptors cluster together and recruit adaptor molecules such as focal adhesion kinases (FAKs), paxillin, and talin to induce a focal adhesion assembly. These structures physically link the ECM to the intracellular environment by interacting with the F-actin cytoskeleton constituent (Chan & Odde,

2008; Martino et al., 2018). Thus F-actin anchored to focal points typically form linear bundles, held together by crosslinking proteins (i.e α-actinin, fascin, filamin). These fibrillar assemblies are able to contract thanks to the presence of the non-muscle myosin II motor proteins and, eventually, give rise to stress fibers (SFs) formation. Pulling on ECM or substrate through the FAs, SFs regulate their own contractility depending on sensed stiffness in a positive-feedback fashion (Ingber, 2008). Briefly, the SFs are composed of F-actin filaments that are interconnected by bipolar bundles of myosin II, a motor protein, and organized to form contractile fibers. The myosin II exploits the energy released by ATP hydrolysis to move relative to the actin filaments bundle towards its barbed end in the process. By this way actin filaments are pulled to both ends of the myosin bundle closer together, inducing thus a contraction of SFs within the overall cytoskeleton. The cycle starts again following the bond of a new ATP molecule that leads myosin to dissociate from actin filament and move towards further upstream end (Mikhaylova et al., 2020). The myosin proteins involved in this mechanism are non-muscle myosin II (NMII) existing in three isoforms (A, B and C). Specifically neuronal cells express predominantly NMII-B (Rochlin et al., 1995). Generally, cells grown on rigid substrates present actin fibers well-organized and assembled in bundles (stress fibers) able to generate larger forces upon contraction (Cai et al., 2006; Mih et al., 2012). The tension and contractility of actin cytoskeleton is regulated by a vast range of proteins, including nucleation-promoting factors (Arp2/3, profilin), capping proteins, depolymerizing factors (ADF/cofilin), stabilizing proteins and crosslinkers (Bugyi & Carlier, 2010; Wiggan et al., 2012). The availability of these proteins, in turn, is regulated by different signaling pathways, often triggered by the activation of FA-associated signaling proteins.

In this regard, the role of the RhoA/ROCK pathway is crucial in the regulation of cell-matrix interaction and stress fibers formation. Briefly, Rho are small GTPases proteins whose activity is regulated by ECM stiffness and, in particular, a stiff matrix promotes Rho activity and thus cell contractility. In brief, a mechanical force transmitted across a focal adhesion activates the small GTPase Rho, which leads to the activation of two primary downstream effectors: ROCK (Rho-associated protein kinase) and the mDia family of F-actin polymerization factors. ROCK is a

serine/threonine kinase that induces myosin II activation by direct phosphorylation of myosin regulatory light chain (MLC) mainly at the Ser-19 residue or by inhibition of MLC phosphatase (MLCP) (Amano et al., 1996; Burridge & Chrzanowska-Wodnicka, 1996). MLC phosphorylation promotes and strengthens actin-myosin interaction and the activation of myosin II ATPase generating contractility (Martino et al., 2018). ROCK is also involved in the phosphorylation and activation of LIM-kinase, which in turn phosphorylates and inactivates cofilin which is an actin depolymerizing factor, to stabilize existing actin filaments (Fukata et al., 2001; Hayakawa et al., 2011).The mDia effector, instead, promotes F-actin polymerization by recruiting Arp2/3 nucleation-factors complex. In figure 2 a summary scheme of RhoA signaling is reported.

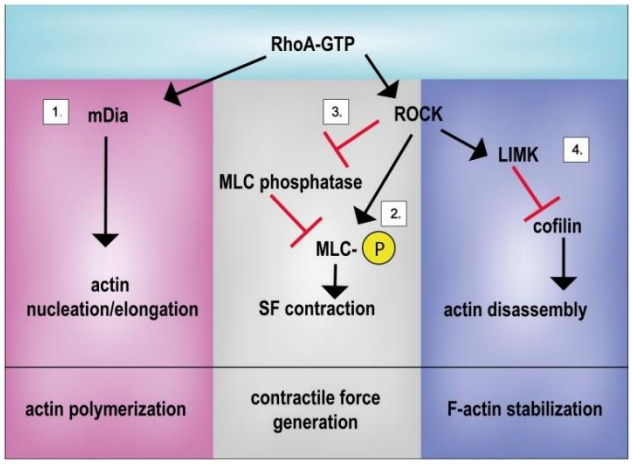

Figure 2. RhoA-GTP and its effectors. *Activated RhoA interacts with effector proteins to lead to actomyosin contractility and actin stablization. (1) mDia effector promotes the actin nucleation/elongation; ROCK effector acts (2) through MLC phosphorylation directly or (3) through MLC phosphatase inhibition; and (4) by phosphorylating LIMK that inhibits cofilin promoting, by this way, actin stabilization. LIMK, LIM kinase; mDia, Diaphanous-related formin-1; MLC, myosin light chain; ROCK, Rho-associated protein kinase; SF, stress fiber. Adapted from* (Martino et al., 2018).

Since Rho/ROCK signalling is required for the development of contractile fibers, the inhibition of any of these players alters the cell ability to perceive the real stiffness of surrounding microenvironment (Riveline et al., 2001; Sit & Manser, 2011). In this regard, it has been observed that in cells cultured on stiff substrates and treated with drugs inhibiting cytoskeleton contractility, such as the Y-27632 molecule, a ROCK inhibitor, or blebbistatin, an NM-II inhibitor, the formation of stress fibers is impaired and the CSK develop isotropic mechanical properties (Kim et al., 2015).

In the nervous system the actin CSK is particularly relevant by its critical role in synapses formation and modulation. It has been demonstrated that actin-generated forces mediate navigation/pathfinding and branching of neurites' growth cones, the leading tips of growing nerve processes. These structures are fundamental to explore the microenvironment and to reach and interact with appropriate targets to form synaptic connections. Specifically, the motility of the growth cones appears to be driven by two cyto-mechanical processes: the actin polymerization cycle and actin-myosin interactions. The first is mainly involved in the filopodia/lamellipodia extension/protrusive phase; the second seems instead to mediate the retraction phase (Dent et al., 2011; Smith, 1988). The mechanical properties of growth cones were experimentally measured, and these experiments revealed that they are extremely soft structures (E = 106 ± 21 Pa, using SFM-based micro-rheology) and weak force generators (Betz et al., 2011).

Additional studies explored the role of the actin CSK and related motor protein, the myosin II, in two neuronal sub-cellular compartments, the dendritic spines and the axon initial segment (AIS), critical for neuronal signalling. Dendritic spines, that are characterized by different shapes and sizes, are important for functions such as learning and memory (Yuste & Bonhoeffer, 2001), instead AIS is the site in which the action potentials are initiated (Brian D. Clark et al., 2009). In 2006, in a specifically designed experimental framework, Ryu J. and colleagues have demonstrated that the actomyosin contraction is fundamental not only to shape spine morphology and regulate their motility, but also for the synaptic activity *per se*. Indeed, it has been shown that an inhibition of actomyosin contractility with blebbistatin (30 minutes treatment), changed dendritic spines shape and reduced excitatory signals transmission (Ryu et al., 2006). In a different study, carried out by Evans M. and co-workers, it was highlighted that myosin II and actin fibers are key elements for the structural plasticity of AIS, regulating its assembly and rearrangement (Evans et al., 2017). This involvement of actomyosin contractility in this specialized neuronal compartment was further confirmed by the group of Berger S (Berger et al., 2019).

1.1.4 The time frame of biomechanical processes

Mechanical cues are ubiquitously present in the cellular environment and continuously stimulate cells inducing a wide range of biological effects on both short-term (fractions of seconds to minutes) and long-term (hours to days) time scales (Kanoldt et al., 2019). Perceived mechanical stimuli are converted into biochemical signals in the intracellular compartments initiating, in this way, several cellular responses.

Among all the cellular adaptations that take place in relatively short times, we can mention the change of ion channels conformation. Every ion channel could behave to a certain extent as mechanosensors (Martinac, 2014). In fact, the kinetics of opening of ion channels is also affected by the tensional state of the plasma membrane in which they are embedded (Kamkin & Kiseleva, 2009). A change in the bilayer elasticity can determine a change in the conformation or opening kinetic of a channel protein, leading to altered ions fluxes as, for example, in calcium ions. Calcium constitutes an important intracellular second messenger responsible for the initiation of several pathways, such as ones involving Rho/ROCK, with the consequent contraction of cytoskeletal actomyosin fibers (Haws et al., 2016), regulation of cell motility (Lee et al., 1999), or growth cone retraction (Franze et al., 2009). Other responses that can be actuated by cells in a very short-term scale following mechanical cues consist in the reorganization of focal adhesions size and compositions within the plasma membrane (from seconds to minutes) (Verma et al., 2015). In particular, it has been shown that cells grown on compliant substrates exhibit immature, small and punctuated FAs. By contrast, cells cultured on stiffer substrates are characterized by mature large FAs, able to exert stronger pulling forces on the extracellular matrix (Pelham & Wang, 1997; Simon W. Moore et al., 2010).

On the other hand, mechanical cues can also trigger cell responses characterized by longer time scale. These processes involve, for example, the genes activation (hours to days). Following mechanical stimuli, such as an increase or decrease in ECM stiffness or a direct cell-cell interaction, several proteins/factors translocate into the nucleus activating the transcription of genes specifically involved in the mechano-adaptation process. This is, for example, the case of YAP (Yes-Associated Protein) and TAZ (Transcriptional Coactivator with PDZ-binding Motif) mediated transcription activation

(Halder et al., 2012), a process addressed by the next paragraph (1.1.4). Another example is given by the transcription factor Nuclear Factor kB (NF-kB) involved in the inflammatory response: its nuclear localization increases with matrix stiffness and triggers the transcription of genes encoding markers for inflammation (i.e., interleukins). Interestingly, it has been observed that its activation and nuclear translocation requires hours compared to the days necessary, instead, to YAP/TAZ activation (Ishihara et al., 2013; Lampi & Reinhart-King, 2018). Additionally, it was shown that mechanical cues also interfere with the MAPK (Mitogen-activated protein kinase) and MRTF-A (Myocardin-related transcription factor–A) pathways, involved in the response to ECM remodeling (Hwang et al., 2015; Johnson et al., 2014).

It is worth considering not only the time frame of the cell responses, but also the duration of the stimuli themself. Stimuli can be acute or chronic. Acute stimulation includes the administration of molecule drugs and immediate observation of the effect, for example the exposure to blebbistatin through a glass pipette patching a cell, or the local delivery of drugs in close proximity of cells using a Picospritzer® (Ryu et al., 2006). Chronic stimuli persist over time, usually from days to weeks or more. For instance, cell cultures chronically treated with molecules able to interact with specific nodes of a mechanosensing pathway, or interfacing cells with substrates characterized by different stiffness for several days in vitro. In the latter case, cells will adapt to chronic and passive mechanical cues.

1.1.5 YAP/TAZ localization in relation to substrate stiffness

In response to mechanical and physical cues, cells actuate a series of immediate adaptive actions, that occurs within a time interval which ranges from fractions of seconds to minutes, such as: i) the remodelling of their cytoskeleton; ii) FAs remodelling and maturation; iii) conformational or kinetic changes in ion channels within the plasma membrane. All these adaptation mechanisms are characterized by a fast time-course. In parallel, mechanical events, perceived through membrane receptors (i.e., FAs associated signalling proteins) and cytoskeleton fibers (i.e., actomyosin or MLCP

activity), can lead to the shuttle of various proteins (e.g., NF-kB, ZO-1, beta-catenin, and paxillin) to the nucleus (Gottardi et al., 1996; Huber et al., 1996; Zhou et al., 2017). This relocation into the nucleus is associated to the activation and regulation of the transcription of genes involved in cell biomechanical response. Obviously, these processes require longer time to be activate compared to the first category.

YAP and TAZ are two proteins well known for their role in the Hippo pathway, that regulates organ development in terms of size, shape and position, and plays a critical role also in cancer development and progression (Zhao et al., 2011). The involvement of YAP/TAZ in cell mechanotransduction is now clear too. In the work of Dupont S. and collaborators it has been demonstrated the strong relationship between substrate stiffness and YAP/TAZ expression and intracellular compartmentalization. The YAP/TAZ activity and their cellular localization was tested in mammary epithelial cells (MEC) grown on hydrogels with a range of stiffness from 0.7 kPa (soft) to 40 kPa (stiff), by real-time PCR and immunofluorescence assays, respectively. They demonstrated that YAP/TAZ was inhibited and mainly localized in the cytoplasm in cells interfaced with soft substrates. Conversely, cells let to develop on the stiffer matrices shown enhanced expression of these regulator factors and their nuclear translocation was promoted. In another set of experiments a strong correlation between CKS tension and YAP/TAZ localization was detected, emphasizing the influence of stress fibers on the overall process (Dupont et al., 2011). Interestingly, these results are in contrast with those reported by Das and colleagues, where the integrity of actomyosin fibers and not their contractility was found as determinant for YAP activity and localization (Das et al., 2016). These results are summarized in figure 3 and 4, respectively.

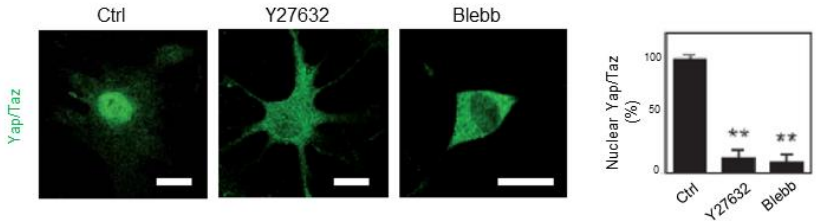

Figure 3 YAP/TAZ localization and cytoskeleton tension. *Confocal immunofluorescence micrographs of mesenchymal stem cells (MSC) control and ones treated with Y27632 or blebbistatin, grown on coverslips, show how the YAP/TAZ localization is regulated by stress fibers contractility. The bar plot summarizes the nuclear quantification of YAP/TAZ in the three examined conditions. The images were taken from* (Dupont et al., 2011).

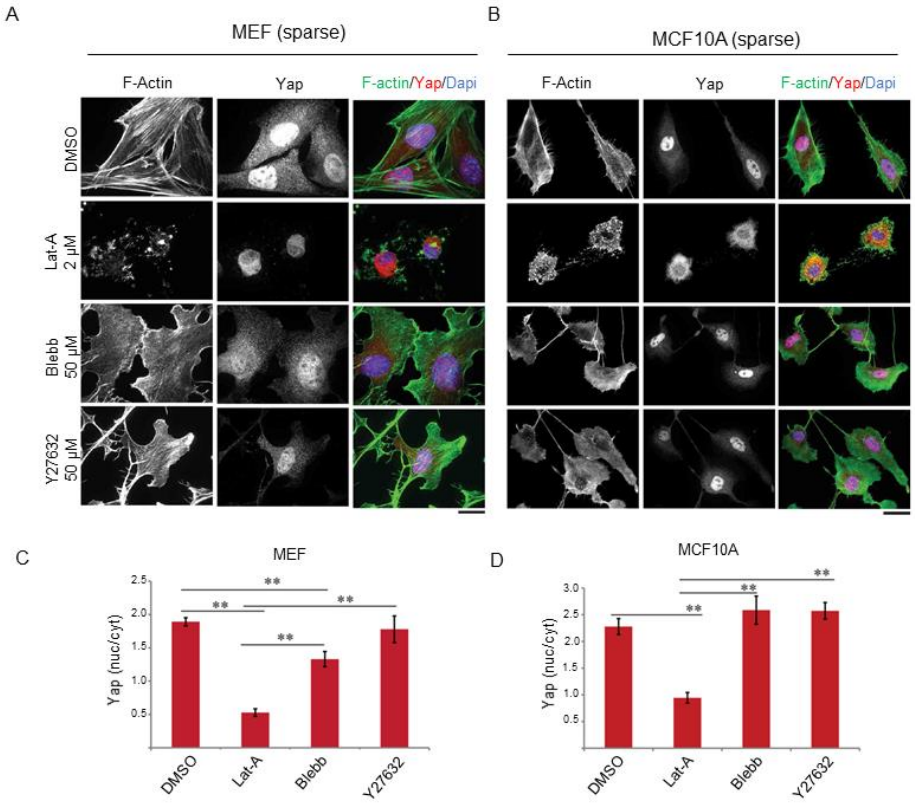

Figure 4 YAP/TAZ localization depends on the cytoskeleton integrity*. The confocal images (A and B) show that in mouse embryonic fibroblasts (MEF) and MCF10A mammary epithelial cells, grown on coverslips and treated with latrunculin-A, the disruption of F-actin caused loss of nuclear YAP and its retention in the cytoplasm. Instead, inhibition of contractility with blebbistatin or Y-27632 induced loss of stress fibers but YAP remained partially localized to the nucleus, similarly to control condition. The graphs C and D summarize these observations. These images were adapted from* (Das et al., 2016).

Despite some minor incongruence, the role of YAP as “mechanotransducer” was assessed in many other works, and it is now clear that its different localization in the cellular compartments, as determined by matrix stiffness, is crucial for neuronal differentiation from stem cells, highlighting the key role of mechanical cues in tuning several (neuro)biological processes (Musah et al., 2014).

1.1.6 Experimental approaches and techniques to study cell mechanobiology

The recent advent of novel (nano)techniques and tools able to measure mechanical properties of biological systems, allowed to increase the knowledge in the field of mechanobiology. In the past, the lack of tools able to generate or detect forces in the range of very low values (from pN to nN) impaired the measurements of mechanical features of cells and materials. Among all the techniques recently developed and exploited to evaluate cell mechano-adaptation and mechanical properties we have to mention the atomic force microscope, the optical and magnetic tweezers, the scanning ion conductance microscopy, the tractional force microscopy, and the use of microposts-decorated surfaces. Some of these biophysical methods are schematically illustrated in figure 5.

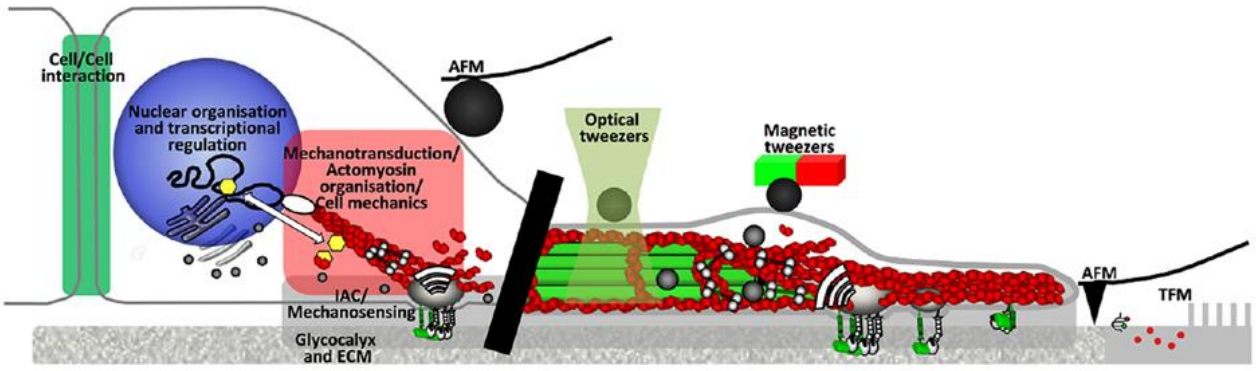

Figure 5 The biophysical methods to study mechanical properties in neuronal cell. *Image was adapted from* (Chighizola et al., 2019).

The atomic force microscopy (AFM) allowed several advances in the analysis of the topography and the biomechanical properties of various tissues, including the nervous one. Specifically, the AFM is a scanning probe microscopy technique that was introduced in 1986 by G. Binnig, C. Quate and C. Gerber transferring the scanning approach initially developed for the scanning tunnelling microscopy (STM) to non-conductive materials. Briefly, the AFM functioning is based on the principle of surface

scanning using an extremely sharp tip mounted on a flexible micromachined silicon probe. This tip is used to image a sample by raster scanning across the surface line by line. As the tip interact with the surface, cantilever bends and this bending determines a change in the optical path constituted by a laser beam reflected by the top of the cantilever. This deflection is constantly tracked by a four-quadrants photodetector (Shahbazian-Yassar, 2013). The figure 6 shows a schematic of AFM components and working principle.

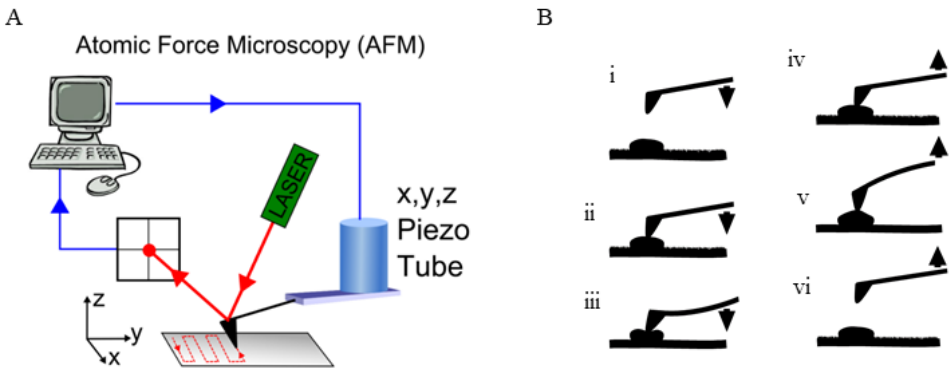

Figure 6 Atomic force microscopy technique. *A) Schematic representation of AFM setup (Adapted from website http://biomechanicalregulation-lab.org/afm). B) Sketch illustrating the functioning of cantilever tip: the tip is placed on the cell, touches and presses it. The deflection degree of cantilever depends on the cell stiffness.*

Another technique exploited to probe cell and subcellular mechanical properties is represented by the optical tweezers, also known as the optical trap or the laser trap. This technique is usually chosen when extremely small forces (in the order of 0.1-100 pN) are required or have to be measured (Killian et al., 2018). This technique is based on the use of a highly focused near infrared (NIR) laser beam to optically trap and manipulate small particles (from fractions of nm to few µm in diameter), such as glass beads or microvesicles, to push/pull the cell membrane generating both compressive or tractional forces. Optical tweezers have been successfully used to investigate the dynamic viscoelastic properties of living cells and tissues (Ayala et al., 2016; Lyubin, 2012; Mohammed et al., 2019).

Magnetic tweezers represent an alternative approach to the optical ones. Unlike optical tweezers, forces are here exerted on paramagnetic beads by means of a controlled magnetic field. An advantage

of this technique is that the paramagnetic beads may be chemically functionalized and, being opaque, they could be easily recognized by optical microscopy (Mohammed et al., 2019). This approach was adopted by T. Grevesse and colleagues, employing fibronectin-coated microbeads, to assess the mechanical properties of two neuronal sub-compartments, namely soma and axon. In their work, they discovered that the cell body was softer and exerted a solid-like response, while the axonal region was stiffer and characterized by a viscous-like response (Grevesse et al., 2015; Mohammed et al., 2019).

Scanning ion conductance microscope (SICM) is another recently introduced tool to probe cell mechanical properties. SICM conjugates, into a unique technique, the resolution of AFM with functional capabilities of conventional light microscopy (Lab et al., 2013). The instrument is composed by a nanopipette mounted on a three-axis piezo-actuator, which can generate force at the tip through hydraulic jets-mediated pressure detecting at the same time any change in ionic currents through the pipette aperture. The applied force may be calibrated by exploiting an AFM cantilever (Sánchez et al., 2008). SICM was used to study mechanical properties of different cell types such as neurons and cardiomyocytes, the latter being able to contract in response to pressure (Lab et al., 2013; Sánchez et al., 2008).

Finally, another approach employed to assess cell mechanobiology is the use of micropillars substrates devices. Cells cultured above these micro-structured substrates could be mechanically stimulated by the passive mechanical cues dictated by micropillars stiffness and geometry or, alternatively, the tangential forces generated by the cells on the substrate could be detected by measuring micropillar bending (Dupont et al., 2011; Gupta et al., 2015).

1.2 Neuronal mechanobiology in the CNS

1.2.1 Extracellular matrix as source of mechanical cues

The contribution of ECM mechanical properties to modulate CNS development, physiology and pathology aroused the interest of many research laboratories. Briefly, the ECM in the adult brain is

almost entirely composed of glycosaminoglycans (GAGs), including hyaluronic acid, proteoglycans (i.e., lecticans) and glycoproteins (i.e., tenascin), and constitutes approximately the 20% of the whole organ mass (Zimmermann & Dours-Zimmermann, 2008). It is possible to distinguish three different compartments in the nervous system ECM: (i) the basement membrane (basal lamina) that surrounds cerebral vessels, (ii) the perineuronal nets (PNNs) surrounding cell bodies and dendrites, and (iii) a diffusely distributed interstitial matrix lying between CNS parenchyma (Lau et al., 2013). A schematic illustration is provided in figure 7.

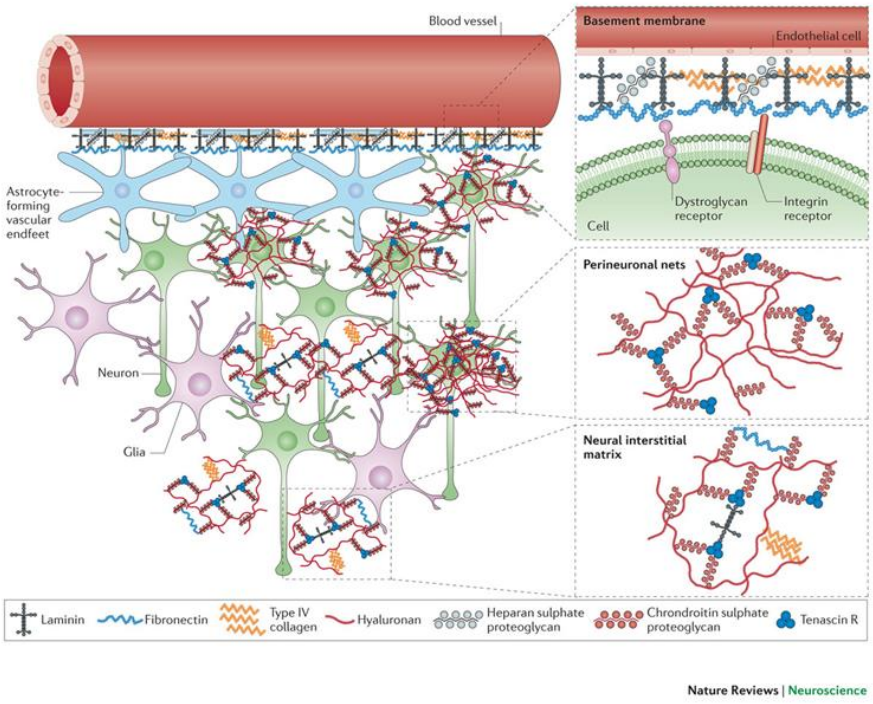

Figure 7. Schematic illustration of ECM in the CNS. *The ECM components are arranged into three different compartments: basement membranes that surrounds cerebral vessels, condensed as perineuronal nets around the cell bodies and dendrites of neurons or diffusely distributed as the neural interstitial matrix between cells of the CNS parenchyma. Image was taken from* (Lau et al., 2013).

ECM performs essential functions in the CNS. First, it provides a biological scaffold for the structure of the nervous tissue (Lu et al., 2011). Secondly, it is involved in the biochemical signalling regulating the diffusion and availability of molecules involved in differentiation and synapse remodelling

(Frantz et al., 2010; Ricks et al., 2014). Furthermore, and more related to the topic of this thesis, the ECM is a source of mechanical stimuli and thus may regulate neuronal behavior and function. Neurons and glial cells, as all cells are subjected to mechanical forces that come in a variety of different forms, and could be generally classified in two main categories: passive (or static) mechanical forces, and active (or dynamic) mechanical forces. The firsts include the contribution of microenvironment stiffness and topography; the seconds refer instead to pushing and pulling forces exerted, for example, by other close cells, by the flow of fluids, by the gravity, and/or by the heart beating transmitted by the dense vascular system sustaining CNS metabolism. All these contributions are summarized in Figure 8 (Urbanczyk et al., 2020).

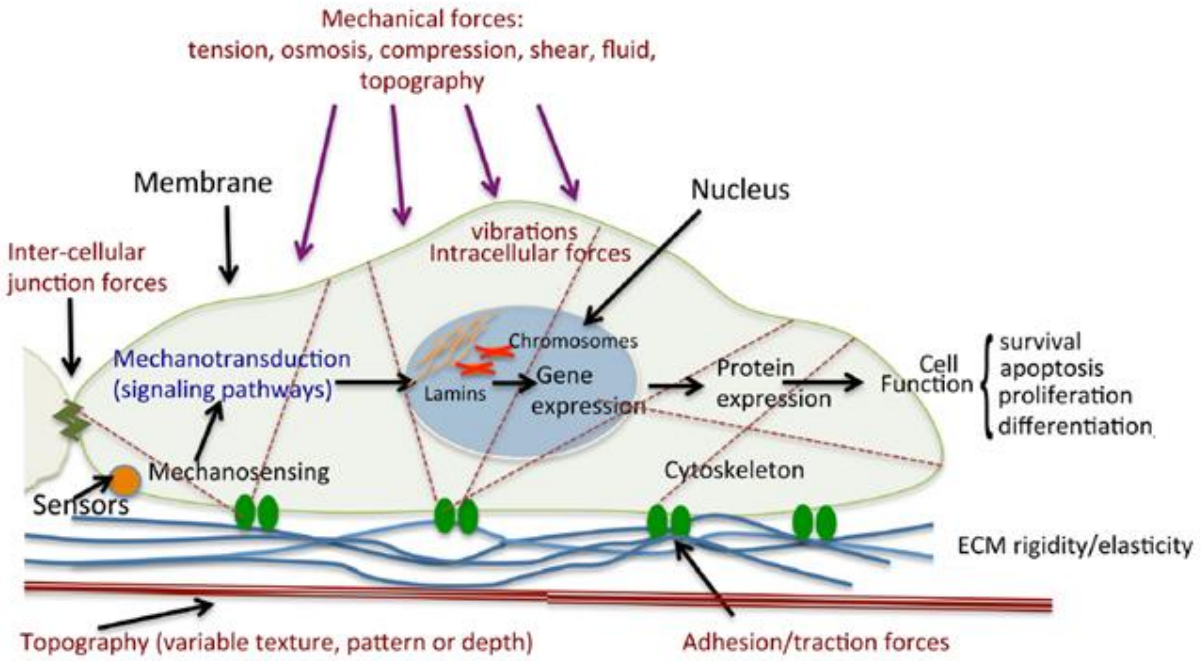

Figure 8 Schematic representation of mechanical contributions from external environment to cell. *Different biomechanical cues are collected by plasma membrane receptors (in green) and converted to biochemical response triggering intracellular pathways. This process regulates cellular activities such as proliferation, migration, differentiation, apoptosis as well as protein secretion in order to remodel the surrounding extracellular matrix. Image was taken from* (Tsimbouri, 2015).

In this thesis, my attention has specifically focused on the role of substrate stiffness, mimicking the contribution of the ECM as main passive mechanical stimulus in the CNS, in the regulation and modulation of neuronal activity and behavior using hippocampal primary cultures as cellular model.

1.2.2 Tissues and substrate stiffness

The CNS is a uniquely complex tissue. Its mechanical properties have become the focus of many recent investigations after their crucial role in modulating its development and overall functionality have been recognized (Tyler, 2018). Several disorders and diseases affecting the CNS are now associated to changes in its mechanical properties. CNS is a compliant, heterogeneous and viscoelastic tissue, these features emerge from the synergic interplay between CNS cellular components and ECM (Barnes et al., 2017). Among mechanical responses, the easier to investigate – and perhaps the most significative – is the stiffness.

The stiffness of the biological matter or of a biomaterial is an important mechanical property, perceived by cells through the mechano-transduction machinery as a passive physical stimulus, and able to deeply affect a wide range of cellular processes.

Briefly, material stiffness can be defined as "the extent to which the material resists to a specific deformation in response to an applied force" (Baumgart & Cordey, 2001). In the simplistic case of traction or compressive uniaxial forces exerted on a perfectly elastic material its value could be simply associated to the Young's elastic modulus (E), whose unit is Pascal (Pa = Newton/m^2, or pN/μm^2 a dimensional scale closer to the cellular one). The Young's modulus can be measured by applying a force to a defined area of a material (stress) and then calculating the resulting unitary change in length (strain). The slope of the stress versus strain plot determines *E* (Figure 9) (Wells, 2008).

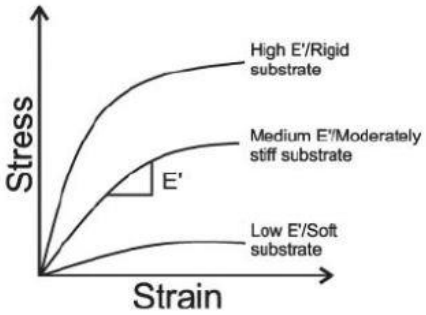

Figure 9 Stress vs Strain curve. *Image was adapted from Jhala D and Vasita R, 2015.*

Different biological tissues are characterized by extremely different values of stiffness. Very soft tissues, such as the fat, characterized by a Young's modulus of just few tens of Pascal, coexist with remarkably stiff tissues, such as the bones, showing a rigidity of the order of billions of Pascals (GPa). In this picture, the CNS is one of the softer tissues (Figure 10), (Budday et al., 2019). Indeed, it is characterized by values of the elastic modulus falling between 0.1 kPa and 10 kPa. Specifically, due to its heterogeneity, it has been shown that the stiffness of the CNS assumes different values of the Young's modulus depending on the tissue region or subregion considered. In the case of the rat hippocampus, the cellular model investigated in this thesis, Elkin SB and collaborators reported that the different layers of the hippocampus possess significantly different rigidities: CA1 *stratum pyramidale* = 140 Pa, CA1 *stratum radiatum* = 200 Pa, CA3 *stratum pyramidale* = 230 Pa, and CA3 *stratum radiatum* = 310 Pa. All these stiffness values were obtained by exploiting AFM technique (Elkin et al., 2007; Moore & Sheetz, 2012).

It is worth noting that tissue stiffness can dramatically change depending on a set of different parameters such as the examined species, the age of the organism, its physiological or pathological state (MacManus et al., 2017).

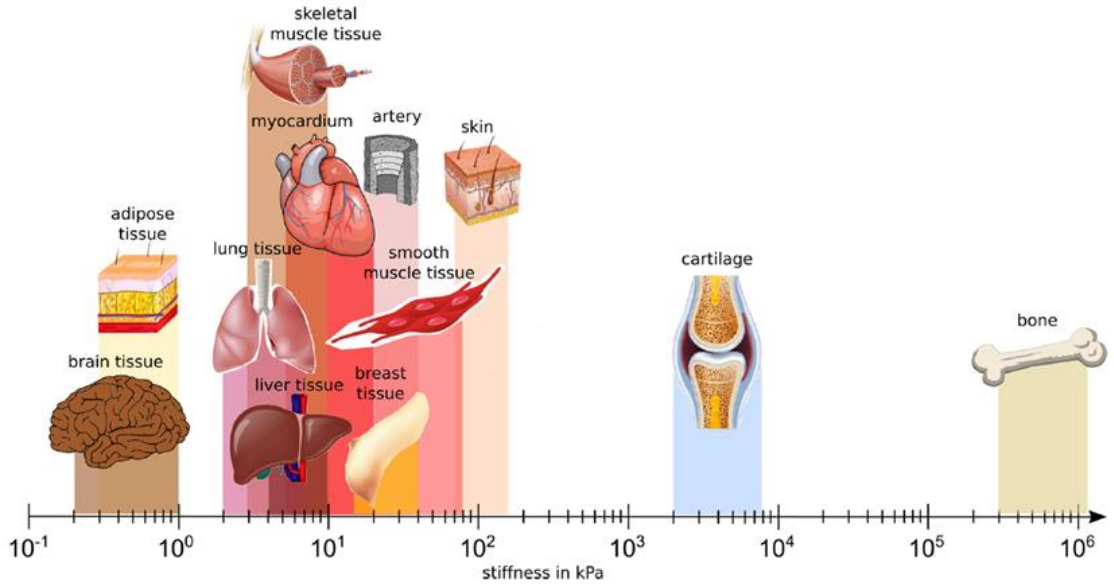

Figure 10 Human body tissues are characterized by different stiffness values. *Images was taken from* (Budday et al., 2019).

1.2.3 Stiffness impact on cellular processes

Many recent studies highlighted the impact of ECM (natural or artificial growth substrates) stiffness on cellular physiology. Several studies have demonstrated that stem cell proliferation and differentiation were both strongly affected by stromal stiffness. In particular, Engler A. and collaborators, in 2006, first described the key role of matrix elasticity in determining cellular phenotypes. Mesenchymal stem cells (MSCs) were grown on poly-acrylamide gels where the stiffness is tuned varying the percentage of bis-acrylamide crosslinker. Depending on the substrate rigidity MSCs differentiate in specific cell type: stiffer gels favour an osteogenic differentiation; cells grown on matrices characterized by an intermediate stiffness (similar to muscle tissue compliance) display a morphology reminiscent of myoblast; finally, the most compliant matrices, closing mimicking brain mechanical properties, induce MSCs to differentiate toward nerve cells. Not only

morphological studies were carried out, but also an accurate analysis of transcriptional profiles of MSCs cultured on different gels confirmed these results. Furthermore, it was also elucidated the crucial role of non-muscle myosin II in the mechano-transduction pathway. In fact, NM-II inhibition impaired MSCs ability to sense substrate rigidity and, consequently, differentiate (Engler et al., 2006). To note, the role of matrix stiffness was studied in the frame of neural stem/progenitor cells (NSPCs) differentiation. Specifically, it was shown that specific values of substrate stiffness (evaluated in terms of Young's modulus) were able to maximize the cellular proliferation ratio (E= 3.5 kPa), while other values (< 1kPa) induced NPSCs to differentiate towards neural cells phenotypes (Leipzig & Shoichet, 2009).

Another well-known cellular process regulated by the substrate stiffness is cell migration. In particular, it is referred to as *durotaxis*, a mechanism by which cells are prone to move toward increasingly stiffer regions. This phenomenon was observed in non-malignant cells, such as fibroblasts, that prefer rigid surfaces compare to the soft ones (Lo et al., 2000), but also in cancer cells, that respond to an increase in extracellular stiffness with an acceleration toward a pro-pathological condition (DuChez et al., 2019). Indeed, substrate rigidity affects cell migration speed and invasiveness. In the 2005 work of S. Peyton, the migration speed of vascular smooth muscle cells (SMCs) was investigated in relation to substrate stiffness. Specifically, cells grown on polyacrylamide substrates characterized by tuneable stiffness, reached a maximum migration speed at a value of stiffness of 51.9 kPa. Furthermore, it was also observed that the migration speed varied as function of the concentration of substrate-coating proteins: an increase in this concentration induced cells to move more quickly on compliant matrices (Peyton & Putnam, 2005).

Numerous studies pointed out that matrix stiffness is directly implicated also in tumour onset and evolution. It has been shown that tumoral microenvironment is characterized by a reduction of tissue compliance. This stiffening is due to an abnormal and increased secretion of trophic factors from cancer cells leading to a remodelling of the extracellular matrix molecular composition and structure

toward more compact and entangled structures. Furthermore, high stiffness of tumoral tissue promotes metastatic processes (Emon et al., 2018; Handorf et al., 2015; Reid & Zanivan, 2017).

In summary, matrix stiffness appears to be a key regulator of different cellular processes spanning from physiological aspects to pathological ones.

1.2.4 Matrix stiffness and neurodegenerative diseases

There is growing evidence highlighting the impact of ECM stiffness in maintaining the correct functionality of the CNS and disruption in the tensional homeostasis of the system was associated to various neurodegenerative disorders (Handorf et al., 2015).

For example, magnetic resonance elastography (MRE) investigations unmasked that the brain stiffness decreases in people affected by Alzheimer's disease. In particular, it was shown that the observed changes in tissue stiffness are mainly localized in the very same areas that are affected by the pathology. Therefore, alterations in neuronal tissue compliance is now under evaluation as hallmark of the onset or progression of neurodegenerative processes and, coupling it to classic biomarkers, as a new tool for the diagnosis of specific (neuro)pathologies (Murphy et al., 2016). Similar changes in brain stiffness were observed in other neuropathologies, such as Parkinson's disease, various forms of epilepsy, and multiple sclerosis. For example, it has been discovered that the brain area affected by parkinsonism, the substantia nigra, undergoes an increase in its rigidity in the presence of the disease. Furthermore, these alterations are prognostic, starting to appear well before the individual displays first motor difficulties (Berg, 2011). On the other hand, an increase in brain stiffness is a typical condition recorded in patients affected by multiple sclerosis. This stiffening seems associated to the inflammatory processes associated to the neuronal demyelination, a key promotor of ECM alteration through the systemic release of pro-fibrotic signalling molecules and factors. This abnormal alteration in tissue mechanical homeostasis impairs cellular functionality and recovery, compromising the correct overall cognitive functions (Urbanski et al., 2019).

The dramatic changes in the stiffness of the nervous tissue occurring during the onset and progression of neurodegenerative diseases hints at a deeper comprehension of the mechanisms correlating matrix stiffness and brain physiology. This will help in developing in vitro models to study neurodegeneration and, in the next future, to design novel treatments to deal with neuropathies. Neuronal scaffolds endowed with specific biochemical and mechanical cues are an example of this approach, potentially able to provide an anti-pathological extracellular microenvironment in order to stop or slow the neuronal disease progression.

1.2.5 Substrate stiffness and neuronal activity

A large portion of mechanobiology studies focuses on the impact ECM/stroma stiffness (i.e. passive mechanical cues), has on different cell phenotypes behavior, in terms of morphological and functional features. In this context, only a minority of studies addressed the role of substrate stiffness in regulating mature neuronal and glial cells activity in the CNS. This is due to the general difficulties in working and measuring physiology of primary neuronal cells when compared to cell lines, and the misconception that (cortical) CNS cells, and in particular neurons, are not mechanosensitive entities. Some preliminary study (Previtera et al., 2010; Zhang et al., 2014) described an alteration in the morphology and electrical activity of neuronal cells when interfaced with substrates characterized by different stiffnesses, but there are incongruencies and lack of a common agreement (Georges et al., 2006; Tanaka et al., 2018) that require to clarify the role played by mechanobiology in CNS organization and signalling processing.

Among all the works that investigated the impact of substrate rigidity on neuronal cells behavior, a relevant portion of them focused just on cell morphology, such as neuronal branching profiles. M. L. Privitera and collaborators have shown that hippocampal cultures were characterized by longer dendrites branches when plated and let to develop on stiff gels compared to soft ones (as shown in figure 11) (Previtera et al., 2010). Anyhow, authors did not explained why and how stiffness can determine different dendritic arborizations. The only hypothesis they attempted referred to a possible

variation in the number and organization of the adhesion points between cells and the substrates – the fundamental cell sensor loci of matrix stiffness. Importantly, this work exploited in-house made substrates to achieve different surface stiffnesses. The different levels of rigidity were obtained changing the monomer/crosslinker ratio (acrylamide/bis-acrylamide). Moreover, all the substrates were pre-treated by a cell-adhesion coating of poly-lysine. In contrast, Tanaka's research group showed, that neuritogenesis was enhanced in neurons interfaced with compliant matrices, where cultured neurons spread out a larger number of processes when compared to those interfaced with harder supports (Tanaka et al., 2018).

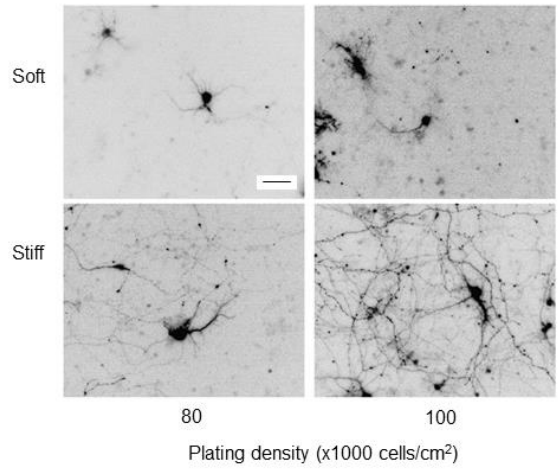

Figure 11 Neuronal morphology changes as function of substrate stiffness. *Representative micrographs of GFP-expressing hippocampal neurons. Cells plated on stiff gels are endowed with complex morphology characterized by a higher number of ramifications and longer branches compare to neurons cultured on soft substrates. Scale bar 50 µm. Images were modified and adapted from* (Previtera et al., 2010) .

In a different approach, both embryonic rat astrocytes and neurons were cultured on soft or stiff gels: while astrocytes displayed an extended morphology with marked stress fibers on hard supports, neurons showed an opposite behavior with actin more pronounced on the soft gels (Georges et al., 2006). Interestingly, these differences in cytoskeletal organization and cellular morphology were not observed in the specific case of cortical neurons – a puzzling result *per se* – and their neurites outgrowth was similar on each substrate used, regardless their stiffness. Therefore, from this study, cortical neurons appeared insensitive to substrate stiffness, at least from the morphological point of view, as reported in figure 12 (Norman & Aranda-Espinoza, 2010).

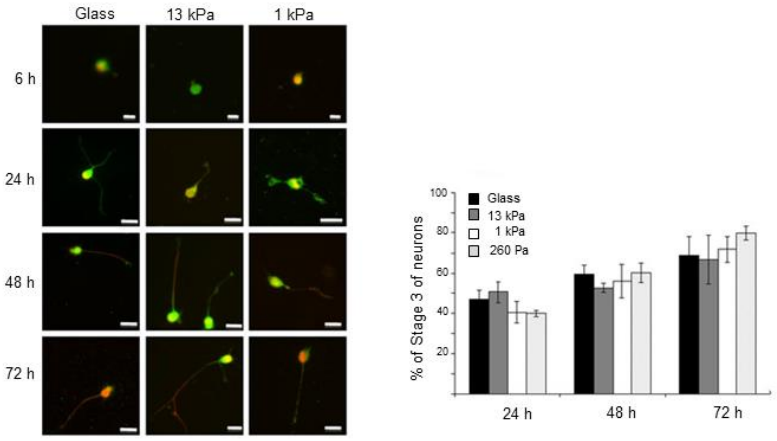

Figure 12 Cortical neurons and their axon growth are insensitive to substrate stiffness. *Fluorescence micrographs show cortical neurons fixed at 6, 24, 48, and 72 h after plating on laminin-coated gels of different stiffness. Cells were stained with MAP2 (green) to identify microtubule associated proteins in neurites, and SMI31 (red) to identify neurofilaments (NF) present only in the axon of each cell. Stage 3 neurons refer to those cells with specified axons (positive staining for SMI31 in one process). No significant differences are observed among different substrates, indicating insensitivity by cortical neurons to stiffness. Images were modified and adapted from* (Norman & Aranda-Espinoza, 2010).

The so far highlighted discrepancies could be, at least in part, explained in terms of the contribution of different external experimental conditions, including: i) the stiffness range chosen for the substrates that was not always fully physiologically representative, ii) the chemical activity or heterogeneity of the material(s) by which the culturing substrates were made, iii) the different contribution of the cell-adhesion coating used. Furthermore, another critical aspect is the degree of maturation of neurons,

their class, the animal model exploited, the plating cell density, and the age of the cultures (i.e., days in vitro - DIV) at the time of the experiments. All these variables might be responsible for the experimental discrepancies observed. For this reason, we deemed it necessary to make order in the field setting on accurate experimental procedures to shed light on the effective impact of matrix mechanical properties on CNS neurons.

Most previous investigations targeted the morphological adaptation of neurons and glial cells to matrices characterized by different stiffness, while little is known about the potential effects that substrate stiffness has on single neurons excitability or on synaptic neuronal networks. In a recent study, Zhang and colleagues demonstrated in 2014 that substrates characterized by different rigidity tuned synaptic activity and function. In particular, the authors demonstrated that Ca^{2+}-mediated currents (as shown in figure 13) and excitatory synaptic transmission were enhanced in stiff supports compared to soft ones (Zhang et al., 2014).

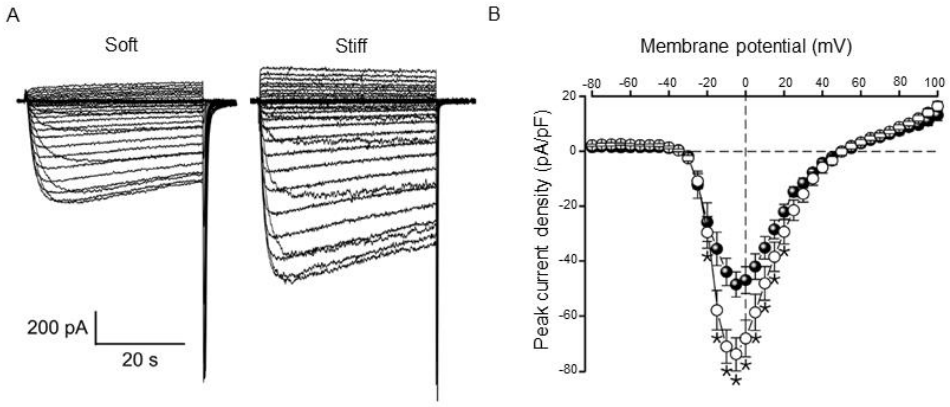

Figure 13 Calcium currents are affected by substrate stiffness. *Soft and stiff substrates refer to PDMS supports characterized by different values of Young's elastic modulus, E ≈50 kPa and E≈500 kPa, respectively. A) Representative traces of Ca currents recorded in neurons grown on soft and stiff substrates. B) I-V curve is reported. Image was adapted from* (Zhang et al., 2014).

The fact that a higher stiffness up-regulates neuronal network activity was later confirmed showing an increased efficacy of excitatory synaptic transmission induced by stiff substrate (Yu et al., 2019). In the work of Wen Y.Q and colleagues it is shown that also matrix proteins can modulate cellular response to substrate stiffness. Specifically, substrates characterized by different stiffness (Soft/stiff:

2/22 kPa) and coated with laminin or fibronectin, regulate differently the neuronal network activity. In particular, neurons on laminin-coated substrates possess a higher number of synaptic connections (observed by pairs recordings) and are characterized by greater calcium oscillations (Wen et al., 2018). In another study, Lantoine J and collaborators have shown that cortical neurons behave differently when grown on stiff or soft micropatterned substrates (although here also space confinement and morphological effects are present together to a varied stiffness). Interestingly, above soft matrices the neuronal network formation was faster because of increased cellular motility (a remarkable different result if compared to other cellular models, see paragraph 1.2.3), while action potentials firing was enhanced by stiffer supports (Lantoine et al., 2016). Summarizing all the results introduced so far, there are increasingly growing evidences that the ECM mechanical and morphological properties play a crucial role in modulating the electrophysiological activity of various types of neurons but, despite the increase in new studies on this topic, the exact biological mechanism underlying this complex electromechanical adaptation remains unclear or, at least, elusive.

1.2.6 Hydrogel-based soft substrates for mechanobiology studies

Researchers investigating cell mechanobiology can take advantage of a large range of different substrates with tuneable stiffness. These relatively new tools open the possibility to mimic tissue compliance and perform *in vitro* experiments aiming to investigate the mechanobiological response of cells to passive mechanical cues.

In this regard, hydrogels are a promising family of materials. In 1997, Pelham and Wang pioneered the exploitation of polyacrylamide (PAA) hydrogels characterized by tuneable Young's modulus as substrates for cell culturing. Specifically, the different rigidity was obtained by varying the amount of the bis-acrylamide cross-linker (Pelham & Wang, 1997). In such a way, PAA hydrogels behave as water-swollen network of polymers whose stiffness could be easily modulated. Furthermore, these materials are characterized by good optical transparency, chemical and thermal stability, resistance to proteolytic degradation and they can be coated with different ECM-like molecules improving cell

adhesion. These features make them an appealing tool for mechanobiology studies (Caliari & Burdick, 2016). Since these first explorations, the PAA hydrogels are now exploited by many different research groups and commercialized by many biotech companies as fully characterized and tested substrates for cell biology studies. A crucial parameter that has to be considered when choosing a stiffness-modulated substrate is the thickness of the compliant film. Since PAA hydrogels are usually bound to glass coverslips, it is necessary to rule out the possibility that cells sense the rigidity of the underlying glass. In that regard, it has been demonstrated that cells are able to perceive the stiffness of an underlying glass or polystyrene substrate when the gels are less than 15 μm thick, resulting in biased and not reproduceable experimental outcomes (Kuo et al., 2012). Therefore, hydrogels substrate rigidity and thickness can play an important role in controlling the mechanosensing behavior in neuronal cell.

1.3 The Hippocampus as an *in vitro* study model

This paragraph focuses on the hippocampus and, specifically, on primary dissociated cultures obtained from this specific region of the CNS, since cells from this region were used as the *in vitro* model in this thesis. I opted to exploit this cellular model since it is a well-characterized and effective model to study the neural behavior. Network activity can be investigated through electrophysiological techniques at different resolution levels (from single-cell and synaptic, up to the whole network level). Furthermore, neuronal networks resulting from this *in vitro* model are characterized by the occurrence of synaptic plasticity phenomena, easily addressable by means of patch-clamping pair recordings. A detailed description of the electrophysiological tools and protocols used to perform neuronal cells and network characterizations is available in the Methods section of the submitted or drafted manuscript which represent the results section of this thesis.

1.3.1 Anatomy

The hippocampus is a brain region highly conserved in mammals and it is part of the so-called hippocampal formation. This formation is composed by the hippocampus itself (*cornus ammonis*),

the *dentate gyrus* (DG), the *subiculum*, the *parasubiculum*, the *presubiculum* and the entorhinal cortex. It is situated in the medial temporal lobe symmetrically organized in both cerebral hemispheres (see Figure 14 a).

The term hippocampus was coined by the anatomist Arantius in the sixteenth century and derives from the Greek word meaning "seahorse", whose it remembers the shape. Afterwards, other neuroanatomists, such as Ramon y Cajal and Rafael Lorente de Nò, studied and characterized this complex and fascinating structure. Cajal, in particular, distinguished two regions within it, the superior and the inferior, thus classified based on the size of pyramidal neurons: the top region was characterized by small pyramidal neurons, the lower portion mainly constituted by larger pyramidal neurons (Dudek et al., 2016). Lorente de Nò, instead, divided the hippocampus in three circuital subregions (CA3, CA2 and CA) and, subsequently, he added a fourth region (CA4), which coincides with the DG. This nomenclature is still used today (Amaral & Lavenex, 2007).

The Hippocampus possess a cortical-like organization characterized by a three-layers structure where each layer is called differently depending on the considered region. In particular, the deeper layer is composed of a set of afferent and efferent axons and interneurons. This layer is named *hilus* and *stratum oriens* for the DG and CA regions, respectively. The middle layer is instead rich of large pyramidal cells and interneurons and researchers refer to it as granule layer within the DG and as pyramidal layer in the hippocampus. The most external layer is cell-free and we usually refer to it as the DG molecular layer. In CA regions this layer is organized in three sublayers: the *stratum lucidum*, the deepest, which receives input from the DG and is present only in CA3; the *stratum radiatum*, made up of the apical dendrites of the neurons situated in the pyramidal layer; and the *stratum lacunosum-moleculare*, including the apical tufts of the apical dendrites (Van Strien et al., 2009). A representation of these layers is described in figure 14 B.

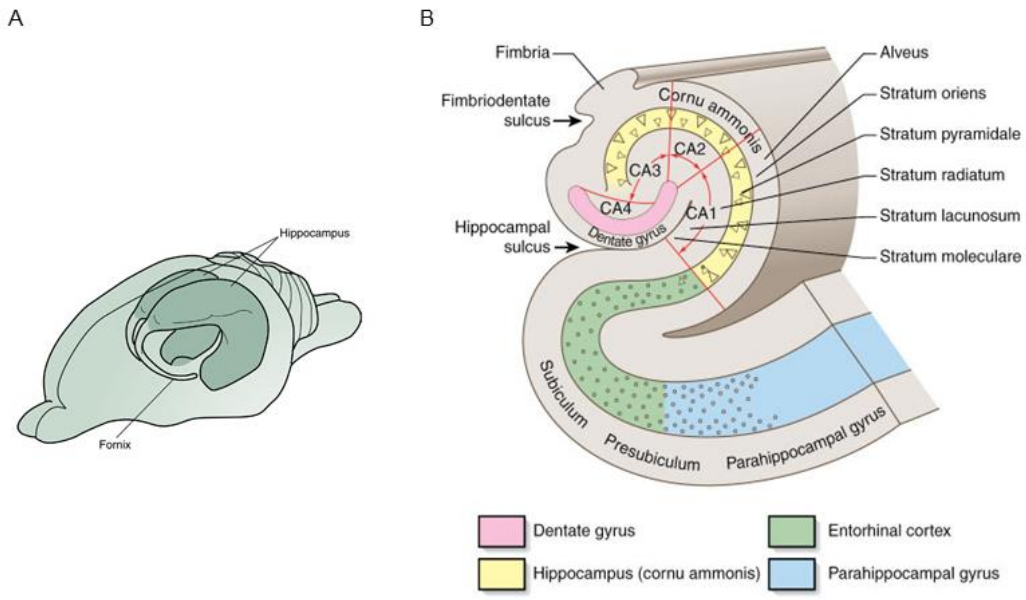

Figure 14 Schematic representation of hippocampus. *A) Sketch of the localization of two hippocampi inside the rat brain (image adapted from Hammond, 2015) B) A schematic organization of hippocampal layers.*

1.3.2 Functions and role of the hippocampus

The hippocampus is an important and fascinating subject of study in neuroscience. Initially, the neuroanatomists believed that the hippocampus had a role in the olfactory system because of its anatomical proximity, but the experiments conducted by Alf Brodal demonstrated that the anosmic mammals, such as the dolphins, unable to sense odours, were equipped with a robust hippocampal structure (Brodal, 1947; Compston, 2010).

It has not taken long time to realize that, instead, the hippocampus plays a fundamental role in the memory and learning processes. It is noteworthy the case of patient HM, who underwent anterograde and partial retrograde amnesia following the removal of his hippocampus (Preilowski, 2009). Thanks to the numerous connections the hippocampus establishes with the other brain regions, it is also reputed to be involved in many other functions as, for instance, the spatial navigation, in which hippocampus demonstrated able to generate and store a cognitive map of the external environment through “place cells”, a highly specialized kind of pyramidal neurons (Eichenbaum, 2017; O’Keefe et al., 1971). Furthermore, the phenomenon of synaptic plasticity, such as long term potentiation

(LTP) and long term depression (LTD), massively occurs in this small and complex structure (Lynch, 2004). Its contribution in the regulation of hypothalamic functions by affecting the release of adrenocorticotropic hormones was also well recognized (Anand & Dhikav, 2012).

Therefore, being the hippocampus the cortical region where these crucial functions are carried out, it is particularly relevant to know if and how its intrinsic mechanical properties, such as stiffness, can affect them.

1.3.3 Hippocampal cultures

In the late 70s, the pioneering neuroscientists G.A Banker and W.M Cowan developed a method to obtain hippocampal primary cultures from embryonic rats. This novel methodology has, *de facto*, revolutionized the way neuroscientist and neurobiologist deal with neuronal cells. Briefly, cells were dissociated by trypsin and plated at low density on poly-lysine-coated coverslips in an enriched medium. Neuronal cells successfully survive this strong "pruning" process and, after a few hours, neurons started to adhere to the substrate and to extend new born processes: axons and dendrites. After about one week in culture, a large portion of the cells adopted a pyramidal morphology resembling the neurons typically observed in hippocampal areas (as shown in figure 16) (Banker & Cowan, 1977).

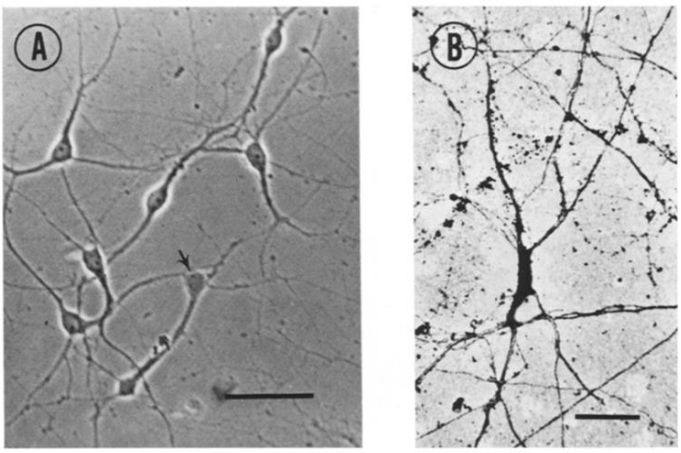

Figure 15 Hippocampal neurons in culture. *A) Representative micrograph of primary hippocampal cultures at 7 DIV. Arrow indicates a non-neuronal cell. Scale bar 50 µm. B) a hippocampal neuron at 11 DIV. Note the typical shape assumed by pyramidal neuron. Scale: 25 µm. Images was taken from* (Banker & Cowan, 1977).

In the subsequent years, the preparation method of hippocampal cells was refined and optimized allowing neurophysiologists to perform a plethora of morphological and functional studies, previously impossible or extremely difficult to accomplish. For example, several experiments focused on the study of hippocampal neurons morphology when grown on substrates characterized by different topographical and mechanical properties arises (see paragraph 1.2.6). Furthermore, electrophysiological studies allowed to characterize the passive properties of neurons, as well as active ones, or the synaptic currents in the neuronal networks.

Therefore, dissociated primary hippocampal cells have proved to be a powerful and reliable tool to investigate the neural network formation and maturation, the cellular and molecular mechanism underlying synaptic plasticity and therefore memory and learning, the electrical activity by electrophysiological techniques, and the interactions of this class of neurons with different drugs or materials. Despite the fact that dissociated neurons explanted from a three-dimensional native environment lose their original cytoarchitecture, they are still able to recapitulate connections patterns and remain viable for 2-4 weeks. A further important advantage connected to the use of dissociated primary hippocampal cells instead of immortalized cell lines is the difficulty using the latter cell model to have mature and electrically active synaptic junctions (Bradford, 2015).

For all the listed reasons, researchers are widely using the hippocampus as a reference model to study *in vitro* neuronal adaptation to different external conditions, synaptogenesis and neuronal plasticity. In addition, the hippocampus can be easily recognized and so isolated during the dissection, a critical aspect if we aim to work with phenotypically homogenous cell cultures. Therefore, all these features make this brain region one of the most captivating in neurobiology and suitable also for mechanobiology studies.

1.3.4 Glial cells

Neurons have always been considered the main actors responsible for the functioning of the nervous system, but another class of cells, named neuroglia, revealed to play a pivotal role too.

Rudolf Virchow, a famous pathologist of the XIX century, coined the word “neuro-glia” in 1856. Specifically, Virchow used the German term “Neurenkitt”, translated as ‘nerve-glue’, in reference to the filling and neuronal support role that he had observed in glial cells (Somjen, 1988). In fact, for a long time the glial cells were considered “silent” cells of nervous system because of the absence of excitable properties. The neurophysiologists who studied glial cells with electrophysiology techniques finding only passive membrane currents (Abbott, 1985).

Even if the name glia remains, its concept has undergone a revolution in modern neuroscience: from a purely support function for neurons to a clear and strong active role in the nervous system (Agulhon et al., 2008).

Neuroglia performs fundamental neurobiological functions providing trophic and structural support to neurons and participate to the modulation of the synaptic transmission, for example by releasing synaptically active molecules, as gliotransmitters (i.e., glutamate and ATP). Thus, neurons and glial cells influence each other: glia contributes in the modulation of synapses formation and strength, neurons affect proliferation, differentiation and the overall morphology of glial cells (Fields & Stevens-Graham, 2002; Stogsdill & Eroglu, 2017).

In the CNS three main classes of glial cells can be identified: astrocytes, oligodendrocytes and microglia. In this section, they will be briefly described.

The astrocytes play a fundamental role in CNS. They are able to take up nutrients from the blood crucial to neuronal survival (Pellerin et al., 2007). Related to their trophic function, astrocytes constitute a fundamental source of glucose, being the only cells in the brain synthesizing glycogen. The glucose captured is oxidized to pyruvate, an essential energetic substrate for neurons. In this regard, astrocytes are able to store glycogen, which is catabolized in case of hypoglycemia, allowing the neuronal survival (Proia et al., 2016). Furthermore astrocytes are involved in the formation and maintenance of the blood brain barrier (BBB) (Correale & Villa, 2009; Haddad-Tóvolli et al., 2017; Janzer & Raff, 1987). Astrocytes act as bridge between the neuronal circuitry and blood vessels: in response to neuronal activity they regulate the blood flow (Attwell et al., 2010). Recently it has been

observed that astrocytes are involved in synaptic maintenance by controlling the formation, strength and turnover of synapses (Clarke & Barres, 2013). Additionally, they participate in the pruning of synapses (N. J. Allen, 2014). Lastly, they regulate extracellular ion concentrations, in particular concerning the sequestration and redistribution of K^+, so modulating the neuronal excitability in terms of ability to repolarize the plasma membrane (Kofuji & Newman, 2004).

Oligodendrocytes are responsible for myelinization process of axons in CNS. Differentiating oligodendrocytes undergo complex morphological changes to generate numerous long processes that enwrap different axons forming the myelin sheaths (Snaidero & Simons, 2014).

Microglia cells are specialized macrophage involved in neuro-immune response; they mainly protect nervous system by potential injuries(Van Rossum & Hanisch, 2004). Specifically, microglia change morphology upon physio- and pathological state. In physiological condition, microglia cells are characterized by a ramified morphology, named 'resting microglia' surveying the CNS stroma in order to detect dysfunction, injury or diseases (Nimmerjahn et al., 2005). During inflammatory events, instead, microglia rapidly transform into an activated state, adopting an amoeboid morphology, and migrate toward the lesion site releasing cytokines. In addition to this main function, microglia play an important role in neuronal apoptosis (Färber & Kettenmann, 2005) and, together with the astrocytes, regulate synapse pruning (Schafer & Stevens, 2015).

Therefore, accumulating literature sustain the active role that glial cells play in the CNS.
Given these fundamental functions, it is also relevant to evaluate the contribution of glial cells in the mechanical properties of CNS and whether and how this category of cells responds to stiffness variations.

2. Aims

Neuronal mechanobiology is a relatively recent research field aiming at investigating the correlation between the mechanical and functional adaptation of neuronal cells and networks when perturbed by mechanical cues, both static or dynamic (Tyler, 2012). Several studies have highlighted the crucial role of mechanical cues in shaping the nervous system and modulating its behavior (Georges et al., 2006; Norman & Aranda-Espinoza, 2010; Previtera et al., 2010; Zhang et al., 2014). Anyhow, despite the rising number of researches on the topic, a further effort is necessary to decipher all the subtle and intricate contributions of mechanical forces in triggering and/or modulating cell and tissue functionality. Indeed, for example, the development of effective *in vitro* models to investigate the impact of mechanical cues on the functionality of the CNS could be of extraordinary importance to investigate pro-pathological vs physiological mechanical cues, an aspect linked to the onset of neurodegenerative diseases as Alzheimer or multiple sclerosis as well as to CNS ageing.

The primary aim of this thesis has been to evaluate the impact of environmental stiffness, a passive mechanical cue, on the mechanoadaptation of hippocampal neuronal networks from an unusual functional perspective. My research outcomes contributed to increase the knowledge of CNS cell mechanoadaptation and set up both an effective experimental framework and a methodology to study the role of stiffness in modulating neuronal electrical activity.

During the first part of my PhD, I investigated whether or not and, in the eventuality, how substrate stiffness could impact the development and morphology of neuronal networks and modulate their electrical activity by exploiting a multi-technique approach including, among others, immunohistochemistry, calcium imaging, atomic force microscopy, and the patch clamp technique. The latter electrophysiology tool, in particular, allowed me to evaluate the degree of neuronal circuit formation and synaptic connections highlighting spontaneous and evoked electrical activities in cultured cells. In parallel to these studies involving neurons, I conducted a preliminary investigation

on the morphological and functional adaptation of the other cell phenotype broadly expressed in my cultures, the astrocytes.

Subsequently, I attempted to highlight the mechanisms governing neuronal mechanoadaptation and, in particular, the ones responsible for the modulation of neuronal electrical activity. This task was accomplished by exploiting molecules able to interfere with cellular mechanosensing inhibiting cytoskeleton contractility.

Finally, I attempted to develop a model to explain why mechanoadaptation in neuronal cells is associated with an alteration in their spontaneous electrical activity and excitability. In my hypothesis, a key role is played by the amount of cholesterol present in cell plasma membranes and in the ability of stiff/soft substrates to alter cholesterol cell homeostasis. Dysregulated cholesterol levels in neuronal plasma membranes appeared associated with an altered transmembrane tensional state and, in turn, altered ion channels kinetics.

The second aim of this thesis is to investigate the impact of the surface chemistry on primary hippocampal cultures and its potential ability to modulate electrical and mechanical properties of neuronal cells. Therefore, as a side project, I explored how surface-immobilized chemical moieties impact on the process of mechanoadaptation. For this purpose, I interfaced neuronal cells to a layer of graphene chemically functionalized with phenylacetic acid and subsequently evaluated cell morphology, stiffness, and electrical activity.

All these results have been included in my thesis as submitted manuscripts and/or drafts ready for submission. Specifically, regarding the collateral projects I was involved in during my PhD, it is worth noting that they could not be accomplished without the collaboration with Dr Elisabeth Prats (CIBER/CSIC, Madrid, ES) and Dr Alejandro Criado Fernandez (CIC biomaGUNE, San Sebastian, ES). They have provided us with the graphene substrates and performed the surface chemical functionalization.

The third aim of this work is to evaluate how mechanical and chemical properties of substrates synergically cooperate in modulating the neuronal network behavior. My investigation of the mechanical and chemical contribution of three-dimensional double-walled carbon nanotubes (DWCNTs) foams on neuronal network development, survival and functionality was possible through a collaboration with Prof Maurizio Prato (University of Trieste, IT, and CIC biomaGUNE, San Sebastian, ES).

As an appendix section of the thesis, I included a preliminary study I have conducted in collaboration with Prof Gianluca Turco group (University of Trieste, IT) on the impact of polycaprolactone (PCL) electrospun membranes on the development and activity of primary neuronal cell networks.

3. Results

In this chapter results are reported as manuscript drafts to be submitted or manuscript drafts in preparation. All data are confidential.

3.1 Compliant environments downregulate neuronal activity by reshaping cholesterol homeostasis in primary hippocampal cultures

Compliant environments downregulate neuronal activity by reshaping cholesterol homeostasis in primary hippocampal cultures

Zummo, F.; Ballerini, L.; Scaini, D.

Affiliations

Neurobiology Sector, International School for Advanced Studies (I.S.A.S.), Trieste, Italy

Francesca Zummo, Laura Ballerini, Denis Scaini

Department of Medicine, Imperial College London, London, United Kingdom

Denis Scaini

Corresponding author

Correspondence to: dscaini@sissa.it (https://orcid.org/0000-0001-8398-8074)

Abstract

The extracellular environment provides mechanical cues relevant to cell and tissue physiology. Equally, neuronal cells actively sense and adapt to these stimuli and, through elusive molecular pathways, translate mechanical signaling into changes in functional behaviors. Increasing attention has been drawn to the ECM/substrate stiffness, but its role in regulating neuronal signaling in the central nervous system (CNS) remains poorly understood. Here, we investigated how stiffness impacts neuronal behavior, attempting to shed some light on the mechanism linking compliance-mediated mechanical and electrical adaptation. Our data showed that compliant substrates downregulate neuronal electrical activity. A similar effect was obtained perturbing the mechano-sensing pathway in hippocampal neurons grown on stiff substrates by molecular inhibition of actomyosin contractility. We deeper probed whether a possible alteration of plasma membrane lipid composition, specifically cholesterol, occurs. We discovered a progressive increase of cell plasma membrane cholesterol in neuronal cultures that perceive a compliant surrounding environment.

Introduction

Many cells can detect and adapt to extracellular mechanical cues through processes referred to as mechanosensing and mechanoadaptation (Humphrey et al., 2015). Recent studies have demonstrated that mammalian central nervous system cells are also able to sense (micro)environmental mechanical stimuli. These could manifest in the form of passive cues, as stromal stiffness (Dupont et al., 2011; C. Zhang et al., 2020), or active ones, as in the case of push-pulling forces directly exerted by neighboring cells through their processes (Siedlik et al., 2017). Neuronal mechanoadaptation manifested in the form of altered behavior, impacting cell development, morphology and functionality (Lantoine et al., 2016; Previtera et al., 2010; Wen et al., 2018; Q. Y. Zhang et al., 2014). For instance, a substrate characterized by a rigidity mimicking the brain tissue induces preferential neuronal differentiation in nerve cells (Engler et al., 2006; Iwashita et al., 2019), or stimulate neuronal over neuroglial growth in cortical neuronal cultures (Georges et al., 2006). The mechanical properties of the cell-supporting substrate play a critical role in neuronal motility and spreading as well. In this regard, it has been demonstrated that stiff substrates could promote neuronal recruitment (durotaxis) in spinal cord explants (Fabbro et al., 2012; Shellard et al., 2021) and processes spreading (Oakes et al., 2018). By contrast, too compliant substrates are usually associated with reduced cell adhesion and thereby altered dynamics in the cytoskeleton-mediated neurite extension-retraction events (Previtera et al., 2010)

Furthermore, there are increasing pieces of evidence demonstrating that the extracellular environment's mechanical properties, recapitulated by culturing substrates of different stiffnesses, can critically impact neuronal functionality in terms of spontaneous electrical activity and synaptic connectivity/transmission (Lantoine et al., 2016; Wen et al., 2018; Q. Y. Zhang et al., 2014).

Unfortunately, the underlying mechanisms responsible for neuronal mechanoadaptation, especially regarding the latter functional aspect, appear to be highly elusive and difficult to catch from a neurobiological perspective.

A full comprehension of neuronal mechanoadaptation could have significant implications not only in increasing our fundamental knowledge about neuronal cell physiology and biochemistry but, above all, for the great repercussions it could have in coping with neurodegenerative diseases. A continuously rising number of studies pointed out the intimate relationship between the functional alteration characterizing cells affected by a neurodegenerative process and a profound alteration of the mechanical properties of the involved tissue. Specifically, injuries at the CNS level or neurodegenerative diseases have proved to remodel neuronal tissue mechanical properties, usually inducing local stiffening (Handorf et al., 2015). Local stiffness changes are associated, among others, with ageing (Arani et al., 2015), glial scar formation after traumatic injury (Cooper et al., 2019), Alzheimer's disease (Murphy et al., 2016) and multiple sclerosis (Urbanski et al., 2019).

These and other studies have recognized the critical impact that the comprehension of neuronal mechanoadaptation could have in developing novel approaches and treatments to alleviate or backward the effect of neuro-impairing phenomena. A complete picture explaining how the mechanical property of cell-interfaced substrates influences neuronal functionality is still lacking. Still, with this work, we started to shed some light on some of the biochemical phenomena responsible for neuronal mechanoadaptation. We evaluated through a multidisciplinary approach the impact of substrate stiffness on neuronal morphology, electrical activity and tensional homeostasis. Subsequently, trying to mimic mechanoadaptation by acting on different cellular mechanisms responsible for mechanosensing, we highlighted a crucial role of plasma membrane cholesterol.

Results

Substrate compliance does not affect neuronal network formation but impacts cell branching.

In order to investigate the contribution that the environmental stiffness has on the behavior of central nervous system (CNS) nerve cells, we cultured dissociated hippocampal cells on gel substrates of different compliance. Stiffnesses have been chosen closer as possible to the values characterizing CNS compartments (Barnes et al., 2017; Budday et al., 2019). Specifically, dissociated rat hippocampal cells were cultured above commercially available poly-acrylamide (PAA) hydrogels

characterized by Young's moduli of 50 kPa, 8 kPa, and 1 kPa as confirmed by atomic force microscopy validation experiments (Figure S1a, see Methods for details). Neurons plated on glass coverslips were instead used as control cultures (Cellot et al., 2009; N. Pampaloni et al., 2018; Rago et al., 2019). Many reports have described the successful growth of different cell types on PAA-based hydrogel substrates (Cozzolino et al., 2016; Pelham & Wang, 1997; Serna-Márquez et al., 2020), but the ex vivo development and functional analysis of primary neuronal cells responses and network activity were rarely investigated (Georges et al., 2006; Previtera et al., 2010). All the three hydrogel substrates allow the growth of cells with comparable mature cellular morphologies than controls, as pointed out by scanning electron micrographs giving a qualitative idea of cell shapes and arborization (Figure 1a). We further probed network cellular composition by quantifying the surface density of neuronal and glial cells after 8–10 days in vitro (DIV), using immunofluorescence markers for neurons (targeting class III β-tubulin) and for astrocytes (targeting the glial fibrillary acidic protein, GFAP) in all culture groups (Figure 1b). No significant differences were detected across the four conditions, as highlighted in the box plots in Figure 1c. These data demonstrated that cells adapt on all hydrogel substrates in a similar way than on glass controls, giving rise to apparently well-formed neuronal networks. Furthermore, the fact that the number of astrocytes remains similar in all the conditions suggests that the exploited PAA substrates have not proinflammatory effects on CNS cells, as an increase in astrocytes is commonly associated to a neuroinflammation process (Colombo & Farina, 2016; González-Reyes et al., 2017).

Fig. 1: Development of hippocampal neuronal networks on PAA substrates.

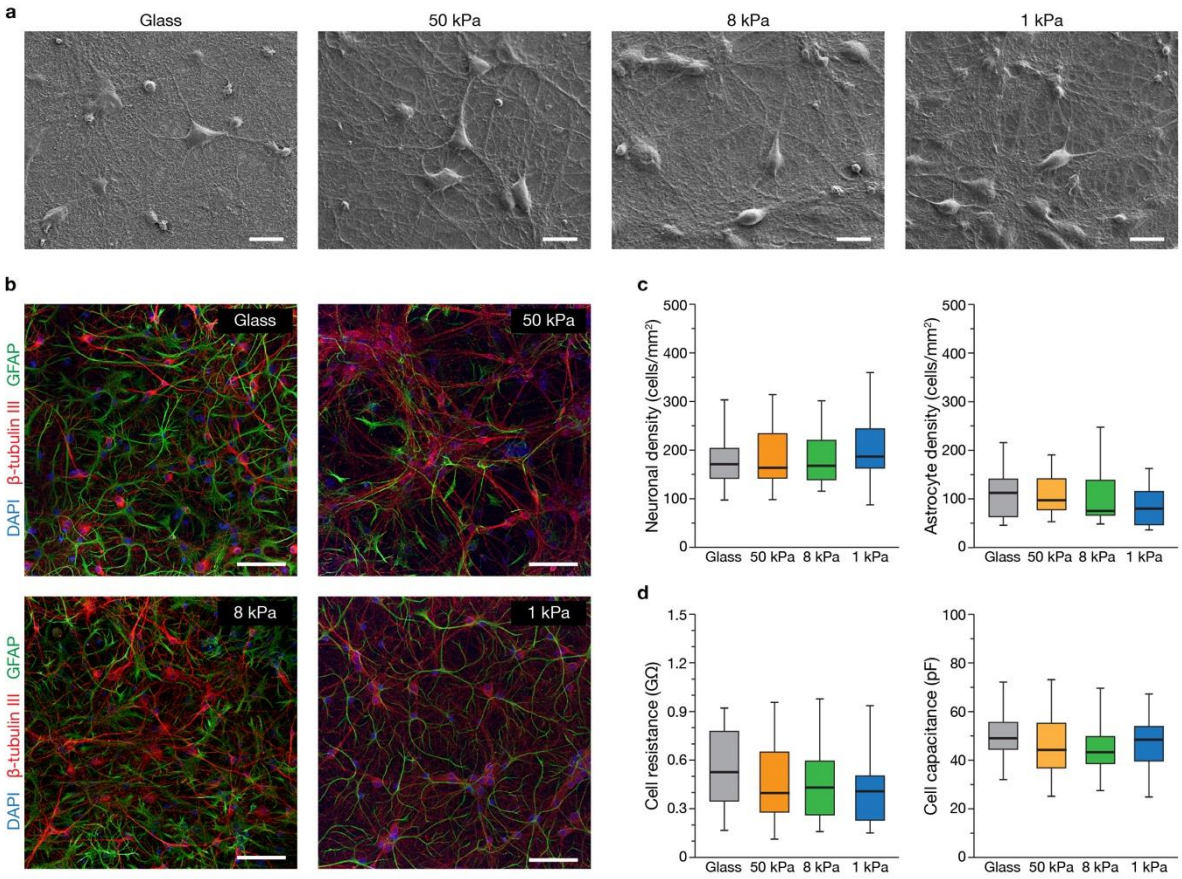

a *Scanning electron micrograph illustrating hippocampal neurons after 8-10 DIV. Scale bar 10 µm.* ***b*** *Fluorescent microscopy images depicting neuronal cultures stained against β-tubulin III, a specific neuronal marker (in red), and GFAP, staining astrocytes (in green), when cultured on glass and PAA gels of different stiffness. Scale bar 100 µm.* ***c*** *Box plots summarizing neuronal (on the left) and glial (on the right) cellular densities among the four substrates. No significant differences were detected across the four groups (25 fields of view analyzed for glass controls, 30 for the 50 kPa, 32 for 8 kPa, and 22 for the 1 kPa condition; images acquired from three independent culture series).* ***d*** *Box plots summarizing the membrane passive properties of patched neurons, revealing to be similar across all conditions (n cells= 33 for glass, n=30 for 50 kPa, n=31 for 8 kPa, n=28 for 1 kPa; from more than three independent culture series). Kruskal-Wallis followed by Dunn's multiple comparison test was performed (* $p < 0.05$, ** $p < 0.01$, *** $p < 0.001$).*

The cell membrane passive properties, input resistance and capacitance, are well-recognized indicators of cell surface extension, cellular healthy state, and membrane integrity (Cellot et al., 2011; Isokawa, 1997). Indeed, we evaluated both values for neurons on every condition and, as summarized in the box-plots in Figure 1d, they were similar across all groups (541.8±233 MΩ and 50.1±9.2 pF

for glass; 445.3 ±241.9 MΩ and 45.19 ±11.4 pF for 50 kPa; 479.3 ±255.9 MΩ and 44 ±8.6 pF for 8 kPa; 417.1±217.2 MΩ and 47.2 ±10.9 pF for the 1 kPa).

Although, at first glance, the morphology of neurons grown on glass controls and on compliant substrates appeared very similar, we wondered if any difference in the complexity of the dendritic arborization took place. To assess this single-cell morphological aspect, we highlighted a limited subpopulation of isolated neurons inducing the expression of the Green Fluorescent Protein (GFP) by calcium phosphate transfection (Figure 2a, see Methods for details). We subsequently performed a Sholl analysis (Binley et al., 2014) on spotlighted neuronal cells for the four conditions (Figure 2b). The Sholl intersection-curve of glass controls appears significantly different from the curves representative of neurons interfaced to the compliant PAA gels that behave similarly (38 cells analyzed for glass; 25 for the 50 kPa substrate, 22 for the 8 kPa substrate and 23 for the 1 kPa substrate). Neurons interfaced to stiff glass control substrates resulted more complex in their arborization and branching profile when compared to neurons cultured on the soft hydrogels that, from the other hand, are characterized by a lower number of branches at similar soma distances. The maximum extension of the cell arborization was the same in all conditions (about 600 μm from the cell soma). We move through this aspect evaluating the surface extension of neuronal cell arborizations (Figure 2c, see Methods for details). Cells developed on glass controls appeared spreaded on a substrate surface significantly larger than neurons on compliant gels where, instead, neurite trees were progressively less extended ($1.7\pm0.6 \cdot 10^5$ μm^2 for glass, $1.2\pm0.7 \cdot 10^5$ μm^2 for the 50 kPa, $1.1\pm0.7 \cdot 10^5$ μm^2 for the 8 kPa, and $1.0\pm0.5 \cdot 10^5$ μm^2 for the 1 kPa). The similar extension in cell branching pointed out by the Sholl analysis (about 600 μm from cell soma) let suppose the increment is due to a widening of the cell branching more than an elongation. We quantified this aspect evaluating the degree of circularity of the different neurite trees (see Methods for details), and our data confirmed that neurons on compliant PAA gels were progressively less circular or, in other words, more elongated (Figure 2d; 0.75±0.19 μm/μm for glass, 0.61±0.19 μm/μm for the 50 kPa, 0.52±0.19 μm/μm for the 8 kPa, and 0.51±0.19 μm/μm for the 1 kPa).

Fig. 2: Evaluation of single-neuron morphology on compliant substrates.

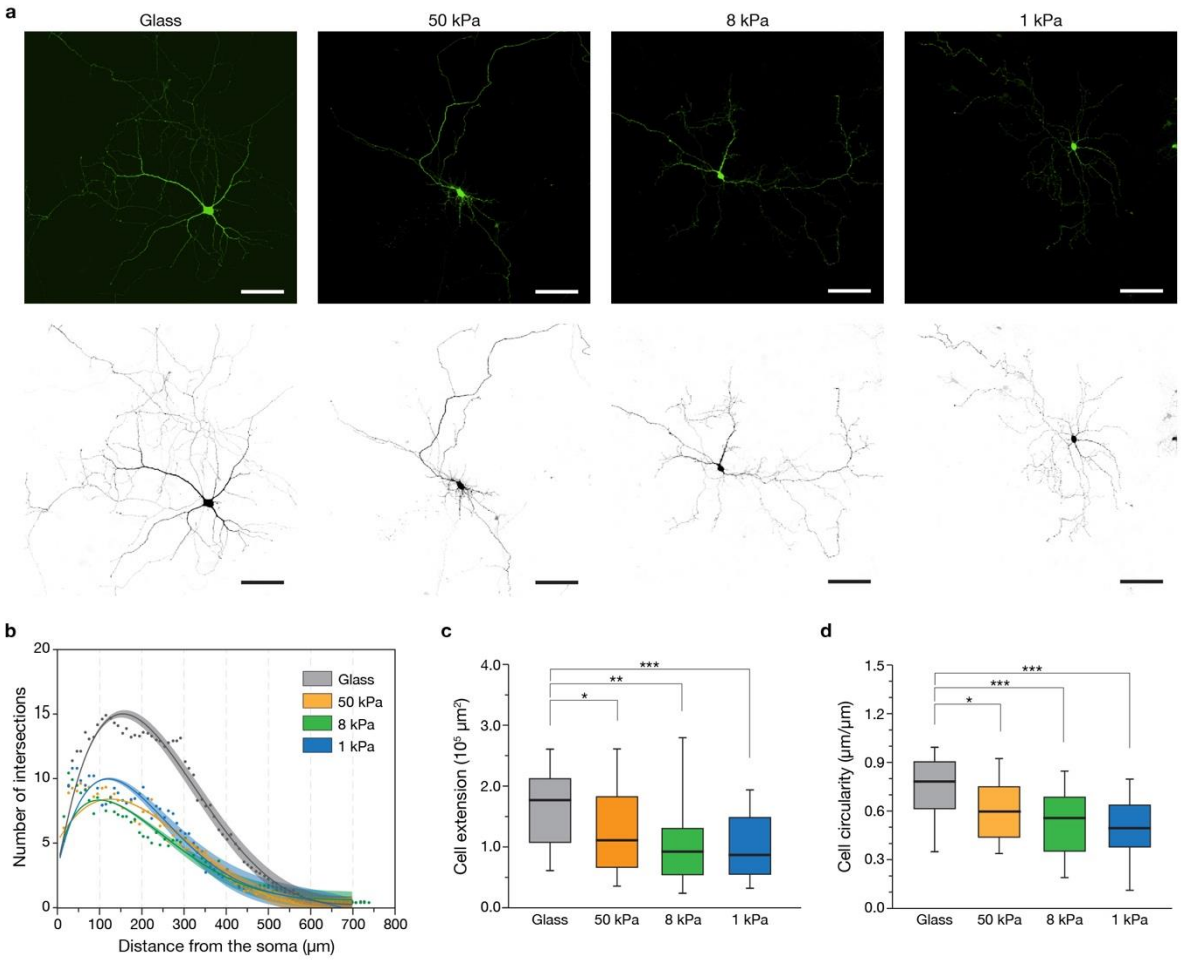

a *Representative fluorescent images of GFP-trasfected neurons cultered on glass and gels (on the top), and the corresponding binarized images used to perform the Sholl analysis (on the bottom).* ***b*** *The resulting Sholl intersection plot gives a quantitative information about the extension of neurite arborizations and branching profiles across the four conditions: at similar distances from the soma, neurons cultured on compliant substrates appear to have a lower number of crossing branches compared to those grown interfaced to glass (average curves were fitted using* 5^{th} *order polynomials showing 95% confidence bands).* ***c*** *Box plots highlighting the differences in surface extension of the neurite trees developed above the four substrates.* ***d*** *Box plots summarizing the degree of cell circularity of neurite arborizations (33 cells analyzed for glass controls, 21 for the 50 kPa, 22 for 8 kPa, and 23 for the 1 kPa condition; images acquired from three independent culture series). Statistical differences evaluated through Kruskal-Wallis followed by a Dunn's multiple comparison non-parametric test (* $p < 0.05$, ** $p < 0.01$, *** $p < 0.001$).*

Compliant substrates induce a reduction in spontaneous postsynaptic currents

In culture, dissociated hippocampal neurons develop in networks characterized by functional synapses giving rise to a spontaneous collective electrical activity as a result of recurrent connections. We recorded spontaneous synaptic activity after 8–10 DIV. This is an indirectly informative of the presence, number and strength of neuronal connections, and the collective number of neuronal interactions (N. P. Pampaloni et al., 2018). To explore the impact that substrates of different stiffness have on the electrical activity of the interfaced neuronal networks we have evaluated network spontaneous postsynaptic currents (PSCs) by whole cell voltage clamp recordings. Heterogeneous postsynaptic currents were detected as inward currents of variable amplitudes (Lovat et al., 2005) in all conditions, as shown in Figure 3a. Our data, summarized in the box plots in Figure 3b, demonstrated that PSCs were significantly reduced in both amplitude and frequency in the networks developed above PAA gels compared to the glass controls (42.47±10.27 pA and 6.09±5.34 Hz for glass, 24.33±12 pA and 1.82±2.56 Hz for 50 kPa, 24.31±14.6 pA and 1.02±1.65 Hz for 8 kPa, 28.21±16.07 pA and 1.13±1.27 Hz for 1 kPa). Indeed, a decrease in the stiffness of the substrate supporting a neuronal network induces a significant decrease in the synaptic activity of the interfaced neuronal network. Interestingly, no significant differences were pointed out among the soft gels, with the three networks behaving similarly in terms of PSCs amplitudes and frequencies. To rule out a possible chemical contribution of PAA on the effect observed on gels, we compared networks developed on pristine glass and on glass functionalized with 3-aminopropyltriethoxysilane (APTES, see Figure S1b and Methods) exposing cells to amino functional groups similar to the ones eventually present on PAA gels. No significant effects on PSC amplitude and frequency were induced by the chemical modification (Figure S1c). Similarly, we excluded an intrinsic functional impact of the cell-adhesion treatment used on PSCs (Polyornithine vs. Matrigel®, Figure S1d and S1e) nor in screening or altering the substrate stiffness perceived by cells (Figure S1e and S1a).

Fig. 3: Spontaneous synaptic activity of hippocampal cells on substrates with different stiffness.

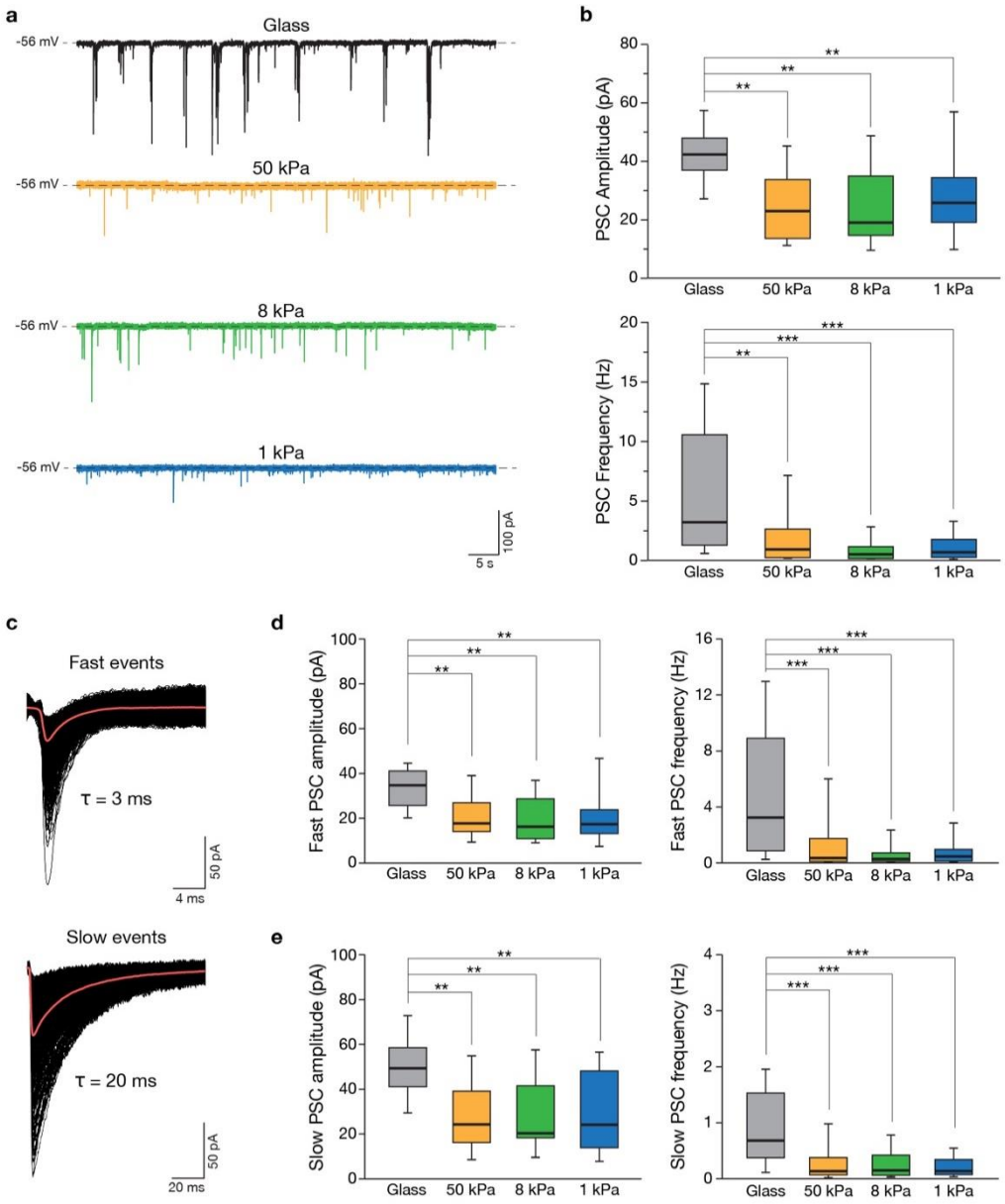

a *Representative traces for each patched neuron.* ***b*** *The box plots show a significant reduction in amplitude (on the top) and frequency (on the bottom) of sPSCs when stiffness decreases.* ***c*** *The synaptic currents were divided on the basis of their kinetics properties (decay time) in fast and slow events; examples of fast (on the top) and slow (on the bottom) events are shown superimposed (average trace reported in red).* ***d*** *and* ***e*** *The box plots summarize a decrease in amplitude and frequency in both cases, fast (**d**) and slow (**e**) events, when neurons were grown on PAA hydrogels (n cells= 33 for glass, n=30 for 50 kPa, n=31 for 8 kPa, n=28 for 1 kPa). Kruskal-Wallis followed by Dunn's multiple comparison test was performed, * p<0.05; ** p<0.01; *** p<0.001.*

Moving further the investigation, we discovered that both fast and slow current components were involved in the overall decrease of electrical activity. For this purpose, we have classified PSCs in fast and slow events based on their kinetic (decay time of about 3 ms for fast events, and about 20 ms for slow ones) as explicated by the traces shown in Figure 3c (Cellot et al., 2011; N. P. Pampaloni et al., 2018). Our analysis highlighted a significant reduction in the amplitude and frequency of fast PSCs (Figure 3d, 34.67±11 pA and 5.19±4.9 Hz for glass, 21.48±11.46 pA and 1.44±2.37 Hz for 50 kPa, 20.31±12.14 pA and 0.70±1.42 Hz for 8 kPa, 21.63±15.25 pA and 0.86±1.14 Hz for 1 kPa) as well as of slow events (Figure 3e, 50.28±15.63 pA and 0.89±0.69 Hz for glass, 27.19±15.42 pA and 0.29±0.42 Hz for 50 kPa, 28.3±19.3 pA 0.26±0.41 Hz for 8 kPa, 29.46± 20.9 pA 0.2±0.23 Hz for 1 kPa). These results suggest that substrate stiffness affects both AMPA- and GABA-mediated current components.

Miniature post-synaptic currents (mPSCs; Figure 4a) were then recorded in a subset of control and gel-interfaced neurons by application of the fast-inactivating voltage-gated sodium channel blocker tetrodotoxin (TTX, 1μM, see Methods), which blocks network activity impairing action potential generation and propagation. Studying mPSCs allows dynamical components to be distinguished from the structural components of the emerging network activity. In particular, mPSCs reflect the stochastic release of vesicles from the presynaptic terminals at individual synapses impinging on the recorded neuron: mPSCs frequency gives information about the pre-synaptic terminals in terms of number of synaptic contacts and quantal size, while their amplitude is related to the number and/or sensitivity of receptors at the postsynaptic side (N. P. Pampaloni et al., 2018; Raastad et al., 1992). As pointed out by the box plots in Figure 4b, we found no significative changes in both amplitude and frequency among the four conditions (17.7±7.6 pA and 0.9±0.5 Hz for glass, n=11 cells; 17.5±7.7 pA and 0.63±0.6 Hz for 50 kPa, n=10; 24.9±7.3 pA and 0.7±0.4 Hz for 8 kPa, n=11; 19.7±8.8 pA and 0.71±0.5 Hz for 1 kPa, n=10). These results suggest that the observed reduction in the

spontaneous network activity in gel-interfaced neurons does not involve structural changes in the number or properties of the synaptic connections.

Surprisingly, when we labeled by immunohistochemistry glutamatergic presynaptic terminals puncta (V-Glut1, see Methods) in neurons cultured on glass and on soft gels (Figure 4c) we found a progressive reduction of the puncta density moving from the stiffest to the softest support (Figure 4d). A significative difference arose between glass controls and the 1 kPa condition (n fields=15 for condition, 1.16±0.27 for glass, 0.87±0.22 for 50 kPa, 0.88±0.27 for 8 kPa, 0.66±0.1 for 1 kPa; n=15 fields per condition; $p<0.001$). This outcome, apparently in contrast with the previous analysis of mPSCs data, could be associated to an internal rearrangement of synaptic puncta distribution and size among the four conditions. To address this possibility, we evaluated from the same set of images the puncta volumetric size (expressed in μm^3, see Methods), and a significative increase in puncta size emerged in neurons cultured on the three gels (Figure 4e; Kolmogorov-Smirnov test, $p<0.001$). These results seem to uncover a compensation mechanism induced by compliant substrates on gel-interfaced neurons inducing a spatial and dimensional reorganization of excitatory puncta: less but larger.

Fig. 4: Evaluation of structural component of synaptic connections.

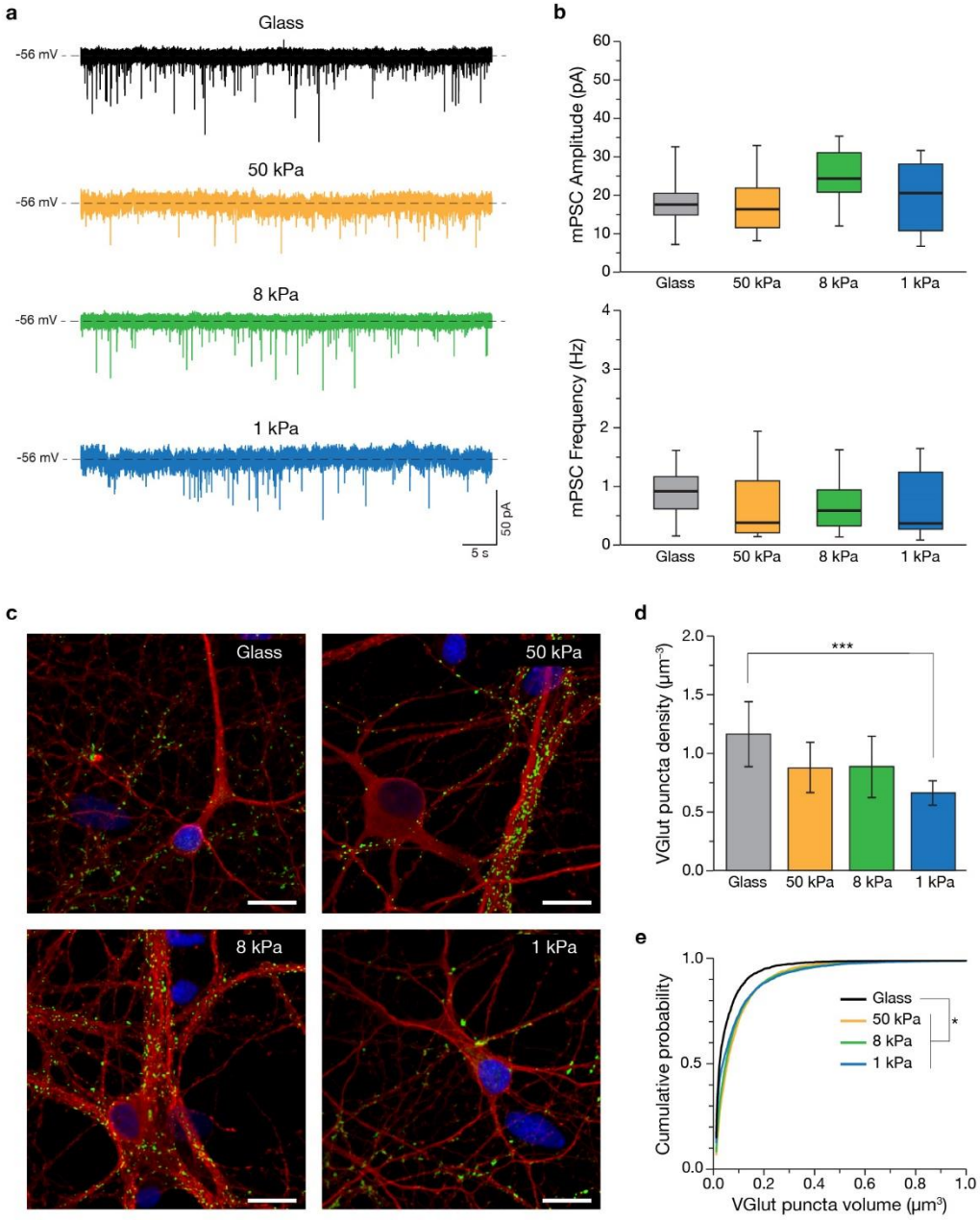

a *Representative traces of miniature postsynaptic currents (mPSCs) of patched neuron for each culture condition.* ***b*** *Box plots summarize amplitude (top) and frequency (bottom) of mPSCs (n=11 cells for glass, n=10 for 50 kPa, n=11 for 8 kPa, n=10 for 1 kPa). No significant differences were detected among the four conditions (one-way ANOVA followed by Tukey's multiple comparison test and Kruskal-Wallis followed by Dunn's multiple comparison test were performed for amplitude and frequency, respectively; P>0.05).* ***c*** *Confocal fluorescence images showing β-tubulin III positive neuronal cells (in red) and V-Glut1 puncta (in green) for the four conditions under investigation.* ***d*** *Box plots summarizing neuronal densities of V-Glut1 positive puncta. A progressive reduction in puncta densities is observable from the stiffest to the softest support (one-way ANOVA followed by Tukey's multiple comparison test, P=0.0003).* ***e*** *Cumulative probability*

plot of puncta size for neurons cultured above the four substrates. A significative increase in puncta sizes on glass-interfaced neurons is revealed when compared to gel-interfaced cells (n fields=15 for each condition; Kolmogorov-Smirnov test, p<0.001).

In the attempt to highlight the mechanisms responsible of the reduced neuronal activity exhibited by networks cultured on compliant substrates, we evaluated single-cell excitability by current-clamp recordings. Glass controls and gel-interfaced neurons were held at –60 mV in standard extracellular solution comparing the basal action potential frequency (Figure S2a). Consistent with previous PSC observations, the action potentials (APs) frequency was significantly lower in neurons grown on the three different hydrogels when compared to neurons cultured on stiff glass, as summarized in the plots in Figure S2b (n cells=15, 1.33±1.05 Hz for glass; n=14, 0.23±0.35 Hz for 50 kPa; n=15, 0.24±0.31 Hz for 8 kPa; n=12, 0.16±0.24 Hz for 1 kPa; $p<0.01$). We then further examined the sustained firing patterns of activity in our two extreme conditions, that are the glass and the 1 kPa gel. Cells were depolarized by current injections of increasing intensity (from 0 to 200 pA, at 10 pA increments). We observed that the same injected current value elicited a lower number of APs in 1 kPa neurons than glass controls (Figure S2c shows two representative plots at 140 pA). Overall, neurons on glass appear significantly more excitable when compared to those cultured above the soft gel (Figure S2d, n=16 cells for glass and n=20 for 1 kPa, data fitted with sigmoidal curves showing 95% confidence bands). In both conditions the sustained action potential firings were characterized by closely spaced action potentials of relatively constant amplitudes, an indication that no accommodation phenomena (Furlan et al., 2007) taking place in neurons interfaced to both substrates.

Altered cell mechanical and electrical properties correlate with substrate stiffness through a mechanosensing pathway

Cells are generally able to perceive the stiffness of the surrounding microenvironment, represented by the underneath substrate in the case of plated cells, via a process referred as mechanotransduction, modulating their functionality and stiffness accordingly (mechanoadaptation) (Alonso & Goldmann,

2016; Lampi & Reinhart-King, 2018; Tee et al., 2011). After having investigated the impact of substrate stiffness on the network electrical activity, we moved further through this scenario evaluating cell stiffnesses among all substrates by means of AFM single-cell force-indentation experiments (Haase & Pelling, 2015; Ulloa et al., 2021). AFM force spectroscopy experiments were performed on neurons cultured on glass and PAA gels after having specifically highlighted neuronal cells' nuclei by immunofluorescence (NeuN, see Methods). Cell stiffness measurements are summarized in Figure 5a. Neuronal cell stiffnesses monotonically decreased following substrate compliance (9.4±4 kPa in Young's Modulus value for glass controls, n=43 cells analyzed; 5.0±2.1 kPa for 50 kPa, n=63 cells; 3.4±1.6 kPa for 8 kPa, n=51; 2.0±1.3 kPa for 1 kPa, n=52). Overall, our data shown that the reduction in cell stiffness well correlates with the reduction in substrate stiffness and with the previously observed reduction in the spontaneous electrical activity. These evidences let suppose that an electromechanical coupling is taking place in our cultured networks.

In order to shed some light on the mechanism linking together compliance-mediated mechanical and electrical adaptation, we decided to study neuronal cells while perturbing the cellular pathway involved in mechanotransduction (Kaunas et al., 2005; Martino et al., 2018). For this purpose, we mimicked the effect of compliant substrates chronically treating hippocampal cells grown on glass coverslips with drugs able to modulate actomyosin contractility and, consequently, mechanoadaptation. For this purpose, we exploited two molecules acting at different levels of the mechanosensing pathway: para-aminoblebbistatin (pBleb), a water-soluble inhibitor of non-muscle myosin II (Várkuti et al., 2016), and Y-27632, a cell-permeable highly potent and selective inhibitor of Rho-associated protein kinase (ROCK) (Kawada et al., 1999).

Fig. 5: Modulation of mechanosensing pathway in hippocampal neuronal cells grown on stiff substrates.

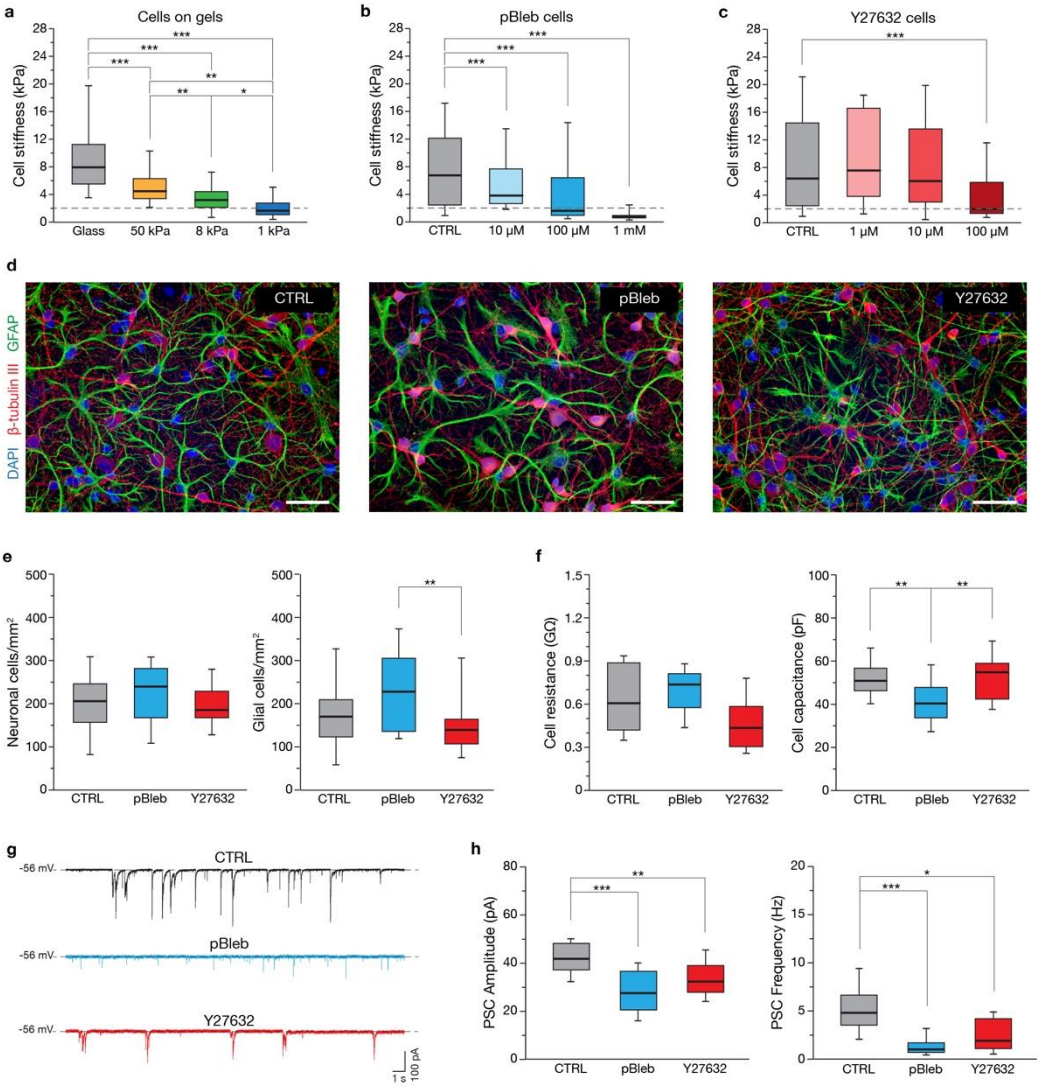

a *Box plots summarizing cell stiffness values measured via AFM when hippocampal cultures grown interfaced to glass and PAA gels of different stiffnesses (50, 8 and 1 kPa).* ***b*** *Box plots depicting stiffness values of cells grown on glass substrates after chronic treatment with para-Blebbistatin at increasing concentrations.* ***c*** *Box plots reporting different cell stiffness values when cells were chronically treated with Y-27632 at increasing concentrations. A concentration of 100 µM was able to induce a cell stiffness comparable to the one characterizing cells grown interfaced to the 1 kPa PAA gel (about 2 kPa, dashed line in the three plots).* ***d*** *Fluorescent microscopy images depicting neuronal cultures stained with β-tubulin III for neurons (red) and GFAP for astrocytes (green); scale bars 40 µm.* ***e*** *Box plots showing summarizing cellular densities of treated cultures: neuronal density (left) and glial density (right). No significant differences were detected in terms of neuronal densities across all three groups, but a significant difference in glial cell densities emerged*

between pBleb-treated and Y-27632-treated samples (Kruskal-Wallis followed by Dunn's multiple comparison test, P = 0.0011). ***f*** *Box plots illustrating the membrane passive properties of neurons, resistance (left) and capacitance (right). The capacitance of pBleb-treated neurons resulted significantly lower than that of the other two conditions.* ***g*** *Three exemplative traces of spontaneous PSCs recorded on each culture condition.* ***h*** *Box plots summarizing the amplitude (left) and the frequency (right) of PSCs. A significant reduction was observed in treated samples compared to control (Kruskal-Wallis followed by Dunn's multiple comparison test, * $p<0.05$; ** $p<0.01$, *** $p<0.001$).*

Both drugs were administered chronically from the 4 DIV while experiments were performed at 8–10 DIV. We have opted to use the two compounds at a concentration able to induce on treated glass-interfaced cells an effect comparable to the softer of our PAA gels (1 kPa). Therefore, we have preliminary treated cells at different concentrations evaluating for every condition cell stiffness (10–1000 µM pBleb, 1–100 µM Y-27632 Figure 5b and 5c, respectively). In both cases we discovered that a concentration of 100 µM was able, in our experimental conditions, to induce a mechanoadaptation, evaluated in terms of neuronal softening, comparable to the 1 kPa gels. Immunofluorescence images acquired at 8–10 DIV demonstrate that both neurons (marked by anti-β-tubulin III antibodies) and glial cells (marked by anti-GFAP antibodies) successfully withstood the two treatments developing well-formed networks (Figure 5d). Cellular morphologies are generally very similar among the three conditions with the exception of pBleb-treated glial cells that, instead, appear qualitatively broadened and less branched. Interestingly, when we quantified network cellular compositions, we found that while neuronal densities were similar in all conditions (Figure 5e, left), an opposite trend emerged between pBleb and Y-27632 treated samples when glial cells densities were evaluated (Figure 5e, right; 225±88.2 cells/mm^2 for pBleb; 139.4±44.4 cells/mm^2 for Y-27632; P=0.001). Similarly, by measuring neuronal passive properties, no differences in terms of membrane resistance were visible, but a significantly lower capacitance came out in pBleb treated samples when compared to the other two conditions (Figure 5f; 633±220.9 MΩ and 51.9±9 pF for control, n=23 cells analyzed; 717.4±205.9 MΩ and 41.5±10 pF for pBleb, n=21 cells; 478±184 and 52.6±11.5 pF for Y-27632, n=23 cells; $p<0.01$).

We evaluated the impact the drug-induced alteration in mechanoadaptation from a functional point of view by measuring PSCs via voltage clamp whole cell recordings (Figure 5g). Both treatments demonstrated able to significantly reduce the amplitude and frequency of spontaneous currents compared to untreated controls (Figure 5h; 5±2.5 Hz and 41±7 pA for control, n=22 cells analyzed; 1.5±1.7 Hz and 28.9±9.9 pA for pBleb, n=24 cells; 2.4±1.8 Hz and 33.9±7.3 pA for Y-27632, n=22 cells). Interestingly, also in these conditions, miniatures postsynaptic currents (mPSCs, Figure S3a) did not appear altered in both currents' amplitude and frequency (Figure S3b, 0.57±0.28 Hz and 13.8±5.5 pA for control, n=8 cells analyzed; 0.5±0.33 Hz and 13.5±3 pA for pBleb, n=7 cells; 0.4±0.26 Hz and 16±4 pA for Y-27632, n=7 cells). This result suggests that no changes in pre- and post-synaptic compartments were induced by pBleb and Y-27632 treatment; a condition similar to what we have observed on gel-interfaced neuronal networks.

The more pronounced effect characterizing pBleb treated cultures suggests that the interruption of cell ability to exert tractional forces to the substrates by a direct inhibition of myosin II contractility plays a key role in neuronal mechanoadaptation. It is worth noting the direct mechanical coupling linking together cell contractility and the tensional state of the plasma cell membrane (Simon et al., 2018) and, therefore, the impact that this could have on the properties of the embedded ion channels (Assmann & Lenz, 2014).

Plasma membrane cholesterol content changes as function of mechanoadaptation

Plasma membrane cholesterol content, acting synergistically with cytoskeleton contractility, is a potent mediator of plasma membrane tension (Al-Rekabi & Contera, 2018; Hong et al., 2012). Indeed, membrane cholesterol content has been shown to modulate membrane mechanical properties as well as ion current in many different cell types (Levitan et al., 2000; Li et al., 2007). To address this possibility, we evaluated using Filipin (see Methods) the amount of cholesterol present within the plasma membranes of pBleb and Y-27632 treated cells in comparison to untreated ones. Filipin is a

naturally fluorescent polyene antibiotic that binds to plasma membrane sterols labeling, in this way, cholesterol. Variations in the intensity and distribution of Filipin-related fluorescent signal across the different conditions allow to highlight any change in cholesterol level in treated cultures (Figure S3c). A significative change in Filipin signal emerged between both treated cellular cultures and the untreated control (Figure S3d; 0.23±0.05 a.u. for glass controls, n=17 fields analyzed; 0.30±0.03 a.u. for pBleb, n= 24 fields; 0.26±0.04 a.u. for Y27632, n=11 fields).

Driven by these results, we wondered if cholesterol depletion from the plasma membrane could be the critical mechanism responsible also of the reduced spontaneous activity and excitability characterizing our gel-interfaced neurons. We moved through this hypothesis evaluating by Filipin staining the amount of cholesterol present in neurons interfaced with PAA gels and comparing that with the basal cholesterol level of control cells plated on glass (Figure 6a). Our data highlighted a monotonical increase of plasma membrane cholesterol content as the stiffness of the substrate decreased. Otherwise, neurons cultured on soft hydrogels have a higher content of cholesterol compared to neurons cultured on stiff glass substrates, as revealed by Filipin fluorescence intensity (Figure 6b; 0.071±0.015 a.u. for glass controls, n=79 fields analyzed; 0.10±0.05 a.u. for 50 kPa, n=133 fields; 0.14±0.08 a.u. for 8 kPa, n=195 fields; 0.19±0.07 a.u. for 1 kPa, n=72 fields; data from three independent experimental sessions).

Fig. 6: Compliant substrates induce changes in the cholesterol content of interfaced hippocampal cultures.

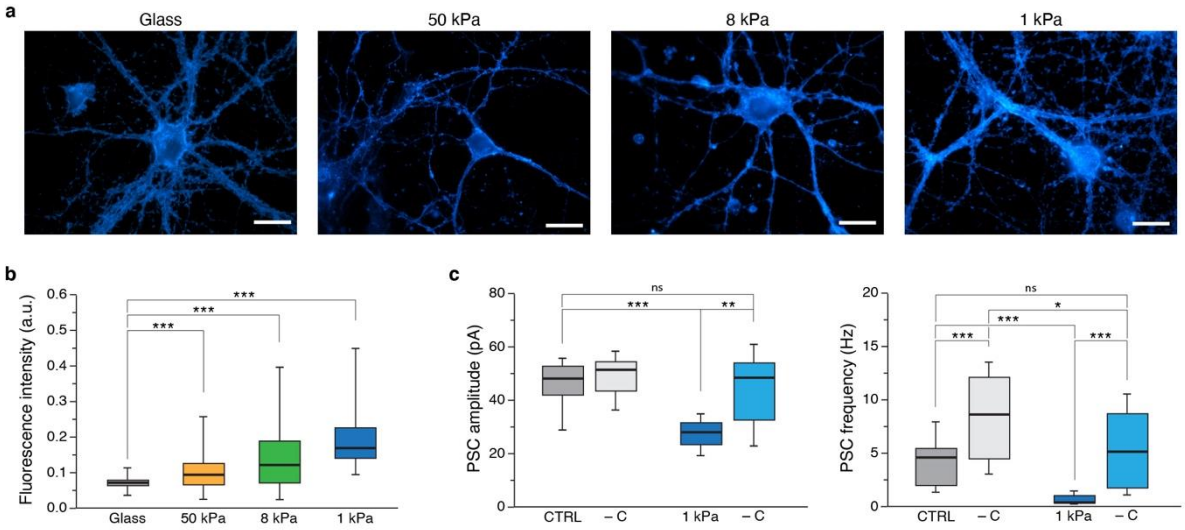

a *Representative fluorescent images highlighting Filipin signals in cells interfaced to the four substrates of different stiffnesses. Scale bars: 20 µm.* ***b*** *Box plots summarizing Filipin signal analysis across the four conditions and uncovering a significant increase in cholesterol content, measured as fluorescence intensity of Filipin, when substrate stiffness decreases (Kruskal-Wallis followed by Dunn's multiple comparison test was performed, p<0.001).* ***c*** *Two graphs summarizing the effect of membrane cholesterol depletion (–C) on amplitudes (left) and frequencies (right) of PSCs recorded on neurons developed above glass and 1 kPa PAA substrates (1 mM MβCD treatment). Two-way ANOVA followed by Bonferroni post-hoc test.*

These results highlighted an effective correlation between the different electrical activity of neurons cultured above complaint PAA gels and an increased content of cellular plasma membrane cholesterol. We attempted to experimentally validate such functional adaptive mechanism by evaluating the spontaneous electrical activity of neuronal networks where membrane cholesterol has been artificially removed. For this purpose, we treated cells cultured above glass and 1 kPa PAA substrates with methyl-β-cyclodextrin (MβCD, 1 mM, see Methods), a sterol scavenger heptasaccharide able to deplete cholesterol from the cell membrane (Christian et al., 1997; Zidovetzki & Levitan, 2007). PSCs analysis (Figure 6c) confirmed a significant increase in neuronal network electrical activity when hippocampal cultures underwent cholesterol depletion. We generally

observed significative increases in PSCs amplitudes and frequencies in neurons developed above both stiff (4.3±2.1 Hz and 46.2±7.9 pA for untreated glass, n=11 cells analyzed; 8.3±3.8 Hz and 49.4±7.2 pA for MβCD treated glass, n=9 cells) and soft substrates (0.51±0.49 Hz and 27.6±4.9 pA for untreated 1 kPa, n=9 analyzed cells; 4.3±3.4 Hz and 44.1±12.7 pA for MβCD treated 1 kPa, n=11 cells). Interestingly, while cholesterol depletion seemed not to induce an increase in PSCs amplitude in glass-interfaced cells, both amplitude and frequency of 1 kPa PSCs were risen by the treatment to a level equivalent to untreated glass values.

Taken together, these results suggest that compliant substrates are able to affect neuronal cells electrical activity by coupling a reduced cytoskeletal tension/contractility to a higher expression of membrane cholesterol. The latter presumably inducing an altered modulation of ion channel activity through an alteration in plasma membrane fluidity (Bukiya et al., 2010; Levitan et al., 2000).

Discussion

Our experiments have shown that primary neuronal networks developed on physiologically compliant substrates behave differently from stiff substrates for mechanical and electrical properties. Compliant substrates have induced softening of the interfaced neuronal cells and revealed detrimental for their electrical activity in terms of amplitude and frequency of spontaneous postsynaptic currents and network excitability. Interestingly, different from what was previously reported in the literature (Q. Y. Zhang et al., 2014), in our experimental conditions, both inhibitory and excitatory synaptic transmissions appeared down-regulated. Overall, these outcomes seemed to indicate that a more general mechanism is here involved, giving rise to a coupled electromechanical adaptation in central nervous system neurons as a response to an altered environmental stiffness.

In the range examined in the study, the stiffness of the surface does not significantly impact network composition, morphology, and neuronal cell membrane passive properties. At 8–10 DIV, neurite trees across the different conditions were characterized by a similar maximal protrusion, but stiffer substrates induce a more centrosymmetric tree-shape and enhanced branching, especially at

intermediate distances from the cell soma. This change could be due to an altered neuritogenesis in the early stage of network development (Tanaka et al., 2018). The modified branching organization could contribute to reshaping neuronal connectivity in the form of increased synaptogenesis. Despite the fact stiff-interfaced networks were characterized by an altered organization and dimensionality of vGlut1-positive puncta, these did not induce a significant alteration in the number and efficacy of synaptic events, as demonstrated by the invariance of miniature postsynaptic currents' amplitudes and frequencies across all the conditions investigated. We hypothesized that this discordance can be ascribable to two factors: (i) stiff substrates significantly increased the number of excitatory-associated puncta, but they were also significantly smaller, and consequently weakened, that on soft substrates; and (ii) neurites protruded from cell soma for similar distances in all the evaluated conditions, meaning that the probability to form new synapses with distant neurons is the same for equally dense cultures.

By the fact the differences in neurite branching could not bear all the differences in electrical activity we observed, we moved into a more neurobiological-focused investigation. Indeed, we impaired cellular mechanosensing by inhibiting cytoskeletal actomyosin-mediated contractility by applying Blebbistatin and Y-27632 drugs, mimicking on glass interfaced cells the same mechanical adaptation observed in neuronal cells developed above the softer of the tested substrates (1 kPa). Despite the broader and partially elusive biological effects these treatments may induce on neuronal cells, treated neurons recapitulated the same coupled reduction in mechanical properties and electrical activity observed in cells developed above soft substrates. This result confirmed the existence of a coupled electromechanical mechanoadaptation in central nervous system cells.

In the attempt to figure out the mechanism responsible for this adaptive connection, it is worth noting the direct mechanical coupling linking together cytoskeletal contractility and the tensional state of the cell plasma membrane in which the ion channels responsible for neuronal electrical activity are embedded. From this consideration, we evaluated in mechanosensing-impaired cultures the amount

of cellular cholesterol, a well-known mediator of plasma membrane tension (Al-Rekabi & Contera, 2018; Hong et al., 2012). Cholesterol levels appeared strongly raised in both Blebbistatin and Y27632 treated cells, with the formers displaying a concomitant more marked reduction in the activity and increased cholesterol content. The critical role of membrane cholesterol in modulating neuronal electrical activity was further demonstrated by cholesterol-depletion experiments performed on cells developed above stiff and soft substrates. Cholesterol depletion in 1 kPa gel interfaced cells was able to regain the level of activity characterizing neuronal networks formed above the stiff substrate.

Taken together, our results provide compelling pieces of evidence showing that substrate stiffness is an essential biophysical factor modulating synaptic activity and excitability in cultured CNS neuronal networks. However, it is not trivial to understand the underlying mechanism linking increased plasma membrane cholesterol levels and diminished electrical activity and excitability. Nevertheless, in the absence of any biochemical model describing the direct dependency of synaptic activity to cellular mechanosensing, we can speculate that a soft environment is effectively detected by CNS neuronal cells in the form of a mechanoadaptation (e.g., through the activation of the non-classical Hippo molecular pathway) modulating cell functionalities by direct altering their biophysical properties or activating (post)translational mechanisms. Reasonably, neurons interfaced with soft substrates will reduce their contractility and decrease their stiffness through cytoskeleton reshaping. Subsequently, presumably through an altered mevalonate pathway, this mechanical adaptation could raise the cholesterol content in the cell and, ultimately, in the plasma membrane. Third, the combined effect of reduced tension exerted in the membrane and an increased amount of inset cholesterol could impact lipid-raft composition and functionality, ion channels kinetics or vesicle fusion and recycling (N. Pampaloni et al., 2018). All these effects have already demonstrated to contribute to the regulation of the electrical activity of neuronal networks (Guo et al., 2009; Mailman et al., 2011; Marquer et al., 2014; Wasser et al., 2007), but further investigations are necessary to figure out the exact weight they have in the overall process.

A deeper comprehension of the mechanisms sustaining the functional mechanoadaptation of CNS cells could inspire new insight into brain functions and, potentially, the factors responsible for the onset of diseases associated with a change in the extracellular matrix or tissue stroma compliance.

Methods

Preparation of primary cultures and cell treatments

Dissociated hippocampal cells were obtained from P2–P4 old rats. Briefly, hippocampi were isolated from rat pups' brain and digested in trypsin (6000 U/mL, Sigma Aldrich) and deoxyribonuclease (1560 U/mL, Sigma Aldrich). After chemical and mechanical digestion, the cell suspension was centrifuged at 800 rpm for 5 minutes, pellet was collected and resuspended in fresh culture medium (see below). Cells were seeded on glass coverslips and on polyacrylamide (PAA) hydrogels bound to glass slides (Matrigen Softslip™, Cell Guidance systems, Easy-coat) of three different values of stiffness (1 kPa, 8 kPa, and 50 kPa, expressed in terms of Young's Modulus). Prior to cell plating, all substrates were coated with a Matrigel® solution composed of Matrigel/Gey's Balanced Salt Solution (GBSS, in ratio 1:50) and poly-L-lysine in ratio 2:1. Every sample was placed in a 35 mm polystyrene petri-dish and, after having placed a drop of cell suspension (300 µL at a concentration of 500.000 cells/mL) above each of them, they were placed in a cell incubator (5% CO_2 at 37 °C) for 1 hour to allow optimum cell adhesion. Subsequently, 2 mL of a culture medium composed by Neurobasal medium (Thermofisher) supplemented with B-27 (2%, Thermofisher), Glutamax® (10 mM, Thermofisher) and Gentamycin (500 nM, Thermofisher) were added to every petri. Cells were then let to develop in an incubator at 37 °C (5% CO_2, 95% RU) for up to 9–10 DIV. Culture medium was replaced with fresh one (1 mL) after 4 DIV. Chronic treatments involving para-aminoblebbistatin (pBleb, Axol) and Y-27632 (Sigma-Aldrich) were performed at the same time-point dissolving the molecules in the fresh-medium to achieve a 100 µM final concentration in petri-dishes. Unless differently stated, all the experiments were performed after 8–10 DIV. APTES-modified surfaces were prepared from standard glass coverslips and cells plated following the procedure described above. Slides were carefully cleaned with a freshly prepared solution of 37% HCl, 30% H_2O_2, H_2O

(1:1:5, by volume) for 5 min and subsequently washed with water, ethanol and acetone. After dried in an oven, substrates were immersed in a APTES solution (5% by volume in toluene, both chemicals from Sigma Aldrich) for 5 min. Before cell plating substrates were rinsed with toluene and acetone and let dry in an oven at 110 °C.

MβCD treatment

Plasma membrane cholesterol depletion was induced in cells developed above glass and 1 kPa PAA substrates using Methyl-beta-cyclodextrin (MβCD) following a procedure already described in one of our previous works (N. Pampaloni et al., 2018). Briefly, 8–10 DIV primary hippocampal cultures growth interfaced with glass and 1 kPa gel substrates were incubated for 1 hour with MβCD at a final concentration of 1 mM. Samples were maintained during this time at 37 °C in a cell incubator (5% CO_2, 95% RU). Immediately after incubation, neuronal PSCs were recorded by patch clamp electrophysiology experiments. Efficacy of cholesterol depletion was validated by Filipin staining at the end of the experimental session. MβCD was prepared in form of stock solution 100 mM dissolving the powder (C4555, from Sigma Aldrich) in deionized water (milliQ), filtered through at 0.2 µm filter, and stored at 4 °C.

Scanning electron microscopy

Hippocampal cells grown on glass control coverslips and PAA-hydrogels substrates were prepared for scanning electron microscopy (SEM) morphological evaluation following a procedure described in literature (N. P. Pampaloni et al., 2018). In brief, samples were fixed in 3% glutaraldehyde (Fluka, Italy) buffered with 0.1 M sodium cacodylate (pH 7.4) for 1 hour at room temperature. Subsequently, samples were progressively dehydrated in water/ethanol solutions at increasing levels of ethanol (50%, 75%, 95%, 99% and 100%, vol/vol, 5 minutes each, 4 °C) and let dry at 4 °C overnight. Before imaging, all samples were Au metalized in a metal sputter coater (Polaron SC7620) in order to avoid charge accumulation during SEM analysis. An accelerating voltage of about 5 keV was used for

sample visualization. SEM characterization was conducted on a Gemini SUPRA 40 SEM (Carl Zeiss NTS GmbH) collecting secondary electrons.

Immunofluorescence

Neuronal cells were fixed in 4% paraformaldehyde in phosphate buffer saline (PBS) solution for 20 minutes at room temperature (RT). Subsequently, samples were incubated for 1 hour in a PBS blocking solution containing 5% fetal bovine serum (FBS) and 0.03 % triton X-100 to permeabilize cell membranes (RT). After careful rinsing in PBS, primary antibodies were added for 1 hour and a half at RT and, after rising with PBS, secondary antibodies were added for 1 hour in dark conditions. Primary antibodies used in our investigations to highlight network morphology and evaluate its cellular composition were: rabbit polyclonal anti-β-tubulin III (T2200, Sigma-Aldrich, 1:250 dilution in blocking solution without Triton), mouse monoclonal anti-GFAP (G3893, Sigma-Aldrich, 1:250 dilution), guinea pig polyclonal anti-vesicular glutamate transporter 1 (AB5905, Sigma-Aldrich, dilution 1:2000), and monoclonal mouse anti-vinculin antibody (V9131, Sigma-Aldrich, 1:400 dilution). As secondary antibodies we have used: Alexa Fluor® 594 goat anti rabbit (A11037, Life Technologies, dilution 1:500 dilution in blocking solution without triton), Alexa Fluor® 488 goat anti mouse (A11029, Life Technologies, 1:500 dilution), Alexa Fluor® 488 goat anti guinea pig (A11073, Thermo Fisher, 1:500 dilution). Cell nuclei were highlighted by with 4',6-diamidino-2-phenylindole (DAPI, D1306, Thermo Fisher, 1:200 dilution) added simultaneously with secondary antibodies. Samples were carefully rinsed two times in PBS and once in milliQ H_2O, and sandwiched with a thin glass slide (L40357, thickness 1 (0.13–0.16 mm), 24 mm × 60 mm, MENZEL-GLÄSER GmbH (DE)) using a liquid mounting medium (Fluoromont-G™, BMS00-4958-02, Thermo Fisher), and then visualized under an inverted epifluorescence microscope (DM6000, Leica, Germany) using a 20× objective (Fluotar L, 0.5 N.A). At least 9 samples per condition from 3 independent culture series were analyzed, collecting 5 fields per sample. All image analyses were conducted using the open-

source program Fiji (Schindelin et al., 2012) and the Wolfram Mathematica technical computation suite (version 12.3.0, Wolfram Research, Inc., USA).

For V-Glut1 analysis, images were acquired with an inverted confocal microscope (Nikon D-Eclipse C1, Nikon Corporation) using a 60× oil immersion objective (PlanFluor λ, 1.4 N.A, Nikon Corporation). Three samples for each condition (glass control, and 50 kPa, 8 kPa, 1 kPa gels) from 3 independent experimental sections were analyzed. For every sample 5 fields (34.89 × 34.89 μm^2, 512 × 512 $pixels^2$) were randomly selected and acquired (11 stacked images at 500 nm Z-spacing) collecting collected. Volocity software (Volocity 3D Image Analysis Software, PerkinElmer, Massachusetts, USA) was used for offline analysis. In every analyzed field, V-Glut1 puncta volume (with volume <2 μm^3) has been normalized to the total β-tubulin III positive volume. Images were collected using identical acquisition settings through each condition. Data analysis was conducted using GraphPad Prism software (version 6.00) and the Wolfram Mathematica technical computation suite (version 12.3.0, Wolfram Research, Inc., USA).

Calcium phosphate transfection

To visualize the morphology and branching profile of isolated neuronal cells when developed interfaced to substrates of different stiffnesses, hippocampal primary neurons were transfected with an eGFP-expressing plasmid (kindly provided by Prof Antonio Mallamaci, SISSA) using a calcium phosphate transfection method (Sun et al., 2013; Thalhammer et al., 2017). Transfection was performed on neuronal cultures at 6 DIV. In brief, cells were rinsed with a pre-transfection medium composed of Neurobasal medium to which it has been added 1% Glutamax® and 1.32% of a 2.5M glucose solution, and subsequently treated with a 50% v/v HEPES-buffered saline water solution (HBS 2×, Invitrogen) containing 2.5 M $CaCl_2$ (5% v/v) and DNA (0.005% w/v). Cells were incubated for 30 minutes and then carefully washed with a post-transfection medium (Neurobasal medium supplemented with 1% Glutamax®,1.32% of a 2.5 M glucose solution and 3% B-27, all from Invitrogen). After keeping cultures in a cell incubator (37 °C, 5% CO_2, 95% RU) for 48–72 hours,

transfection outcomes were checked under a fluorescence microscope. In order to enhance and stabilize neuronal labelling, transfected cells were fixed in 4% paraformaldehyde in a PBS solution for 20 minutes at RT, incubated with blocking solution and then immunolabeled using an anti-GFP primary antibody produced in chicken (GTX13970, 1:800 dilution, GeneTex) and an Alexa Fluor® 488 anti-chicken secondary antibody produced in goat (A11039, 1:800 dilution, Thermo Fisher). Samples were sandwiched with a thin glass slide (L40357, thickness 1 (0.13–0.16 mm), 24 mm × 60 mm, MENZEL-GLÄSER GmbH (DE)) using a liquid mounting medium (Fluoromont-G™, Thermofisher), and then visualized using an inverted confocal microscope (Nikon D-Eclipse C1, Nikon Corporation). Branching profiles were evaluated performing a Sholl analysis (Binley et al., 2014) using the Sholl-analysis plugin available within the open-source program Fiji (Schindelin et al., 2012). Specifically, the number of intersections of neuronal branches with circles of progressively increasing radius and centered on cell soma were evaluated. Further image analysis, including the evaluation of cell areal extension and degree of circularity were conducted on the same set of data using the Wolfram Mathematica technical computation suite (version 12.3.0, Wolfram Research, Inc., USA). Specifically, the area and the ratio between minor/major axis (subtracted from one) of the minimum rectangular box containing the entire neuronal tree define cellular coverage and the degree of circularity.

Electrophysiology experiments

Neuronal network activity was measured performing patch clamp experiments in whole-cell configuration. Electrophysiological recordings were obtained using glass capillaries (OD= 1.5, ID=1.05, cod. 1408411, Hilgenberg) thermally pulled (model PC-10, Narishige Co., Japan) to a final aperture of about 1 µm and a measured resistance when in bath solution of 4–8 MΩ. The so obtained pipettes were filled with an intracellular solution composed of 120 mM K-gluconate, 20 mM KCl, 10 mM HEPES, 10 mM EGTA, 2 mM $MgCl_2$, 2 mM Na_2ATP (all from Sigma, pH 7.3; in average 300 mOsm). The extracellular solution used during the electrophysiological experiments was instead

composed of 150 mM NaCl, 4 mM KCl, 2 mM $CaCl_2$, 1 mM $MgCl_2$, 10 mM HEPES, 10 mM glucose (all Sigma, pH 7.4, in average 320 mOsm). All recordings were performed at room temperature under continuous perfusion of the chamber with fresh extracellular solution (5 mL/min). Samples were placed in a chamber mounted on an inverted microscope. All the recordings of the synaptic activity were collected using a Patch Clamp L/M – EPC 7 patch amplifier (HEKA Electronic, USA) and digitized using a Digidata 1322A (Molecular Devices LLC, US) at 10 kHz sampling frequency using the pClamp 8.2 acquisition software (Molecular Devices LLC, USA). Spontaneous postsynaptic currents (PSCs) were measured by clamping cells at a holding membrane potential of –56 mV (not corrected for the liquid junction potential, calculated to be 14 mV at 20 °C). Miniatures postsynaptic currents (mPSCs) were recorded by application of 1 µM Tetrodotoxin (TTX, Latoxan), a fast Na^+ channels blocker, through the perfusion circuit. All recorded synaptic events were analyzed off-line with the AxoGraph (version 1.7.0, Axon Scientific, US) analysis software. Specifically, for each recording all detected events were averaged evaluating the peak amplitude and kinetic properties of the resulting mean current. Two templates, based on the different kinetic parameters (rise and decay time), were built to further distinguish between glutamate AMPA-receptor and $GABA_A$-receptor mediated postsynaptic currents. The kinetic parameters used were 0.1 ms rise-time and 3 or 20 ms decay time constants (τ) for fast and slow events, respectively. Passive cell-membrane properties were evaluated by applying a −5 mV voltage step for 10 ms repeatedly for 80 times and analyzing the average cell response in terms of current using Clampfit (pClamp 10.3, Molecular Devices LLC, US). Uncompensated series resistance was ≤ 11 MΩ.

Regarding current clamp experiments, voltage traces were collected using a Multiclamp 700B patch-clamp amplifier (Axon CNS, Molecular Devices) and digitized using a Digidata 1440 (Axon CNS, Molecular Devices) at 10 kHz through the pClamp 10.2 acquisition software (Molecular Devices LLC, US). Spontaneous firing activity was measured in every condition holding neurons at –60 mV for each recording. Bridge balance was adjusted accordingly. Traces were analyzed off-line using the pClamp software suite detecting action potentials (APs) by defining an amplitude threshold limit.

Single cell excitability was evaluated on glass and 1 kPa interfaced neurons, the most stiff and compliant substrates used, respectively. Cells were held at –60 mV and depolarized with increasing steps of current (from 0 to 200 pA at 10 pA increments).

Atomic Force Microscopy

PAA substrates and cellular stiffnesses were evaluated by means of atomic force microscopy (AFM) force-indentation experiments. For this purpose, AFM measurements were carried out at room temperature in liquid environment (PBS). Stiffness assessment was conducted taking advantage of the force spectroscopy capabilities integrated in the AFM used for such characterization (JPK NanoWizard® 3, Bruker Nano Surfaces, US). Briefly, during experiments the displacement of an AFM cantilever of calibrated elastic constant is measured while it is pressed against a surface. Data are then converted in a force vs indentation curve, the slop of which is proportional to substrate stiffness. Tip-less cantilevers with a nominal elastic constant of 0.03 nN/nm and a resonance frequency of 10 kHz (CSG11-B/tipless, NT-MDT Co., Russia) were used. A glass bead (8.0±0.4 µm in diameter, No. 9008, Duke Standards™, Fremont CA, USA) was glued at the end of the cantilever by means of a UV-curable glue (Norland Optical Adhesive 61, Norland Products, Inc., USA). Cantilevers' effective elastic constant was measured by means of the thermal method (Lévy & Maaloum, 2002) integrated into the AFM control software.

Force spectroscopy measurements on pristine PAA gels were performed at a constant speed of 2.5 µm/s and triggered to a maximum surface indentation of about 500 nm. Neuronal cell stiffness in networks grown interfaced with substrates of different stiffness (glass and PAA gels, 8–9 DIV) or treated with drugs able to interfere with cellular mechanotransduction (pBleb and Y-27632, 8–10 DIV) was evaluated after having fixed cells in 4% PFA in PBS and made visible their nuclei by NeuN staining. Briefly, cells were incubated with mouse antineuronal nuclei primary antibody (NeuN, AB_2298772, Millipore; used at 1:100 dilution in 5% FBS PBS). After washing in PBS, sections were incubated for 15 minutes with a goat secondary anti-rabbit antibody coupled to an Alexa Fluor®

488 fluorophore (AB_2534088, Thermo Fisher Scientific; used at 1:500 dilution in PBS) for 15 minutes at RT. After careful washing samples with fresh PBS, cells were immediately mounted on the AFM microscope stage and measured. Although cell fixation is known to increase the cell stiffness, it is possible to use this value for a relative comparison of cell mechanical adaptation on the different substrates (Grimm et al., 2014; Jiang et al., 2011; Ulloa et al., 2021) or as reference value to determine the concentrations of drugs to induce a mechanoadaptation similar to the one induced by a compliant substrate. Indentation was conducted by manually placing the cantilever tip above the DAPI-stained cell nucleus. This strategy ensures high measurement reproducibility. Force spectroscopy measurements on cells were performed at a constant speed (2.5 µm/s) and triggered to a maximum sample indentation of 5 nN or to a maximum indentation of 250 nm, representing the 5% of the average maximum cell height (data not shown). Such maximum indentation value avoided any contribution from the underneath substrate to the measured cell stiffness minimizing, at the same time, its susceptibility to cell nucleus stiffness. Substrate or cell stiffnesses were determined using the JPKSPM Data Processing® software by fitting the obtained force-indentation curves with the integrated Hertzian model for a spherical indenter (Sneddon, 1965). PAA substrate stiffness was evaluated averaging stiffness values from 30 randomly-executed measurements per condition (from 3 different batches of substrates). Cell stiffness was obtained averaging values measured from about 100 cells per condition from 3 independent experiments. Neuronal stiffness was described in terms of Young's Modulus (E) and expressed in kPa.

Filipin staining

Cholesterol content of cells' plasma membrane was evaluated using Filipin, a naturally fluorescent polyene antibiotic selectively binding to sterols (Tashiro et al., 2021). After 8–9 DIV, cell cultures were fixed in 4% paraformaldehyde in PBS solution for 20 minutes at RT. Subsequently, samples were carefully rinsed with PBS and incubated for 10 minutes at RT with a 20 mM glycine solution in PBS to quench PFA. Cells were incubated with Filipin (f-9765, Sigma-Aldrich; 1:20 dilution in PBS

from a 1 mg/mL DMSO stock solution) for 2 hours at RT. After rising with PBS, samples were sandwiched with a thin glass coverslip (L40357, thickness 1 (0.13–0.16 mm), 24 mm × 60 mm, MENZEL-GLÄSER GmbH (DE)) using a mounting medium (Fluoromont-G™, Thermofisher) for subsequent analysis. Samples were visualized using an epifluorescence microscope (DM6000, Leica, Germany) endowed with a 100x oil immersion objective (HCX PL FLUOTAR 100×/1.30 OI, Leica GmbH, DE).

Images (148×110 μm^2, 1392×1040 $pixels^2$) were acquired using always the same settings of illumination, CCD (Q Imaging EXI Blue) exposure and gain across the different conditions in order to make possible a direct comparison. From 70 to 210 images per condition (from three independent experimental sessions) were randomly collected. Filipin quantification was performed using an ad-hoc procedure within the Wolfram Mathematica technical computation suite (version 12.3.0, Wolfram Research, Inc., USA). Briefly, images were binarized and the median intensity value evaluated for all Filipin-positive regions. The fluorescence signal was subsequently normalized by subtracting the background fluorescence.

Total internal reflection fluorescence (TIRF)

TIRF experiments were performed to evaluate the number and distribution of focal adhesions (FAs) in hippocampal cultures grown above glass and treated with pBleb and Y-27632. Cellular samples were fixed with 4% PFA for 30 minutes at room temperature (RT). After fixation, samples were incubated for 1 hour in a PBS blocking solution containing 5% fetal bovine serum (FBS) and 0.03 % triton X-100 to permeabilize cell membranes (RT). Subsequently, samples were incubated for 1 hours and a half at RT with a monoclonal mouse anti-vinculin antibody (V9131, Sigma-Aldrich, 1:400 dilution in blocking solution without triton) and a rabbit polyclonal anti-β-tubulin III (T2200, Sigma-Aldrich, 1:250 dilution in blocking solution without triton). Samples, washed with PBS, were subsequently incubated for 1 hours with a goat anti-mouse secondary antibody coupled to Alexa Fluor® 488 (A11029, Life Technologies,1:500 dilution) and Alexa Fluor® 594 goat anti-rabbit

secondary antibody (A11037, Life Technologies, 1:500 dilution), diluted in blocking solution without triton. Samples were sandwiched with a thin glass slide (L40357, thickness 1 (0.13–0.16 mm), 24 mm × 60 mm, MENZEL-GLÄSER GmbH (DE)) using a liquid mounting medium (Fluoromont-G™, Thermo Fisher), and then visualized using an inverted epi-fluorescence microscope equipped with a TIRF module (Nikon Eclipse TiU, Nikon Corporation). Images were acquired in total reflection condition using a high aperture oil-immersion objective (CFI Apochromat TIRF 100×C Oil, Nikon Corporation) and a 488 nm laser (OBIS 488 LS; Coherent, Inc., Santa Clara, CA, USA) at a power sufficient to avoiding photo-bleaching. In our conditions the penetration depth of the evanescent wave was about 150 nm. Samples were visualized using a CCD camera (DS-Qi1, Nikon Corporation) acquiring for every field of view a TIRF image of the vinculin staining and a conventional fluorescence image of β-tubulin III positive regions (426×340 μm^2, 1280×1024 $pixels^2$). FAs were quantified as vinculin-positive puncta exploiting a procedure developed with the Wolfram Mathematica software (version 12.3.0, Wolfram Research, Inc., USA). Briefly, vinculin signal was analyzed exclusively in β-tubulin positive regions. After image binarization, puncta were highlighted using a morphological-matching procedure based on disk of increasing radius (from about 300 nm to 3 μm) and segmented for further analysis. Specifically, for every detected punctum the surface and mean intensity were computed. FAs density was evaluated as the ratio between the total number of puncta and the β-tubulin positive total area for every field of view.

Statistical information

All the described experiments were repeated at least three times using cell cultures from independent experimental sessions. All statistical analysis was performed using the software Prism (version 6.0, GraphPad Software), Igor Pro (version 6.37, WaveMetrics), and the Wolfram Mathematica suite (version 12.1.0, Wolfram Research, Inc., USA). Data distribution was evaluated by Shapiro Wilk test of normality and, based on the result, a bar chart or a box plot was chosen to graphically represent data. Bar charts show mean ± standard deviation (SD). Box plots are plotted as median with boxes

spanning from the 25th (1st quartile, Q1) to the 75th (3rd quartile, Q3) percentiles, with whiskers representing the 5th and 95th percentiles. Statistics between two independent samples were performed with t-test when the distribution was normal. Statistical differences between the three or more conditions (i.e., glass, 50 kPa, 8 kPa, 1 kPa gels, or glass, pBleb, Y-27632 treated samples) were evaluated through a one-way ANOVA followed by a Dunnet post-test. Comparison among multiple independent variables on one continuous dependent variable (i.e., substrate vs MβCD treatment contribution in PSC amplitude and frequency) were instead evaluated through a two-way ANOVA analysis followed by a Bonferroni post-test. The normality distribution of data was evaluated performing Shapiro-Wilk Test. For parametric data Student's t-test for two groups comparisons and one-way ANOVA followed by Tukey's multiple comparison test were performed. For non-parametric data, Mann Whitney for two groups comparison test and Kruskal-Wallis followed by Dunn's multiple comparison test and were used. For the sake of clarity, all the values reported in the text are expressed as mean ± standard deviation (SD). Statistical significance was determined at $P < 0.05$, unless otherwise indicated. Significance was graphically indicated as follows: $*P < 0.05$, $**P < 0.01$, $***P < 0.001$.

References

Al-Rekabi, Z. & Contera, S. (2018). Multifrequency AFM reveals lipid membrane mechanical properties and the effect of cholesterol in modulating viscoelasticity. *Proceedings of the National Academy of Sciences of the United States of America*, *115*(11), 2658–2663. https://doi.org/10.1073/pnas.1719065115

Alonso, J. L. & Goldmann, W. H. (2016). Cellular mechanotransduction. *AIMS Biophysics*, *3*(1), 50–62. https://doi.org/10.3934/biophy.2016.1.50

Arani, A., Murphy, M. C., Glaser, K. J., Manduca, A., Lake, D. S., Kruse, S. A., Jack, C. R., Ehman, R. L. & Huston, J. (2015). Measuring the effects of aging and sex on regional brain stiffness with MR elastography in healthy older adults. *NeuroImage*, *111*, 59–64. https://doi.org/10.1016/j.neuroimage.2015.02.016

Assmann, M. . & Lenz, P. (2014). Membrane tension influences the spike propagation between voltage-gated ion channel clusters of excitable membranes. *Physical Biology*, *115504*.

Barnes, J. M., Przybyla, L. & Weaver, V. M. (2017). Tissue mechanics regulate brain development, homeostasis and disease. *Journal of Cell Science*, *130*(1), 71–82. https://doi.org/10.1242/jcs.191742

Binley, K. E., Ng, W. S., Tribble, J. R., Song, B. & Morgan, J. E. (2014). Sholl analysis: A quantitative comparison of semi-automated methods. *Journal of Neuroscience Methods*, *225*, 65–70.

https://doi.org/10.1016/j.jneumeth.2014.01.017

Budday, S., Ovaert, T. C., Holzapfel, G. A., Steinmann, P. & Kuhl, E. (2019). Fifty Shades of Brain: A Review on the Mechanical Testing and Modeling of Brain Tissue. In *Archives of Computational Methods in Engineering* (Vol. 27, Issue 4). Springer Netherlands. https://doi.org/10.1007/s11831-019-09352-w

Bukiya, A. N., Belani, J. D., Rychnovsky, S. & Dopico, A. M. (2010). *Specificity of cholesterol and analogs to modulate BK channels points to direct sterol – channel protein interactions*. 93–110. https://doi.org/10.1085/jgp.201010519

Cellot, G., Cilia, E., Cipollone, S., Rancic, V., Sucapane, A., Giordani, S., Gambazzi, L., Markram, H., Grandolfo, M., Scaini, D., Gelain, F., Casalis, L., Prato, M., Giugliano, M. & Ballerini, L. (2009). Carbon nanotubes might improve neuronal performance by favouring electrical shortcuts. *Nature Nanotechnology*, *4*(2), 126–133. https://doi.org/10.1038/nnano.2008.374

Cellot, G., Toma, F. M., Varley, Z. K., Laishram, J., Villari, A., Quintana, M., Cipollone, S., Prato, M. & Ballerini, L. (2011). Carbon nanotube scaffolds tune synaptic strength in cultured neural circuits: Novel frontiers in nanomaterial-tissaue interactions. *Journal of Neuroscience*, *31*(36), 12945–12953. https://doi.org/10.1523/JNEUROSCI.1332-11.2011

Christian, A. E., Haynes, M. P., Phillips, M. C. & Rothblat, G. H. (1997). Use of cyclodextrins for manipulating cellular cholesterol content. *Journal Lipid Research*, *38*(11), 2264–2272. https://doi.org/10.1016/S0022-2275(20)34940-3

Colombo, E. & Farina, C. (2016). Astrocytes: Key Regulators of Neuroinflammation. *Trends in Immunology*, *37*(9), 608–620. https://doi.org/10.1016/j.it.2016.06.006

Cooper, J. G., Sicard, D., Bs, S. S., Gulden, S. Van & Kessler, J. A. (2019). *Spinal cord injury results in chronic mechanical stiffening*. 1–48. https://doi.org/10.1089/neu.2019.6540

Cozzolino, A. M., Noce, V., Battistelli, C., Marchetti, A., Grassi, G., Cicchini, C., Tripodi, M. & Amicone, L. (2016). Modulating the Substrate Stiffness to Manipulate Differentiation of Resident Liver Stem Cells and to Improve the Differentiation State of Hepatocytes. *Stem Cells International*, *2016*. https://doi.org/10.1155/2016/5481493

Dupont, S., Morsut, L., Aragona, M., Enzo, E., Giulitti, S., Cordenonsi, M., Zanconato, F., Le Digabel, J., Forcato, M., Bicciato, S., Elvassore, N. & Piccolo, S. (2011). Role of YAP/TAZ in mechanotransduction. *Nature*, *474*(7350), 179–184. https://doi.org/10.1038/nature10137

Engler, A. J., Sen, S., Sweeney, H. L. & Discher, D. E. (2006). Matrix Elasticity Directs Stem Cell Lineage Specification. *Cell*, *126*(4), 677–689. https://doi.org/10.1016/j.cell.2006.06.044

Fabbro, A., Villari, A., Laishram, J., Scaini, D., Toma, F. M., Turco, A., Prato, M. & Ballerini, L. (2012). *Spinal Cord Explants Use Carbon Nanotube Interfaces To Enhance Neurite Outgrowth and To Fortify Synaptic Inputs*. *3*, 2041–2055.

Furlan, F., Taccola, G., Grandolfo, M., Guasti, L., Arcangeli, A., Nistri, A. & Ballerini, L. (2007). ERG conductance expression modulates the excitability of ventral horn GABAergic interneurons that control rhythmic oscillations in the developing mouse spinal cord. *Journal of Neuroscience*, *27*(4), 919–928. https://doi.org/10.1523/JNEUROSCI.4035-06.2007

Georges, P. C., Miller, W. J., Meaney, D. F., Sawyer, E. S. & Janmey, P. A. (2006). Matrices with compliance comparable to that of brain tissue select neuronal over glial growth in mixed cortical cultures. *Biophysical Journal*, *90*(8), 3012–3018. https://doi.org/10.1529/biophysj.105.073114

González-Reyes, R. E., Nava-Mesa, M. O., Vargas-Sánchez, K., Ariza-Salamanca, D. & Mora-Muñoz, L. (2017). Involvement of astrocytes in Alzheimer's disease from a neuroinflammatory and oxidative stress perspective. *Frontiers in Molecular Neuroscience*, *10*(December), 1–20. https://doi.org/10.3389/fnmol.2017.00427

Grimm, K. B., Oberleithner, H. & Fels, J. (2014). Fixed endothelial cells exhibit physiologically relevant nanomechanics of the cortical actin web. *Nanotechnology*, *25*(21). https://doi.org/10.1088/0957-4484/25/21/215101

Guo, J., Chi, S., Xu, H., Jin, G. & Qi, Z. (2009). *Effects of cholesterol levels on the excitability of rat hippocampal neurons*. *7688*. https://doi.org/10.1080/09687680701805541

Haase, K. & Pelling, A. E. (2015). Investigating cell mechanics with atomic force microscopy. *Journal of the Royal Society Interface*, *12*(104). https://doi.org/10.1098/rsif.2014.0970

Handorf, A. M., Zhou, Y., Halanski, M. A. & Li, W. J. (2015). Tissue stiffness dictates development, homeostasis, and disease progression. *Organogenesis*, *11*(1), 1–15. https://doi.org/10.1080/15476278.2015.1019687

Hong, Z., Staiculescu, M. C., Hampel, P., Levitan, I., Forgacs, G. & Monasky, M. M. (2012). *How cholesterol regulates endothelial biomechanics*. *3*(November), 1–6. https://doi.org/10.3389/fphys.2012.00426

Humphrey, J. D., Dufresne, E. R., Schwartz, M. A., Haven, N., Haven, N., Haven, N. & Haven, N. (2015). *Mechanotransduction and extracellular matrix homeostasis*. *15*(12), 802–812. https://doi.org/10.1038/nrm3896.Mechanotransduction

Isokawa, M. (1997). Membrane time constant as a tool to assess cell degeneration. *Brain Research Protocols*, *1*(2), 114–116. https://doi.org/10.1016/S1385-299X(96)00016-5

Iwashita, M., Ohta, H., Fujisawa, T., Cho, M. & Ikeya, M. (2019). Brain-stiffness-mimicking tilapia collagen gel promotes the induction of dorsal cortical neurons from human pluripotent stem cells. *Scientific Reports*, *December 2018*, 1–17. https://doi.org/10.1038/s41598-018-38395-5

Jiang, F., DC, L., F, H. & NA, L. (2011). Probing Mechanical Adaptation of Neurite Outgrowth on a Hydrogel Material Using Atomic Force Microscopy. *Annals of Biomedical Engineering*, *39*(2), 706–713. https://doi.org/10.1007/s10439-010-0194-0.Probing

Kaunas, R., Nguyen, P., Usami, S. & Chien, S. (2005). *Cooperative effects of Rho and mechanical stretch on stress fiber organization*. *102*(44).

Kawada, N., Seki, S., Kuroki, T. & Kaneda, K. (1999). *ROCK Inhibitor Y-27632 Attenuates Stellate Cell Contraction and Portal Pressure Increase Induced by Endothelin-1*. *300*, 296–300.

Lampi, M. C. & Reinhart-King, C. A. (2018). Targeting extracellular matrix stiffness to attenuate disease: From molecular mechanisms to clinical trials. *Science Translational Medicine*, *10*(422), 1–15. https://doi.org/10.1126/scitranslmed.aao0475

Lantoine, J., Grevesse, T., Villers, A., Delhaye, G., Mestdagh, C., Versaevel, M., Mohammed, D., Bruyère, C., Alaimo, L., Lacour, S. P., Ris, L. & Gabriele, S. (2016). Matrix stiffness modulates formation and activity of neuronal networks of controlled architectures. *Biomaterials*, *89*, 14–24. https://doi.org/10.1016/j.biomaterials.2016.02.041

Levitan, I., Christian, A. E., Tulenko, T. N. & Rothblat, G. H. (2000). *Membrane Cholesterol Content Modulates Activation of Volume-regulated Anion Current in Bovine Endothelial Cells*. *115*(April).

Lévy, R. & Maaloum, M. (2002). Measuring the spring constant of atomic force microscope cantilevers: Thermal fluctuations and other methods. *Nanotechnology*, *13*(1), 33–37. https://doi.org/10.1088/0957-4484/13/1/307

Li, S. W. Æ. X., Liang, Æ. C. C. Æ. Y., David, J. P. Æ. & Ma, G. W. Æ. H. (2007). *Membrane Tension Modulates the Effects of Apical Cholesterol on the Renal Epithelial Sodium Channel*. 21–31. https://doi.org/10.1007/s00232-007-9071-7

Lovat, V., Pantarotto, D., Lagostena, L., Cacciari, B., Grandolfo, M., Righi, M., Spalluto, G., Prato, M. & Ballerini, L. (2005). Carbon nanotube substrates boost neuronal electrical signaling. *Nano Letters*, *5*(6), 1107–1110. https://doi.org/10.1021/nl050637m

Mailman, T., Hariharan, M. & Karten, B. (2011). Inhibition of neuronal cholesterol biosynthesis with lovastatin leads to impaired synaptic vesicle release even in the presence of lipoproteins or geranylgeraniol. *Journal of Neurochemistry*, *119*(5), 1002–1015. https://doi.org/10.1111/j.1471-4159.2011.07474.x

Marquer, C., Laine, J., Dauphinot, L., Hanbouch, L., Lemercier-neuillet, C., Pierrot, N., Bossers, K., Le, M., Corlier, F., Benstaali, C., Saudou, F., Thinakaran, G., Cartier, N., Octave, J., Duyckaerts, C. & Potier, M. (2014). *Increasing membrane cholesterol of neurons in culture recapitulates Alzheimer ' s disease early phenotypes*. 1–13.

Martino, F., Perestrelo, A. R., Vinarský, V., Pagliari, S. & Forte, G. (2018). Cellular mechanotransduction: From tension to function. *Frontiers in Physiology*, *9*(JUL), 1–21. https://doi.org/10.3389/fphys.2018.00824

Milescu, L. S., Bean, B. P. & Smith, J. C. (2010). Isolation of somatic Na+ currents by selective inactivation of axonal channels with a voltage prepulse. *Journal of Neuroscience*, *30*(22), 7740–7748. https://doi.org/10.1523/JNEUROSCI.6136-09.2010

Murphy, M. C., Jones, D. T., Jack, C. R., Glaser, K. J., Senjem, M. L., Manduca, A., Felmlee, J. P., Carter, R. E., Ehman, R. L. & Huston, J. (2016). Regional brain stiffness changes across the Alzheimer's disease spectrum. *NeuroImage: Clinical*, *10*, 283–290. https://doi.org/10.1016/j.nicl.2015.12.007

Oakes, P. W., Bidone, T. C., Beckham, Y., Skeeters, A. V & Ramirez-san, G. R. (2018). *Lamellipodium is a myosin-independent mechanosensor*. https://doi.org/10.1073/pnas.1715869115

Pampaloni, N. P., Lottner, M., Giugliano, M., Matruglio, A., D'Amico, F., Prato, M., Garrido, J. A., Ballerini, L. & Scaini, D. (2018). Single-layer graphene modulates neuronal communication and augments membrane ion currents. *Nature Nanotechnology*, *13*(8), 755–764. https://doi.org/10.1038/s41565-018-0163-6

Pampaloni, N., Scaini, D., Perissinotto, F., Bosi, S., Prato, M. & Ballerini, L. (2018). Sculpting neurotransmission during synaptic development by 2D nanostructured interfaces. *Nanomedicine: Nanotechnology, Biology, and Medicine*, *14*(7), 2521–2532. https://doi.org/10.1016/j.nano.2017.01.020

Pelham, R. J. & Wang, Y. L. (1997). Cell locomotion and focal adhesions are regulated by substrate flexibility. *Proceedings of the National Academy of Sciences of the United States of America*, *94*(25), 13661–13665. https://doi.org/10.1073/pnas.94.25.13661

Previtera, M. L., Langhammer, C. G. & Firestein, B. L. (2010). Effects of substrate stiffness and cell density on primary hippocampal cultures. *Journal of Bioscience and Bioengineering*, *110*(4), 459–470. https://doi.org/10.1016/j.jbiosc.2010.04.004

Raastad, M., Storm, J. F. & Andersen, P. (1992). Putative Single Quantum and Single Fibre Excitatory

Postsynaptic Currents Show Similar Amplitude Range and Variability in Rat Hippocampal Slices. *European Journal of Neuroscience*, *4*(1), 113–117. https://doi.org/10.1111/j.1460-9568.1992.tb00114.x

Rago, I., Rauti, R., Bevilacqua, M., Calaresu, I., Pozzato, A., Cibinel, M., Dalmiglio, M., Tavagnacco, C., Goldoni, A. & Scaini, D. (2019). Carbon Nanotubes, Directly Grown on Supporting Surfaces, Improve Neuronal Activity in Hippocampal Neuronal Networks. *Advanced Biosystems*, *3*(5), 1–13. https://doi.org/10.1002/adbi.201800286

Schindelin, J., Arganda-Carreras, I., Frise, E., Kaynig, V., Longair, M., Pietzsch, T., Preibisch, S., Rueden, C., Saalfeld, S., Schmid, B., Tinevez, J. Y., White, D. J., Hartenstein, V., Eliceiri, K., Tomancak, P. & Cardona, A. (2012). Fiji: An open-source platform for biological-image analysis. *Nature Methods*, *9*(7), 676–682. https://doi.org/10.1038/nmeth.2019

Serna-Márquez, N., Rodríguez-Hernández, A., Ayala-Reyes, M., Martínez-Hernández, L. O., Peña-Rico, M. Á., Carretero-Ortega, J., Hautefeuille, M. & Vázquez-Victorio, G. (2020). Fibrillar collagen type I participates in the survival and aggregation of primary hepatocytes cultured on soft hydrogels. *Biomimetics*, *5*(2). https://doi.org/10.3390/BIOMIMETICS5020030

Shellard A, Mayor R. Durotaxis: The Hard Path from In Vitro to In Vivo. Dev Cell. 2021 Jan 25;56(2):227-239. doi: 10.1016/j.devcel.2020.11.019. Epub 2020 Dec 7. PMID: 33290722.

Siedlik, M. J., Varner, V. D., Nelson, C. M. & Engineering, B. (2017). *HHS Public Access*. 4–12. https://doi.org/10.1016/j.ymeth.2015.08.019.Pushing

Simon, C., Caorsi, V. & Sykes, C. (2018). *Interplay between membrane tension and the actin cytoskeleton determines shape changes Interplay between membrane tension and the actin cytoskeleton determines shape changes*.

Sneddon, I. N. (1965). The relation between load and penetration in the axisymmetric boussinesq problem for a punch of arbitrary profile. *International Journal of Engineering Science*, *3*(1), 47–57. https://doi.org/10.1016/0020-7225(65)90019-4

Sun, M., Bernard, L. P., Dibona, V. L., Wu, Q. & Zhang, H. (2013). *Calcium Phosphate Transfection of Primary Hippocampal Neurons*. *November*, 1–7. https://doi.org/10.3791/50808

Tanaka, A., Fujii, Y., Kasai, N., Okajima, T. & Nakashima, H. (2018). Regulation of neuritogenesis in hippocampal neurons using stiffness of extracellular microenvironment. *PLoS ONE*, *13*(2), 1–16. https://doi.org/10.1371/journal.pone.0191928

Tashiro, Y., Yamazaki, T., Shimada, Y., Ohno-iwashita, Y. & Okamoto, K. (2021). *Axon-dominant localization of cell-surface cholesterol in cultured hippocampal neurons and its disappearance in Niemann – Pick type C model cells*. *20*, 2015–2021. https://doi.org/10.1111/j.1460-9568.2004.03677.x

Tee, S., Fu, J., Chen, C. S. & Janmey, P. A. (2011). Cell Shape and Substrate Rigidity Both Regulate Cell Stiffness. *Biophysj*, *100*(5), L25–L27. https://doi.org/10.1016/j.bpj.2010.12.3744

Thalhammer, A., Contestabile, A., Ermolyuk, Y. S., Soong, T. W., Goda, Y., Cingolani, L. A., Thalhammer, A., Contestabile, A., Ermolyuk, Y. S., Ng, T., Volynski, K. E. & Soong, T. W. (2017). Alternative Splicing of P / Q-Type Ca 2 + Channels Shapes Presynaptic Plasticity Article Alternative Splicing of P / Q-Type Ca 2 + Channels Shapes Presynaptic Plasticity. *CellReports*, *20*(2), 333–343. https://doi.org/10.1016/j.celrep.2017.06.055

Ulloa, L. S., Perissinotto, F., Rago, I., Goldoni, A., Santoro, R., Pesce, M., Casalis, L. & Scaini, D. (2021). *Carbon Nanotubes Substrates Alleviate Pro-Calcific Evolution in Porcine Valve Interstitial Cells*. 1–20.

Urbanski, M. M., Brendel, M. B. & Melendez-Vasquez, C. V. (2019). Acute and chronic demyelinated CNS lesions exhibit opposite elastic properties. *Scientific Reports*, *9*(1), 1–13. https://doi.org/10.1038/s41598-018-37745-7

Valente, P., Lignani, G., Medrihan, L., Bosco, F., Contestabile, A., Lippiello, P., Ferrea, E., Schachner, M., Benfenati, F., Giovedì, S. & Baldelli, P. (2016). Cell adhesion molecule L1 contributes to neuronal excitability regulating the function of voltage-gated Na+ channels. *Journal of Cell Science*, *129*(9), 1878–1891. https://doi.org/10.1242/jcs.182089

Várkuti, B. H., Képiró, M., Horváth, I. Á. & Végne, L. (2016). A highly soluble , non-phototoxic , non-fluorescent blebbistatin derivative. *Nature Publishing Group*, *May*, 2–11. https://doi.org/10.1038/srep26141

Wasser, C. R., Ertunc, M., Liu, X. & Kavalali, E. T. (2007). Cholesterol-dependent balance between evoked and spontaneous synaptic vesicle recycling. *Journal of Physiology*, *579*(2), 413–429. https://doi.org/10.1113/jphysiol.2006.123133

Wen, Y. Q., Gao, X., Wang, A., Yang, Y., Liu, S., Yu, Z., Song, G. B. & Zhao, H. C. (2018). Substrate stiffness affects neural network activity in an extracellular matrix proteins dependent manner. *Colloids and Surfaces B: Biointerfaces*, *170*, 729–735. https://doi.org/10.1016/j.colsurfb.2018.03.042

Zhang, C., Tan, Y., Feng, J., Huang, C., Liu, B., Fan, Z., Xu, B. & Lu, T. (2020). *Exploration of the E ff ects of Substrate Sti ff ness on Biological Responses of Neural Cells and Their Mechanisms*. https://doi.org/10.1021/acsomega.0c04279

Zhang, Q. Y., Zhang, Y. Y., Xie, J., Li, C. X., Chen, W. Y., Liu, B. L., Wu, X. A., Li, S. N., Huo, B., Jiang, L. H. & Zhao, H. C. (2014). Stiff substrates enhance cultured neuronal network activity. *Scientific Reports*, *4*, 12–15. https://doi.org/10.1038/srep06215

Zidovetzki, R. & Levitan, I. (2007). *Use of cyclodextrins to manipulate plasma membrane cholesterol content : Evidence , misconceptions and control strategies*. *1768*, 1311–1324. https://doi.org/10.1016/j.bbamem.2007.03.026

Acknowledgements

We are grateful to M. Grandolfo for microscopy assistance, L. Casalis for the support in setting up TIRF experiments, M. Lazzarino for the guide in performing AFM experiments and analyzing the resulting data, L. Cingolani and F. Cesca for the help in setting and conducting calcium phosphate transfections, and to Prof A. Malamacci to have kindly provided us the eGFP-expressing plasmid. This work was funded by the European Union's Horizon 2020 Research and Innovation Program under the Grant Agreement 737116 (to L.B). D.S. acknowledges the support of the European Union's Horizon 2020 research and innovation program under the Marie Skłodowska-Curie grant agreement no. 838902.

Ethics declarations

Animal use ethical statement

All animal procedures were conducted in accordance with the National Institutes of Health and with international and institutional standards for the care and use of animals in research. All experiments were performed in agreement with the Italian law (decree 26/14) and the European Union (EU) guidelines (2007/526/CE and 2010/63/UE) and were approved by the local authority veterinary service and by our institutional (SISSA-ISAS) ethical committee. All efforts were made to minimize animal suffering and to reduce the number of animals necessary to accomplish our studies. Animal use was approved by the Italian Ministry of Health.

Competing interests

The authors declare no competing interest for all content of the work.

Supplementary Information

Fig. S1: Evaluation of contribution of chemical groups exposed on culture surface.

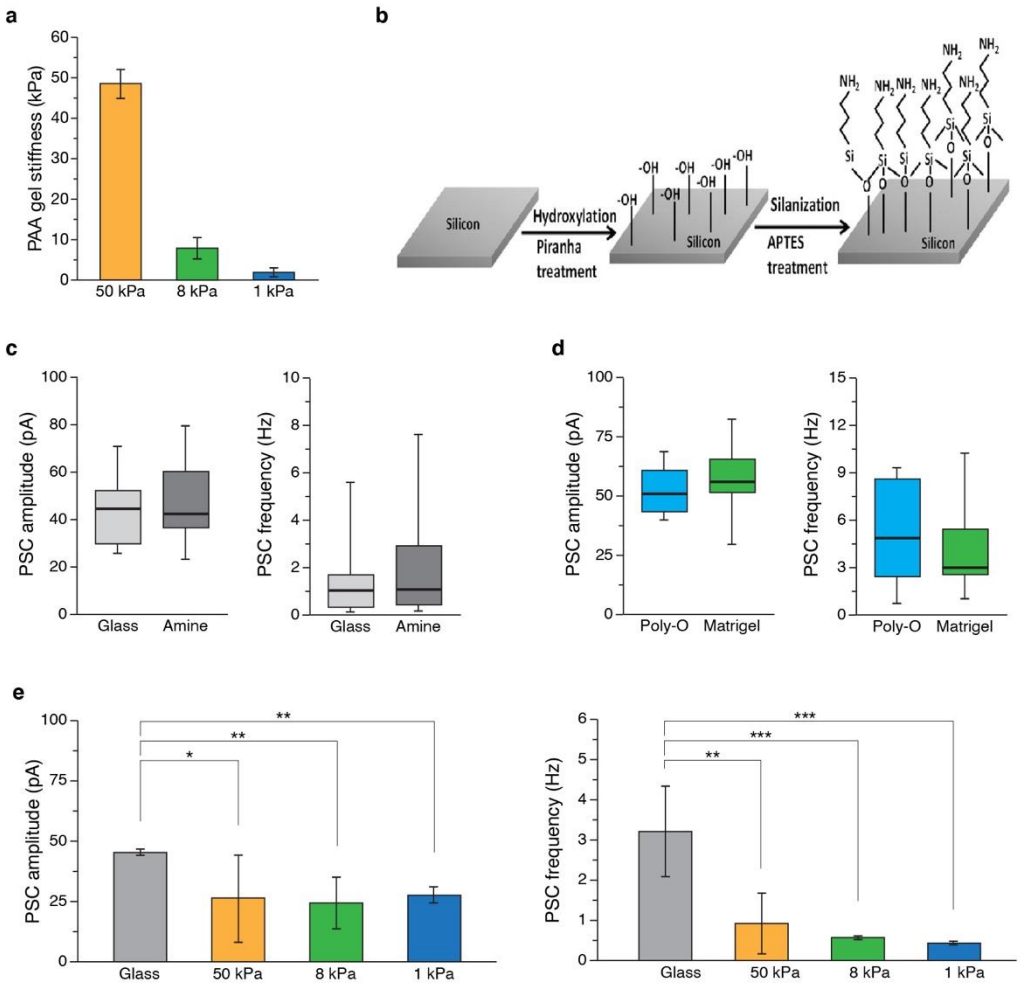

a *A bar plot showing the stiffness values for the three PAA gels as revealed by atomic force microscopy experiments.* ***b*** *Sketch of glass surface functionalization with 3-Aminopropyltriethoxysilane (APTES) mimicking the amino functional groups eventually present on PAA gels.* ***c*** *Box plots of amplitude (on the left) and frequency (on the right) of PSCs recorded on glass and APTES interfaced neurons do not reveal any significant effects induced by the chemical modification of the surface.* ***d*** *Box plots revealing no significant differences in terms of amplitude and frequency of PSCs between Matrigel® and polyornithine treated glass substrates.* ***e*** *Bar plots illustrating similar variations in hippocampal neurons PSCs' amplitudes and frequencies when PAA-substrates were coated with collagen type I. Kruskal-Wallis followed by Dunn's multiple comparison test was performed, * $p<0.05$; ** $p<0.01$; *** $p<0.001$.*

Fig. S2: The cell excitability on substrates with different stiffness.

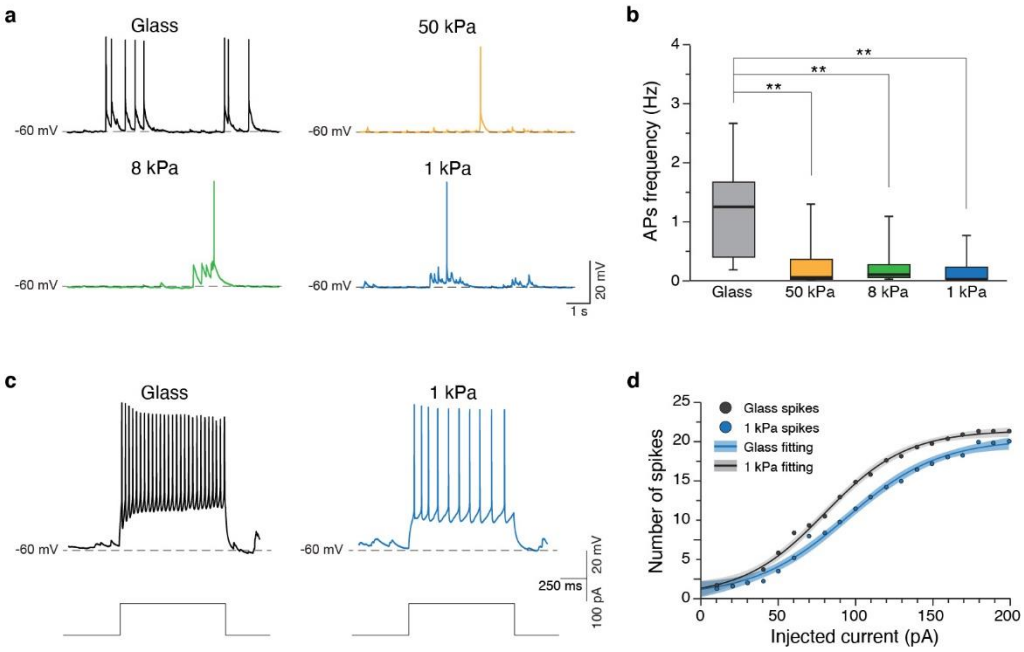

a *Representative current-clamp recordings of neurons grown (8–10 DIV) on glass and soft gels (50, 8 and 1 kPa).* ***b*** *Box plots summarizing the spontaneous neuronal firing activity across the four conditions (n cells=15 for glass, n=14 for 50 kPa, n=15 for 8 kPa, n=12 for 1 kPa; Kruskal-Wallis followed by Dunn's multiple comparison test was performed, ** p<0.01).* ***c*** *Cell excitability was evaluated by depolarizing cell membranes with injections of current at increasing amplitudes (from 0 to 200 pA at 10 pA increments). In the panel two representative traces depicting action potentials trains evoked by a 140 pA current injection for glass and 1 kPa conditions.* ***d*** *Plot showing the average number of spikes evoked by the increasing steps of currents characterizing the two conditions: glass (black points, n=16), and the 1 kPa gel (blue points, n=20). Points were fitted using sigmoidal curves showing 95% fitting confidence bands. Values are represented as mean mean±SEM.*

Fig. S3: Miniatures postsynaptic currents (mPSCs).

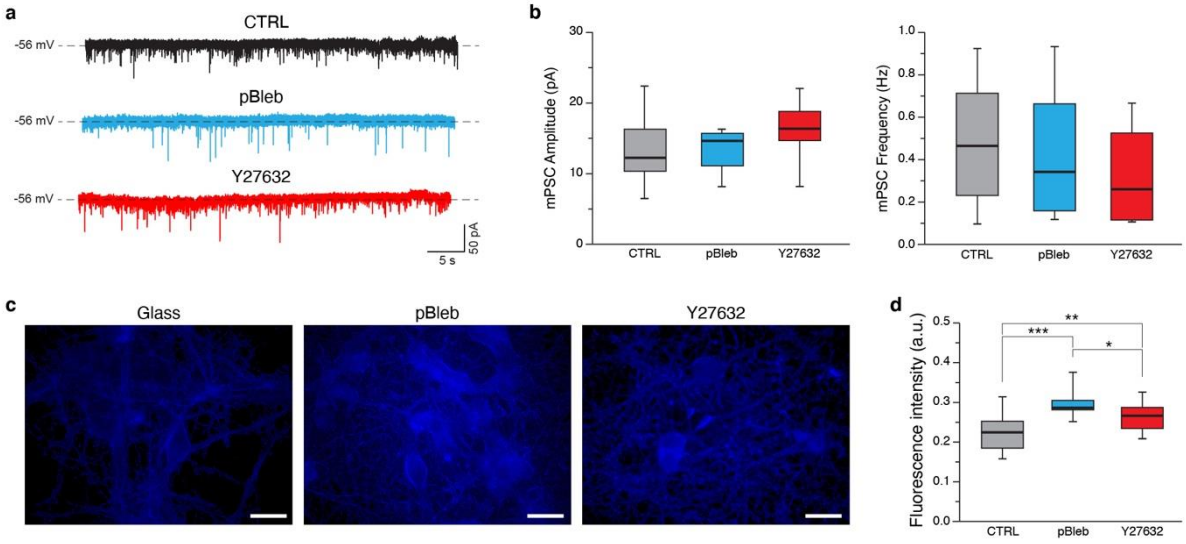

a *Representative mPSCs traces of patched neurons for each chronical treatment: control (in black), para-aminoblebbistatin (in blue), and Y-27632 treated (in red).* ***b*** *Box plots summarizing amplitude (left) and frequency (right) of mPSCs. No significant differences emerged between the three conditions. One-way ANOVA followed by Tukey's multiple comparison test. p>0.05.* ***c*** *Three representative fluorescent images depicting the Filipin signal across the three experimental conditions. Bar scales: 20 µm.* ***d*** *Box plot summarizing the differences in Filipin signal between treated cultures (pBleb and Y27632) and untreated controls, all cultured above glass substrates (Kruskal-Wallis followed by Dunn's multiple comparison test was performed, * p<0.05; ** p<0.01, *** p<0.001). Significant differences between two independent conditions with no-normal distribution was evaluated through a Mann-Whitney U Test.*

Fig. S4: Impaired mechanosensing induce reorganization in neuronal cell focal adhesions.

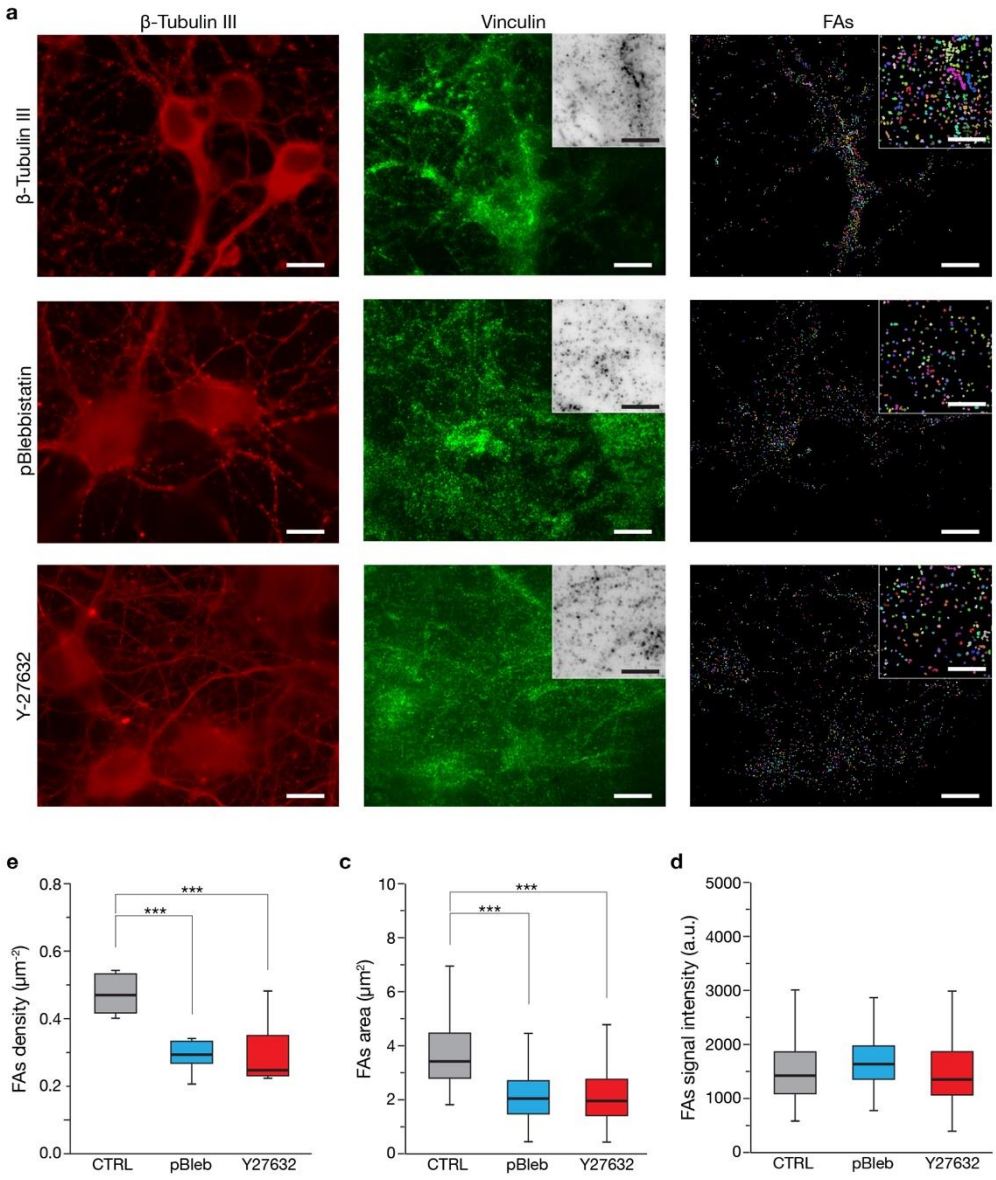

a *Representative TIRF images of hippocampal cells developed above glass substrates. Neurons were revealed within untreated cultures (top row), pBleb-treated (central row) and Y27632-treated (bottom row) targeting the β-Tubulin III protein (first column, in red). Focal adhesions were highlighted by staining and visualizing membrane-associated vinculin (central column, in green). Vinculin images were binarized (magnified inset) and segmented (left column, in the insets magnified). Scale bars: images 10 μm, insets 5 μm.* ***b*** *Box plot summarizing focal adhesion densities in terms of vinculin puncta across the three conditions. Significant differences were detected between treated and untreated conditions (One-way ANOVA followed by Tukey's multiple comparison test, p <0.001).* ***c*** *Box plot showing puncta size. A statistically significant difference emerged among the experimental groups (One-way ANOVA followed by Tukey's multiple comparison test, p <0.001).* ***d*** *Box plot depicting the average intensity signal of vinculin puncta between the three conditions. No significative differences emerged between treated and untreated cultures.*

3.2 Bidirectional modulation of neuronal cells electrical and mechanical properties through pristine and functionalized graphene substrates

Bidirectional modulation of neuronal cells electrical and mechanical properties through pristine and functionalized graphene substrates

Francesca Zummo[1] ǂ, Pietro Esposito[1] ǂ, Huilei Hou[2], Cecilia Wetzl[2], Gemma Rius[3], Raphaela Tkatchenko[3], Anton Guimera[3,4], Philippe Godignon[3,4], Maurizio Prato[2,5], Laura Ballerini[1], Elisabet Prats-Alfonso[3,4*], Alejandro Criado[2,6*], Denis Scaini[1,7*]

[1] Neuroscience Area, International School for Advanced Studies (SISSA), Trieste, Italy

[2] Center for Cooperative Research in Biomaterials (CIC biomaGUNE), Basque Research and Technology Alliance (BRTA), San Sebastián, Spain

[3] Institut de Microelectrònica de Barcelona, IMB-CNM (CSIC), Esfera UAB, Bellaterra 08193, Spain

[4] Centro de Investigación Biomédica en Red en Bioingeniería, Biomateriales y Nanomedicina (CIBER-BBN), Madrid 28029, Spain

[5] Department of Chemical and Pharmaceutical Sciences, University of Trieste, Trieste, Italy

[6] Universidade da Coruña, Centro de Investigacións Científicas Avanzadas (CICA), Rúa as Carballeiras, 15071, A Coruña, Spain

[7]Nanomedicine Research Laboratory, Department of Medicine, Imperial College London, Hammersmith Hospital, London, UK

ǂ Equally contributing authors

*** Correspondence:**

Denis Scaini: dscaini@ic.ac.uk

Alejandro Criado: a.criado@udc.es

Elisabet Prats-Alfonso: elisabet.prats@csic.es

Keywords: hippocampal neurons, graphene, chemical functionalization, synaptic activity, cell stiffness.

Abstract

In recent years, the quest for surface modifications to promote neuronal cell interfacing and modulation has risen. This course is justified by the requirements of emerging technological and medical approaches attempting to effectively interact with central nervous system cells, as in the case of brain-machine interfaces or neuroprosthetic. In that regard, the remarkable cytocompatibility and ease of chemical functionalization characterizing surface-immobilized graphene-based nanomaterials (GBNs) make them increasingly appealing for these purposes. Here, we compared the (morpho)mechanical and functional adaptation of rat primary hippocampal neurons when interfaced with surfaces covered with pristine single-layer graphene (pSLG) and phenylacetic acid-functionalized single-layer graphene (fSLG). Our results confirmed the intrinsic ability of glass-supported single-layer graphene to boost neuronal activity highlighting, conversely, the downturn inducible by the surface insertion of phenylacetic acid moieties. fSLG-interfaced neurons showed a significant reduction in spontaneous postsynaptic currents (PSCs), coupled to reduced cell stiffness and altered focal adhesion organization compared to control samples. Overall, we have here demonstrated that graphene substrates, both pristine and functionalized, could be alternatively used to intrinsically promote or depress neuronal activity in primary hippocampal cultures.

Introduction

Graphene is an atomically-thin carbon-based nanomaterial currently exploited in many research fields (Randviir et al., 2014), as well as industrial sectors (Torrisi et al., 2012; X. Zhou et al., 2011), including advanced biomedical applications (Nayak et al., 2011; G. Reina et al., 2017; Ryoo et al., 2010; Zhang et al., 2011). In regard to the latter application, graphene unusual physicochemical properties, such as its high carrier mobility, optical transparency and ease of chemical functionalization open to novel approaches in the design and fabrication of advanced neuronal tools as, for example, implanted brain sensors, smart stimulation electrodes or neuroprosthetic devices (Franceschi Biagioni et al., 2021; Lu et al., 2016; Shin et al., 2016). In this framework, the possibility to functionalize graphene with a plethora of molecules (Xu et al., 2016), drastically expands material

capabilities making possible, for example, to tune cellular adhesion (Jeong et al., 2016), reduce inflammatory responses (K. Zhou et al., 2016), or introduce chemical moieties (Karki et al., 2020). Among all chemical functionalization able to alter surface physicochemical properties, the amino (-NH_2) and carboxyl groups (-COOH) have demonstrated to induce cell adhesion and promote cell growth (Deng et al., 2015; Keselowsky et al., 2004; Ren et al., 2009), presumably through an improved cell wettability associated to surface charging and protein adsorption (Arima & Iwata, 2007).

Unfortunately, despite hopes raised by recent development in graphene applications, the understanding of its functional interactions with brain tissue when chemically functionalized is still limited, particularly concerning the synergic effect of chemical moieties and graphene innate effect on neuronal excitability. Indeed, single-layer graphene has demonstrated intrinsic ability to induce a boosting in the electrical activity of interfaced neuronal cells (Kitko et al., 2018; N. P. Pampaloni et al., 2018; Tang et al., 2013). This effect has been reconducted to the ability of graphene to perturb the distribution of extracellular ions at the interface with neurons giving rise to altered ion currents, associated to increased firing rate. Apparently, the graphene–ion interactions responsible of the effect take place when single-layer graphene is laid on electrically insulating substrates but vanish on electrically conductive ones (N. Pampaloni et al., 2018). Other studies reconducted graphene-induced neurotransmission potentiation to an alteration in cholesterol homeostasis impacting the number, release probability, and recycling rate of synaptic vesicles (Kitko et al., 2018). A common aspect of all these studies is to have validated the possibility to potentiate the spontaneous electrical activity of a neuronal network simply by facing it with graphene. This remarkable result opens to the possible use of the material for neuromodulation. However, the limitation to induce only network excitation limits the effectiveness of neuromodulation due to the lack of the ability to downregulate the electrical activity.

In the present study, we attempted to respond to this need interfacing primary neurons from rat hippocampus to pristine single-layer graphene (pSLG) and phenylacetic acid functionalized graphene

(fSLG), comparing their properties to those of cells plated on glass controls. The carboxyl group conveyed by the phenylacetic acid surface insertion, in particular, has already demonstrated to allow effective cell attachment and development with a very mild effect on cell vitality and functionality (J. W. Lee et al., 2006; Ren et al., 2009). Indeed, this chemical group represents a good validation molecule to investigate the impact of a chemical functionalization on graphene. We aimed at disclosing the synergic impact of graphene and chemical groups on neuronal network development focusing, in particular, on its effect on neuronal cell electrical and biomechanical properties. To pursue the investigation, we directly plated cells on graphene substrates and evaluated network morphology and composition by immunofluorescence, electrical activity by patch-clamping recordings, and cell stiffness by Atomic Force Microscopy (AFM) force-spectroscopy experiments.

Materials and Methods

Preparation of single-layer graphene substrates

Single-layer graphene (SLG) was growth by chemical vapor deposition (CVD) on flat Cu foils and subsequently transferred onto supporting glass substrates. In brief, graphene was grown using a Black MagicPro 4" reactor on a 25 μm thick copper foil (99.8% metal basis, Alfa Aesar, UK). Prior to the CVD process, copper foils had been cut in 6×5 cm^2 samples, cleaned in acetic acid and acetone, and finally rinsed in isopropyl alcohol (IPA). The two-steps growth process consisted of a 10 minutes Cu surface reduction at 1000 °C by flowing 400 standard cubic centimeters per minute (sccm) of H_2, 600 sccm of Ar and 150 sccm of N_2, followed by a 20 minutes graphene growth at 970 °C using methane as carbon precursor (10/100 sccm CH_4/ H_2 ratio). A 700 nm thick sacrificial layer of polymethyl methacrylate (PMMA) was spin-coated above the graphene (7% 950k MW dissolved in anisole, Micro Resist technology GmbH, DE) and after a soft backing, specimens of about 10×10 mm^2 in side size were cut out. The graphene layer was separated from copper using an electrochemical delamination process (De La Rosa et al., 2013) and, after washing in deionized water, transferred onto supporting glass coverslips (12×24 mm^2, No. 1, 0.13–0.16 mm in thickness, ORSAtec GmbH,

DE). Before the transfer procedure, supporting substrates were ultrasonicated in acetone and isopropanol (IPA) to assure the required cleanness and activated with an UV-ozone treatment (UVO, 5 minutes). After transfer, samples were let dry and baked at 180 °C for 2 minutes. The PMMA sacrificial layer was removed by immersing samples in acetone and then in IPA, 30 minutes in each solvent. pSLG substrates were used as transferred while, in fSLG, phenyl acetic acid moieties were immobilized on the surface. The functionalization was accomplished by placing some of the pSLG substrates in a glass beaker with distilled water (10 mL). Then, a distilled water solution of 4-(carboxymethyl)phenyl diazonium tetrafluoroborate (10 mg, 20 mM final concentration, synthesized following a published diazotization procedure (Franco et al., 2020) was slowly added with a syringe pump (2.5 mL/h) for 1 h at room temperature (RT). Substrates were subsequently removed from the solution and cleaned by immersion (3 times) in distilled water and dried over a stream of N_2.

The graphene materials were characterized by Raman spectroscopy and AFM. To evaluate the quality of graphene obtained and to quantify the functionalization degree, the ratio between the D (~1345 cm^{-1}) and G (~1589 cm^{-1}) Raman band intensities of graphene (I_D/I_G) were employed (Bottari et al., 2017). Raman spectra were recorded with a Renishaw inVia^{TM} Raman spectrometer equipped with a green laser (λ = 532 nm) and plotted after baseline correction by means of the Wire 4.4 software. An average defect density (*nD*) of $4.38 \cdot 10^{-4}$ nm^{-2} was obtained for fSLG samples. Defects were interpreted as changes in the graphene lattice C hybridization from sp^2 to sp^3 induced by the covalent modification (Cançado et al., 2011). Topographical changes of the surface of graphene were evaluated performing AFM analysis (see Atomic Force Microscopy section).

Cell cultures preparation

Dissociated hippocampal cells were derived from P0–P3 old rats as described in literature (Cellot et al., 2011; Lovat et al., 2005; N. Pampaloni et al., 2018; Rago et al., 2019). Briefly, rat hippocampi were isolated and digested in trypsin and deoxyribonuclease (6000 U/mL and 1560 U/mL, respectively, both from Sigma Aldrich). After digestion, the cell suspension was centrifuged (800 rpm for 5 minutes), and pellet collected and resuspended in a fresh culture medium composed of

Neurobasal-A medium (Thermo-Fischer) supplemented by B27 (2%, Gibco) and Glutamax® (10 mM, Gibco). Cells were plated on pSLG and fSLG substrates, and on polyornithine-coated glass coverslips controls at a nominal concentration of 10^6 cells/mL (300 µL for 45 minutes). Prior to cell plating, all substrates were sterilized for 30 minutes under UV light. Cultures were maintained in incubation conditions (37 °C, 5% CO_2, 95% RU) in 35 mm petri dishes containing about 2 mL of culture medium. All the experiments were performed after 8–10 days in vitro (DIV).

All animal procedures were conducted in accordance with the National Institutes of Health and with international and institutional standards for the care and use of animals in research. All experiments were performed in agreement with the Italian law (decree 26/14) and the European Union (EU) guidelines (2007/526/CE and 2010/63/UE) and were approved by the local authority veterinary service and by our institutional (SISSA-ISAS) ethical committee. All efforts were made to minimize animal suffering and to reduce the number of animals necessary to accomplish our studies.

Immunofluorescence

Cells were fixed with 4% paraformaldehyde (PFA) in phosphate buffered saline (PBS) for 20 minutes. Subsequently, samples were incubated for 1 h at RT in a PBS blocking solution containing 5% fetal bovine serum (FBS) and 0.03% triton X-100 to permeabilize cell membranes. After rinsing in PBS, primary antibodies were added for 1 h at RT and, subsequent to a PBS washing, secondary antibodies were added for 45 minutes in dark conditions (Cellot et al., 2016; Rago et al., 2019). As primary antibodies were used: mouse monoclonal anti-NeuN (MAB377, Sigma-Aldrich, 1:500 dilution), rabbit polyclonal anti-GFAP (HPA056030, Sigma-Aldrich, 1:500 dilution), rabbit polyclonal anti-β-tubulin III (T2200, Sigma-Aldrich, 1:250 dilution), and mouse monoclonal anti-GFAP (G3893, Sigma-Aldrich, 1:250 dilution). As secondary antibodies were instead used: AlexaFluor® 594 goat anti-mouse (A11032, Sigma-Aldrich, dilution 1:500) and anti-rabbit (A11037, Life Technologies, dilution 1:500), and AlexaFluor® 488 goat anti-mouse (A11029, Life Technologies, dilution 1:500) and anti-rabbit (A11034, Sigma-Aldrich, dilution 1:500). Unspecific cell-nuclei staining was performed using 4′,6-diamidino-2-phenylindole (DAPI, D1306, Thermo Fisher, dilution 1:200).

Samples were mounted on common microscope glass slides (Fisher Scientific) using Fluoromount-G™ Mounting Medium (Thermofisher). NeuN and DAPI stainings were used to compute neuronal *vs* non neuronal cell densities. Specifically, images 636 µm × 636 µm (1024 pixels × 1024 pixels) were acquired with an epifluorescence microscope (DM6000, Leica Microsystems) using 20× objective (0.5 N.A). Three visual fields per condition were randomly collected (2 samples per condition per session from three independent cell-culture series). The offline analysis was conducted semi-automatically in Fiji (Schindelin et al., 2012), using the cell-count plugin developed by Ivan V. Grishagin (Grishagin, 2015). Cell shape and network morphology were instead highlighted by immunolabeling neurons against β-tubulin III, and astrocytes against the glial fibrillary acidic protein (GFAP). Images were acquired using a confocal microscope (Nikon eclipse C1 equipped with Ar/Kr and He/Ne lasers) using a 60× oil-immersion objective (Plan Apo, 1.40 NA, Nikon Corporation). Images were recorded at 212 µm × 212 µm (1024 pixels × 1024 pixels) collecting about 14 focal planes per field (600 nm Z-stacks step-length).

Electrophysiology

All patch-clamp recordings were performed in voltage clamp mode in whole-cell configuration at RT. The glass pipettes, thermally pulled to achieve a final resistance of 4–8 MΩ, were filled with an intracellular solution composed by 120 mM K-gluconate, 20 mM KCl, 10 mM HEPES, 10 mM EGTA, 2 mM $MgCl_2$ and 2 mM Na_2ATP (pH 7.3; 300 mOsm in osmolarity, all compounds from Sigma Aldrich) and immersed in an extracellular recording solution composed by 150 mM NaCl, 4 mM KCl, 2 mM $CaCl_2$, 1 mM $MgCl_2$, 10 mM HEPES and 10 mM glucose (pH 7.4; about 320 mOsm in osmolarity, all compounds from Sigma Aldrich). Data were collected using a Patch Clamp EPC 7 patch amplifier (HEKA Electronic, USA) and digitized using a Digidata 1322A (Molecular Devices LLC, US) at 10 kHz sampling frequency using the pClamp 8.2 acquisition software (Molecular Devices LLC, USA). Cell membrane passive properties (input resistance R_i, and membrane capacitance C_m), were measured by averaging the cell response to 80 voltage steps (−5 mV, 10 ms in duration) in terms of currents through the Clampfit software (pClamp 10.3, Molecular Devices LLC,

US). Uncompensated series resistance was less than 11 MΩ. Spontaneous post-synaptic currents (PSCs) were recorded by clamping the membrane voltage at −56 mV holding potential (value not corrected for the liquid junction potential, calculated to be equal to −14 mV). Miniature post-synaptic currents (mPSCs) were instead recorded in presence of 1 µM Tetrodotoxin (TTX, Latoxan), a specific blocker of fast-activating voltage-gated Na^+ channels. The analysis of synaptic events was performed offline using the AxoGraph neuronal event detection software (version 1.7.0, Axon Scientific, US). Specifically, for each recording all events detected were averaged and the peak amplitude and kinetic properties of the resulting mean current were measured. The presence and contribution of glutamate AMPA-receptor and $GABA_A$-receptor mediated postsynaptic currents in the overall electrical activity were discriminated based on their distinctive kinetic properties (rise and decay time). Specifically, fast events are characterized by a rise-time of about 100 µs and a decay time of less than 3 ms in terms of time constant (τ), while slow events are characterized by a similar rise-time but a decay time larger than 20 ms. In our experimental conditions, fast-decaying ($\tau<5$ ms) PSCs are generally mediated by the glutamate AMPA-receptor type, while slow-decaying events ($\tau>20$ ms) are mediated by the $GABA_A$-receptor type (N. P. Pampaloni et al., 2018).

Atomic force microscopy

Glass control, pSLG and fSLG substrate surfaces were characterized by AFM. A commercial Solver PRO AFM instrument (NT-MDT Co., RU) was used in no-contact mode in air (normal pressure and RT). Both topographic and phase signal images were acquired using silicon AFM tips (Etalon® HA-NC rectangular cantilevers, spring constant 12 nN/nm, resonant frequency 235 kHz, probe tip radius 10 nm, NT-MDT Co., RU). Images of 2.5×2.5 μm^2 (512×512 $pixels^2$) were acquired at 1 lines/second scan speed. The open-source SPM analysis software Gwyddion (Nečas & Klapetek, 2012) was used to process and analyze all AFM images. Root mean square line-roughness (R_{RMS}) was defined internally to the software and corresponds to the average of the height deviations from the mean line of the selected profile.

The stiffness of neuronal cells interfaced to glass, pSLG and fSLG substrates were evaluated by means of AFM force-indentation experiments. Measurements were carried out at RT in liquid environment (PBS). Stiffness assessment was conducted taking advantage of the cell-mechanics analysis capability integrated in the AFM tool (JPK NanoWizard® 3, Bruker Nano Surfaces, US). Experiments were performed using tip-less cantilevers with a nominal elastic constant of 0.03 nN/nm and a resonance frequency of 10 kHz (CSG11-B/tipless, NT-MDT Co., Russia) on which apex a glass bead (8.0±0.4 µm in diameter, No. 9008, Duke Standards™, Fremont CA, USA) was glued using a UV-curable glue (Norland Optical Adhesive 61, Norland Products, Inc., USA). Cantilevers' effective elastic constants were determined by the software-integrated thermal method (Lévy & Maaloum, 2002). Neuronal cell stiffness has been evaluated after having fixed cells in 4% PFA in PBS and made them visible by NeuN staining. Despite the fact that cell fixation is known to increase the cell stiffness, it has been shown that it is possible to use these values to perform a relative comparison of cell mechanical adaptation on the three different substrates (Grimm et al., 2014; Jiang et al., 2011; Ulloa et al., 2021). Indentation was conducted by manually placing the cantilever tip above the NeuN-stained cell soma. This strategy ensures high measurement reproducibility. Measurements were performed at a constant speed of 2.5 µm/s and triggered to a maximum applied force of 5 nN and never exceeded an indentation depth of 250 nm, representing the 5% of the average measured cell height (data not shown). Such maximum indentation avoided any contribution from the underneath substrate to the measured cell stiffness minimizing, at the same time, its susceptibility to cell nucleus stiffness. Cell stiffnesses were determined using the JPKSPM Data Processing® software by fitting the obtained force-indentation curves with the integrated Hertzian model for a spherical indenter (Sneddon, 1965). Averaging values were computed from measurements performed on about 200 cells per condition from 3 independent experiments. Neuronal stiffness was reported in terms of Young's Modulus (E) and expressed in kPa.

Total internal reflection fluorescence (TIRF)

TIRF experiments were performed to evaluate the number and distribution of focal adhesions (FAs) in hippocampal cultures grown above glass, pSLG and fSLG substrates. Cellular samples were fixed with 4% PFA for 30 minutes at RT. After fixation, samples were incubated for 1 h in a PBS blocking solution containing 5% fetal bovine serum (FBS) and 0.03% triton X-100 to block non-specific sites and permeabilized cells. Subsequently, they were incubated for 1 hours and a half at RT with a monoclonal mouse anti-vinculin antibody (V9131, Sigma-Aldrich, 1:400 dilution in blocking solution without triton) and a rabbit polyclonal anti-β-tubulin III (T2200, Sigma-Aldrich, 1:250 dilution in blocking solution without Triton). Then, samples, washed with PBS, were incubated for 1 h with a goat anti-mouse secondary antibody coupled to Alexa Fluor® 488 (A11029, Life Technologies, 1:500 dilution) and Alexa Fluor® 594 goat anti-rabbit secondary antibody (A11037, Life Technologies, 1:500 dilution), diluted in blocking solution without triton. Samples were mounted on standard microscope glass slides (7525M, J. Melvin Freed, US) using a liquid mounting medium (Fluoromont-G™, ThermoFisher), and then visualized using an inverted epi-fluorescence microscope equipped with a TIRF module (Nikon Eclipse-TiU, Nikon Corporation). Images were acquired in total reflection condition using a high aperture oil-immersion objective (CFI Apochromat TIRF 100×C Oil 1.49 N.A., Nikon Corporation) and a 488 nm laser (OBIS 488 LS; Coherent, Inc., Santa Clara, CA, USA) at a power sufficient to avoiding photo-bleaching. In our conditions the penetration depth of the evanescent wave was about 150 nm. Samples were visualized using a CCD camera (DS-Qi1, Nikon Corporation) acquiring for every field of view a TIRF image of the vinculin staining and a conventional fluorescence image of β-tubulin III positive regions (426×340 μm^2, 1280×1024 $pixels^2$). FAs were quantified as vinculin-positive puncta exploiting a procedure developed within the Wolfram Mathematica software suite (version 12.3.0, Wolfram Research, Inc., USA). Briefly, vinculin signal was analyzed exclusively in β-tubulin positive regions. After image binarization, puncta were highlighted using a morphological-matching procedure based on disks of increasing radius (from 300 nm to 3 μm) and segmented. For every condition, the area of every detected punctum

was computed and averaged. FAs density was evaluated as the ratio between the total number of puncta and the area of β-tubulin positive regions.

Statistical analysis

All the described experiments were repeated at least three times using cell cultures from independent experimental sessions. All statistical analysis was performed using the Prism software (version 6.0, GraphPad). Data distribution was evaluated by Shapiro Wilk test of normality and, based on the result, a bar chart showing mean ± standard deviation (SD) or a box plot representation was chosen to graphically represent data. Box plots are plotted as median with boxes spanning from the 25^{th} (1^{st} quartile, Q1) to the 75^{th} (3^{rd} quartile, Q3) percentiles, with whiskers representing the 5^{th} and 95^{th} percentiles. Statistics between two independent samples were performed with t-test when the distribution was normal. For parametric data Student's t-test was used to compare two independent conditions, while comparisons between more than two conditions were performed performing a one-way ANOVA analysis followed by Tukey's multiple comparison post-hoc test. For non-parametric data, Mann Whitney for two groups comparison test or Kruskal-Wallis followed by Dunn's multiple comparison test were used. For the sake of clarity, all the values reported in the main text are expressed as mean ± SD. Statistical significance was determined at $P < 0.05$, unless otherwise indicated. Significance was graphically indicated as follows: $*P < 0.05$, $**P < 0.01$, $***P < 0.001$.

Results

Materials fabrication and characterization

Single-layer graphene was grown on flat Cu foils, separated from copper using an electrochemical delamination process, and subsequently transferred onto supporting glass substrates (Figure 1A). The quality of CVD-grown pSLG and the effectiveness of chemical functionalization of fSLG were assessed by Raman spectroscopy analysis (Figure 1B). Specifically, the distinctive graphene Raman spectrum is characterized by the signature bands so-called D, G and 2D (Dong et al., 2011; Nguyen et al., 2013; A. Reina et al., 2009). The D peak, localizes at about 1345 cm^{-1}, is larger when chemical

or structural non-idealities are present, such as impurities or defects, but it can also be correlated with covalent chemical functionalization (Criado et al., 2015). The G peak, placed at about 1589 cm^{-1}, is characteristic of sp^2 hybridization showing the structural order and purity in all graphitic materials whereas, the 2D peak, sited at about 2689 cm^{-1}, is characteristic of the atomically-thick 2D nature of graphene films. For instance, peaks' characteristics analysis allows the discrimination between single- versus multi-layered graphene, as reported in literature (Faugeras et al., 2009; Ferrari et al., 2006; Malard et al., 2009). Precisely, it is well-known that the ratio of the intensity of the 2D and G bands (I_{2D}/I_G) is indicative of the number of graphene layers. A $2<I_{2D}/I_G<3$ ratio is indicative of monolayer graphene, $1<I_{2D}/I_G<2$ of bilayer graphene, while $I_{2D}/I_G<1$ is associated to the multilayer one. In addition, the presence of single-layer graphene can be also evinced by analyzing the shape of the 2D peak, where a full width at half maximum (FWHM) value of about 38 cm^{-1} is indicative of a single-layer material, even in the presence of I_{2D}/I_G value falling between 1 and 2. Based on measured I_{2D}/I_G and $FWMH_{2D}$ values, we can state that the graphene films grown on the Cu foil at 970 ºC was mainly a monolayer with a contingent distribution of double layer nucleation sites.

Pristine SLG was chemically modified through a radical reaction employing 4-(carboxymethyl)phenyl diazonium tetrafluoroborate (Figure 1C). The diazonium salt reacts with graphene through a single electron transfer (SET) mechanism, resulting in a change in the hybridization of carbon atoms within the graphene lattice from sp^2 to sp^3 (Paulus et al., 2013). To confirm and evaluate the chemical modification, graphene samples were characterized by Raman spectroscopy and AFM. Based on Raman scattering, the successful chemical modification was confirmed by a significant increment in the I_D/I_G ratio (Figure 1D). The increased intensity of the D peak evidenced the change in the hybridization of carbon atoms, as defects in the structure of graphene, which would be purely sp^2.

The quantification of the degree of chemical functionalization was carried out by evaluating the defect density (*nD*) (Cançado et al., 2011) using the following relation:

$$nD\ (cm^{-2}) = \frac{(1.8 \pm 0.5\ ) \times 10^{22}}{\lambda_L^4} \cdot \left(\frac{I_D}{I_G}\right)$$

where λ_L is the excitation wavelength. It is worth noting that this equation is valid for Raman data obtained from graphene samples with distances between defects ≥ 10 nm. Thus, the fSLG samples showed a moderate average $nD = 4.38 \cdot 10^{-4}$ nm^{-2} (Table S1).

The morphology of pristine and phenylacetic acid functionalized SLG films were characterized by AFM and compared to bare glass coverslips control substrates (Figure 1E). Line profile analysis revealed an increase in surface roughness as compared to glass (Ctrl), for both pSLG and fSLG (Figure 1E, bottom; R_{RMS}=0.18 nm for Ctrl, R_{RMS}=0.61 nm for pSLG, and R_{RMS}=1.24 nm for fSLG), as apparent in the three topographical reconstructions. The qualitative change in SLG surface morphology after the chemical modification, quantified in terms of an increased roughness, can be correlated to the well-known oligomers derived from the generated phenyl radicals (Hossain et al., 2010).

Graphene substrates support the development of hippocampal neuronal networks

Despite the fact that several reports have already demonstrated the successful development of hippocampal cell cultures interfaced with graphene substrates (Fabbro et al., 2016; Kitko et al., 2018; N. P. Pampaloni et al., 2018; Rauti, Secomandi, et al., 2020; Tang et al., 2013), this aspect has not been evaluated on chemically functionalized graphene yet. In order to explore the potential effects of graphene and its chemical functionalization on cell development and network composition we cultured primary hippocampal neurons on both pSLG and fSLG supports. Neurons plated directly on glass coverslips were used as control cultures (Cellot et al., 2009; Lovat et al., 2005; N. Pampaloni et al., 2018; Rago et al., 2019).

Both graphene substrates, pSLG and fSLG, demonstrated able to sustain a similar growth and development of hippocampal cells with respect to the glass control condition. We qualitatively investigated the network size and phenotypical composition evaluating the density of neuronal and non-neuronal cells. Specifically, we marked the nuclei of all the cells of our cultures using 4′,6-

diamidino-2-phenylindole (DAPI) and specifically highlighted neurons by immunolabelling them against NeuN, a protein localized in nuclei and perinuclear cytoplasm of most of the neurons in the central nervous system of mammals (Sarnat et al., 1998) (Figure 2A). An automatic procedure was used to binarize images and classify cells as neuronal or non-neuronal (Figure 2A, inlets). The non-neuronal constituent of primary hippocampal cultures is neuroglia (Jäkel & Dimou, 2017) which, in our experimental conditions, is mainly composed by astrocytes (Cellot et al., 2016; Lovat et al., 2005; Rauti, Cellot, et al., 2020). No significant differences were detected across all three substrates in terms of neuronal density (Figure 2B) or neuroglia density (Figure 2C). Similarly, the ratio between neuronal and glial cells appeared to be similar among all the three conditions (Figure 2D).

Graphene substrates alter neuronal electrical activity

To assess the impact of graphene substrates on the cellular morphology of the interfaced networks we revealed by immunofluorescence the shape of neurons and astrocytes. For that purpose, we marked the neuronal cytoskeletal components β-tubulin III and the glial fibrillary acidic protein (GFAP), while cells nuclei were stained using DAPI (Figure 3A). Confocal micrographs show that cells adopt a healthy morphology without any apparent difference among the three conditions.

We further extended our investigation performing a functional analysis of the spontaneous synaptic activity characterizing our neuronal networks interfaced to graphene and glass for 8–10 DIV. Voltage-clamp electrophysiological experiments were conducted patching neurons within the three conditions and recording network spontaneous post-synaptic currents. Heterogeneous PSCs were detected as inward currents of variable amplitudes (Lovat et al., 2005) in all conditions, as showed by the three representative traces in Figure 3B.

Plasma membrane passive properties, measured for each patched neuron, provided further indications about cell viability and membrane integrity in cells developed above pSLG and fSLG substrates. We compared the results with glass controls and no significant differences were identified in terms of input resistance and membrane capacitance over the three experimental groups (Figure 3C; 519±208

MΩ and 54.8±8.5 pF for Ctrl, n=23 cells; 438±134 MΩ and 51.7±9.6 pF for pSLG, n=16; 493±188 MΩ and 47.2±9.1 pF for fSLG, n=16).

The appearance in all of our traces of spontaneous post-synaptic events was both evidence of functional synaptic formation and an index of network efficacy (Lovat et al., 2005; N. P. Pampaloni et al., 2018). Interestingly, the quantification of the amplitude and frequency of PSCs in pSLG and fSLG interfaced neurons revealed a different functional adaptation of these networks when compared to glass. Specifically, our data highlighted that while PSCs amplitudes of networks developed above glass and pSLG were almost identical, pSLG interfaced neuronal networks showed a significant enhancement in the frequency of synaptic currents with respect to controls (Figure 3D, grey and blue boxes; 32.62 ± 7.65 pA and 1.31±0.56 Hz for glass controls, n=23 cells; 33.76±5.11 pA and 2.33±1.24 Hz for pSLG, n=16). In contrast, fSLG induced in interfaced networks a significant reduction in both PSCs amplitude and frequency in comparison with pSLG and glass (Figure 3D, red boxes; 21.74±8.4 pA and 0.48±0.40 Hz for fSLG, n=16 cells).

In addition, we wondered if both inhibitory and excitatory components of PSCs were similarly affected by the two substrates. For this purpose, we have offline analyzed and classified PSCs in slow and fast events based on their kinetic (Figure 3E; τ = 22.3±6.64 ms for slow events, and τ = 3.79±1.31 ms for fast ones) and respectively associated to excitatory and inhibitory events. This approach is supported by the fact that, in our experimental conditions, fast-decayings (τ<5 ms) are mediated by the glutamate AMPA-receptor type, while slow-decayings (τ>20 ms) by the $GABA_A$-receptor type (Cellot et al., 2011; N. P. Pampaloni et al., 2018). pSLG did not significantly affect the amplitude and frequency of slow PSCs in interfaced networks which, on the other hand, were both reduced in cultures developed above fSLG (Figure 3F; 39.22 ± 5.32 pA and 0.49±0.33 Hz for glass controls, n=23 cells; 44.44 ± 8.49 pA and 0.55±0.42 Hz for pSLG, n=16; 23.44±10.44 pA and 0.07 ± 0.09 Hz for fSLG, n=16). Regarding fast components, PSC amplitudes were not significantly altered by pSLG but reduced by fSLG (in comparison to glass controls). In terms of frequencies, instead, they were upregulated by pSLG and downregulated by fSLG substrates (Figure 3G; 24±7.1 pA and 0.7±0.4 Hz

for glass controls, n=15 cells; 23±5.2 pA and 1.7±1 Hz for pSLG, n=11; 16.8±3.9 pA and 0.44±0.39 Hz for fSLG, n=16 cells). Interestingly, while pSLG seemed to affect more the fast PSCs components than the slow, fSLG substrates similarly impaired both components. From these evidences we can infer that the two graphene substrates, pSLG and fSLG, did induce an alteration in neuronal spontaneous activity through two distinct mechanisms.

To move through this idea, we tested if the changes in synaptic activity detected in our experiments could result from a structural reassembling at the synaptic level. We measured miniature postsynaptic currents (mPSCs) by application of TTX (Figure 4A). For each condition we evaluated the amplitude and frequency of mPSCs. The former gives an indication about the number of neurotransmitter receptors localized at the post-synaptic terminal, whereas the latter is mainly influenced by the pre-synaptic release probability and by the number of synaptic contacts (N. P. Pampaloni et al., 2018; Raastad et al., 1992). Interestingly, no significant difference in amplitudes nor frequencies were detected among the three conditions (Figure 4B; 13.2±6.2 pA and 1.1±0.85 Hz for glass, n=10 cells analyzed; 13.9±7.2 pA and 1±0.5 Hz for pSLG, n=10; 15.2±6.8 pA and 0.8±0.7 Hz for fSLG, n=10). Consequently, we can rule out that pristine or phenylacetic acid modified graphene substrates alter the structural functionality of synapses at pre- and post-synaptic level, excluding that such phenomenon stay behind the observed changes in network activity.

Focal adhesion organization and cell stiffness

To point out if the two graphene substrates may have had an impact on focal adhesions (FAs), we attempted an evaluation of their distribution and size using total internal fluorescence microscopy (TIRF). For this purpose, we performed an immunostaining assay fluorescently labelling vinculin, a cytoskeletal protein associated with the cytosolic protein complex of FAs, together with β-tubulin III (highlighting neuronal cytoskeleton), after 8–9 DIV (Figure 5A; top and bottom rows, respectively). FAs analysis was conducted visualizing vinculin-positive regions by TIRF, confining in this way the analysis to a volume extending just about a hundred of nanometers from the graphene surface (see Materials and Methods). This approach made possible to exclude from the analysis the majority of

the signal coming from cytosolic vinculin not associated to FAs. β-tubulin III signal was instead acquired as a normal epi-fluorescence signal. We evaluated vinculin puncta density among the three kinds of substrates highlighting a significant reduction in puncta densities in graphene substrates (Figure 5B; 0.49±0.12 puncta/μm^2 for glass controls, n=12 fields analyzed; 0.37±0.05 puncta/μm^2 for pSLG, n=12; 0.31±0.11 puncta/μm^2 for fSLG, n=12). Interestingly, when we estimated the average area of vinculin puncta detected across the three conditions, we observed that pSLG and fSLG induced an opposite effect when compared with glass controls. Neuronal cells interfaced with pSLG were characterized by larger puncta, while cells interfaced with fSLG presented significantly smaller ones than controls (Figure 5C; 0.157±0.015 μm^2 for glass controls, n=12 fields analyzed; 0.173±0.010 μm^2 for pSLG, n=12; 0.125±0.011 μm^2 for fSLG, n=12). These values allow us to assume that different mechanisms were involved in FAs modulation by pSLG and fSLG.

In order to evaluate if pSLG and fSLG substrates impacted the cellular mechanoadaptation of interfaced hippocampal neurons, we have evaluated cell stiffness across the three experimental conditions. The rigidity of a cell is determined by a complex tensional equilibrium established within the cell as an adaptation to the mechanical and chemical cues provided by the extracellular environment (Azadi et al., 2019). In in vitro systems, this condition includes the compliance of the culturing substrate (Byfield et al., 2009; Tee et al., 2011), its chemical functionalization (Peyton et al., 2006), or micro and nano morphology (Yang et al., 2020). All these factors could induce cell stiffening or softening through an alteration in cytoskeletal structure/organization eventually mediated by a reshaping of FAs number and dimensions too (Gupta et al., 2016; Saphirstein et al., 2013). In our study, we have probed cell stiffness values of cells interfaced with pSLG, fSLG and glass control by means of AFM force-indentation experiments (Luo et al., 2016). We have described cell stiffness in terms of Young's elastic modulus (E), a parameter commonly accepted to qualitatively quantify the rigidity of a cell (Ding et al., 2017). We discovered that pSLG did not affect neuronal cell stiffness but, conversely, fSLG interfaced cells appeared significantly softer than glass

controls (Figure 5A; 6.2 ± 2.6 kPa for glass controls, n=168 cells analyzed; 6.2 ± 2.8 for pSLG, n=203; 4.0 ± 4.0 kPa for fSLG, n=140).

Discussion

Herein, we fabricated high-quality single-layer graphene films by CVD on flat Cu foils and subsequently transferred them on supporting glass coverslips. We chemically functionalized graphene substrates with carboxyl groups by surface insertion of phenylacetic acid moieties. Both pristine graphene films (pSLG) and functionalized ones (fSLG) were characterized by high chemical and structural quality, and demonstrated to be nanometrically flat on a length scale comparable with neuronal cells processes (about 1–5 μm). Indeed, from a surface morphology point of view, the two graphene substrates were perceived by the cells to be comparatively as even as control glass substrates (Figure 1) (Baranes et al., 2012; Fan et al., 2002; Rajnicek et al., 1997).

The ability of graphene substrates to sustain proper cell adhesion and development was evaluated by interfacing them with primary cultures of rat hippocampus. We assessed the content of neuronal and glial cells above pristine and carboxyl-functionalized graphene substrates in comparison to glass controls and no significative differences emerged between the cellular networks developed above the three substrates (Figure 2). This result confirmed once again the extremely good cyto-compatibility of graphene-based materials (W. C. Lee et al., 2011; Li et al., 2011; N. P. Pampaloni et al., 2018) and, for the first time, allowed us to state that a similar behavior is also found in the case of a covalent insertion of phenylacetic acid moieties on it.

Subsequently, we moved to a multi-technique approach, combining immunofluorescence, patch-clamping electrophysiology and scanning probe microscopy to evaluate the morphological and functional adaptation of the neuronal networks developed interfaced to graphene substrates for 8–9 DIV. Overall, our results demonstrate that the morphology of hippocampal cell networks developed above pSLG and fSLG substrates are almost identical to that of glass controls. Electrophysiology showed that also neuronal passive properties (R_m and C_m) were not significantly different, an indication of similar plasma membrane condition and cellular dimensions (Cellot et al., 2011).

Interestingly, network spontaneous activity was significantly higher in terms of frequency on pSLG-interfaced networks, but lower in fSLG-interfaced ones (in the latter case also current amplitude was lower). This result highlighted an opposite modulation of neuronal cells electrical activity by the two graphene substrates, presumably indicating that two different adaptation mechanisms are involved. Further analysis revealed that while the boosting effect observed in pSLG samples is mainly associable to an increase in the frequency of just the fast fraction of events. In contrast, in the case of fSLG, the reduction in both amplitude and frequency affected similarly slow and fast components (Figure 3). These shreds of evidence let us suppose that pristine graphene potentiates neuronal excitatory signaling, mainly attributed to the fast components, AMPA-mediated currents, while carboxyl-functionalized substrates impaired both excitatory and inhibitory activity. The origin of this different selectivity can be traced back to the different spatial distribution of excitatory and inhibitory synapses in hippocampal neurons: the former usually having axo-dendritic localization, and the latter frequently axo-somatic one (Megías et al., 2001). Indeed, excitatory synapses will generally be spatially closer to the graphene surface than inhibitory ones.

Starting from this evidence, we extended our investigation to the synaptic adaptation of the network by measuring the miniature PSCs of TTX-silenced networks among the three conditions. This study allowed to decouple within the network activity the contribution of dynamical components from structural components. We discovered that both graphene substrates have no effect on both the amplitude and frequency of miniature events compared to controls (Figure 4). This result suggests that the alterations in the spontaneous postsynaptic activity described earlier in graphene-interfaced neurons do not involve any structural changes in the presynaptic release probability or the number of synaptic contacts, as well as on postsynaptic receptor sensitivity (Raastad et al., 1992).

To rule out the possibility that graphene substrates alter the network electrical activity as a side effect of a more complex, surface-mediated, tensional adaptation of the cell, we evaluated two cellular aspects connected to surface properties and mechanoadaptation: the focal adhesions organization and the cellular stiffness. In the first case, compared to controls, we highlighted a reduction in FAs

densities among graphene substrates, which are particularly significative in fSLG-interfaced cells. Interestingly, FAs size was oppositely regulated by the two substrates: pSLG cells presented larger FAs while fSLG were significantly smaller. This result apparently underlines for cells on pSLG an adaptive mechanism where fewer FAs are compensated by their larger size. Conversely, in fSLG-interfaced cells, this compensation is not activated and both the number and the size of FAs were reduced. Because FAs represent the fundamental cellular structure responsible for cytoskeleton-mediated cellular mechanoadaptation, we evaluated through AFM force-indentations the stiffness of neuronal cells developed above graphene substrates. We pointed out that, while the stiffness of pSLG-interfaced neurons did not change compared to control cells, fSLG cells resulted significantly softer than controls (Figure 5). Cell softening may be the eventual result of an impaired ability of the cell to adjust its internal tension through actomyosin-mediated cytoskeletal reorganization (Lessey et al., 2012) mainly due to the low density and size of the FAs that mechanically link the cell and the extracellular environment. Indeed, for the first time, we have shown how the physicochemical properties of a carboxyl-functionalized graphene substrate could impact not only the electrical activity of interfaced cells, but also their mechanoadaptation.

Conclusion

This study compared the (morpho)mechanical and functional adaptation of rat primary hippocampal neurons when interfaced with surfaces covered with pristine single-layer graphene and functionalized graphene endowed with carboxylic functional groups. Our results confirmed the intrinsic ability of single-layer graphene layered on glass to boost spontaneous neuronal activity highlighting, on the other hand, the reduction in the electrical activity inducible by the -COOH functionalization. On these substrates, neurons showed a significant decrease in the frequency of spontaneous postsynaptic currents, coupled to a reduced average cell stiffness and altered focal adhesion organization in respect to controls. The reduced electrical activity observed in fSLG-interfaced neurons may be an indirect consequence of the altered mechanical properties of the cells or, instead, the result of an independent

functional adaptation mechanism taking place in neurons. Further studies will be necessary to address this open question about neuronal mechanoadaptation.

Overall, we have here demonstrated that two graphene substrates, pristine and carboxylic-functionalized, could be alternatively used to intrinsically promote or depress neuronal activity in primary hippocampal cultures.

Conflict of Interest

The authors declare that the research was conducted in the absence of any commercial or financial relationships that could be construed as a potential conflict of interest.

Author Contributions

Conceived and designed the experiments: D.S., A.C., and E.P.A. Performed the experiments: P.E., F.Z., H. H., C.W., R.T., A.C., G.R. and E.P.A. Formal data analysis: F.Z., P.E., and D.S. Funding acquisition: D.S., L.B., A.G. and M.P. Resources: A.G., P.G., L.B., and M.P. Wrote the original paper: D.S., F.Z., A.C., and E.P.A.

Funding

This work was funded by the European Union's Horizon 2020 Research and Innovation Program under the Grant Agreement 737116, and under Grant Agreements 785219 and 881603 of the Graphene Flagship. D.S. acknowledges the support of the European Union's Horizon 2020 research and innovation program under the Marie Skłodowska-Curie grant agreement no. 838902. M.P., as the recipient of the AXA Bionanotechnology Chair, is grateful to the AXA Research Fund for financial support. This work was performed under the Maria de Maeztu Units of Excellence Program from the Spanish State Research Agency-grant no. MDM-2017- 0720. A.C. thanks Xunta de Galicia for his research grant Atracción de Talento (no. ED431H 2020/17). G.R. acknowledges funding from RYC-2016-21412. H.H. acknowledges funding from Juan de la Cierva - Incorporación no. IJC-2018-037396-I.

Acknowledgments

We are grateful to L. Casalis for the support in setting up TIRF experiments and performing AFM topographical characterizations, and to M. Lazzarino for the guide in performing AFM experiments and analyzing cell-stiffness data. This work has made use of the Spanish ICTS Network MICRONANOFABS partially supported by MICINN and the ICTS 'NANBIOSIS', more specifically by the Micro-NanoTechnology Unit of the CIBER in Bioengineering, Biomaterials and Nanomedicine (CIBER-BBN) at the IMB-CNM.

References

Arima, Y. & Iwata, H. (2007). Effect of wettability and surface functional groups on protein adsorption and cell adhesion using well-defined mixed self-assembled monolayers. *Biomaterials*, *28*(20), 3074–3082. https://doi.org/10.1016/j.biomaterials.2007.03.013

Azadi, S., Tafazzoli-Shadpour, M., Soleimani, M. & Warkiani, M. E. (2019). Modulating cancer cell mechanics and actin cytoskeleton structure by chemical and mechanical stimulations. *Journal of Biomedical Materials Research - Part A*, *107*(8), 1569–1581. https://doi.org/10.1002/jbm.a.36670

Baranes, K., Chejanovsky, N., Alon, N., Sharoni, A. & Shefi, O. (2012). Topographic cues of nano-scale height direct neuronal growth pattern. *Biotechnology and Bioengineering*, *109*(7), 1791–1797. https://doi.org/10.1002/bit.24444

Bottari, G., Ángeles Herranz, M., Wibmer, L., Volland, M., Rodríguez-Pérez, L., Guldi, D. M., Hirsch, A., Martín, N., D'Souza, F. & Torres, T. (2017). Chemical functionalization and characterization of graphene-based materials. *Chemical Society Reviews*, *46*(15), 4464–4500. https://doi.org/10.1039/c7cs00229g

Byfield, F. J., Reen, R. K., Shentu, T. P., Levitan, I. & Gooch, K. J. (2009). Endothelial actin and cell stiffness is modulated by substrate stiffness in 2D and 3D. *Journal of Biomechanics*, *42*(8), 1114–1119. https://doi.org/10.1016/j.jbiomech.2009.02.012

Cançado, L. G., Jorio, A., Ferreira, E. H. M., Stavale, F., Achete, C. A., Capaz, R. B., Moutinho, M. V. O., Lombardo, A., Kulmala, T. S. & Ferrari, A. C. (2011). Quantifying defects in graphene via Raman spectroscopy at different excitation energies. *Nano Letters*, *11*(8), 3190–3196. https://doi.org/10.1021/nl201432g

Cellot, G., Cilia, E., Cipollone, S., Rancic, V., Sucapane, A., Giordani, S., Gambazzi, L., Markram, H., Grandolfo, M., Scaini, D., Gelain, F., Casalis, L., Prato, M., Giugliano, M. & Ballerini, L. (2009). Carbon nanotubes might improve neuronal performance by favouring electrical shortcuts. *Nature Nanotechnology*, *4*(2), 126–133. https://doi.org/10.1038/nnano.2008.374

Cellot, G., Lagonegro, P., Tarabella, G., Scaini, D., Fabbri, F., Iannotta, S., Prato, M., Salviati, G. & Ballerini, L. (2016). PEDOT:PSS interfaces support the development of neuronal synaptic networks with reduced neuroglia response in vitro. *Frontiers in Neuroscience*, *9*(JAN), 1–11. https://doi.org/10.3389/fnins.2015.00521

Cellot, G., Toma, F. M., Varley, Z. K., Laishram, J., Villari, A., Quintana, M., Cipollone, S., Prato, M. &

Ballerini, L. (2011). Carbon nanotube scaffolds tune synaptic strength in cultured neural circuits: Novel frontiers in nanomaterial-tissaue interactions. *Journal of Neuroscience*, *31*(36), 12945–12953. https://doi.org/10.1523/JNEUROSCI.1332-11.2011

Criado, A., Melchionna, M., Marchesan, S. & Prato, M. (2015). The Covalent Functionalization of Graphene on Substrates. *Angewandte Chemie - International Edition*, *54*(37), 10734–10750. https://doi.org/10.1002/anie.201501473

De La Rosa, C. J. L., Sun, J., Lindvall, N., Cole, M. T., Nam, Y., Löffler, M., Olsson, E., Teo, K. B. K. & Yurgens, A. (2013). Frame assisted H2O electrolysis induced H2 bubbling transfer of large area graphene grown by chemical vapor deposition on Cu. *Applied Physics Letters*, *102*(2). https://doi.org/10.1063/1.4775583

Deng, Y. H., Li, L. H., He, J., Li, M., Zhang, Y., Wang, X. M., Cui, F. Z. & Xia, H. (2015). Self-assembled monolayers of alkanethiolates on surface chemistry groups in osteosarcoma cells. *Molecular Medicine Reports*, *11*(2), 975–981. https://doi.org/10.3892/mmr.2014.2876

Ding, Y., Xu, G. K. & Wang, G. F. (2017). On the determination of elastic moduli of cells by AFM based indentation. *Scientific Reports*, *7*, 1–8. https://doi.org/10.1038/srep45575

Dong, X., Wang, P., Fang, W., Su, C. Y., Chen, Y. H., Li, L. J., Huang, W. & Chen, P. (2011). Growth of large-sized graphene thin-films by liquid precursor-based chemical vapor deposition under atmospheric pressure. *Carbon*, *49*(11), 3672–3678. https://doi.org/10.1016/j.carbon.2011.04.069

Fabbro, A., Scaini, D., León, V., Vázquez, E., Cellot, G., Privitera, G., Lombardi, L., Torrisi, F., Tomarchio, F., Bonaccorso, F., Bosi, S., Ferrari, A. C., Ballerini, L. & Prato, M. (2016). Graphene-Based interfaces do not alter target nerve cells. *ACS Nano*, *10*(1), 615–623. https://doi.org/10.1021/acsnano.5b05647

Fan, Y. W., Cui, F. Z., Hou, S. P., Xu, Q. Y., Chen, L. N. & Lee, I. S. (2002). Culture of neural cells on silicon wafers with nano-scale surface topograph. *Journal of Neuroscience Methods*, *120*(1), 17–23. https://doi.org/10.1016/S0165-0270(02)00181-4

Faugeras, C., Amado, M., Kossacki, P., Orlita, M., Sprinkle, M., Berger, C., De Heer, W. A. & Potemski, M. (2009). Tuning the electron-phonon coupling in multilayer graphene with magnetic fields. *Physical Review Letters*, *103*(18), 1–4. https://doi.org/10.1103/PhysRevLett.103.186803

Ferrari, A. C., Meyer, J. C., Scardaci, V., Casiraghi, C., Lazzeri, M., Mauri, F., Piscanec, S., Jiang, D., Novoselov, K. S., Roth, S. & Geim, A. K. (2006). Raman spectrum of graphene and graphene layers. *Physical Review Letters*, *97*(18), 1–4. https://doi.org/10.1103/PhysRevLett.97.187401

Franceschi Biagioni, A., Cellot, G., Pati, E., Lozano, N., Ballesteros, B., Casani, R., Coimbra, N. C., Kostarelos, K. & Ballerini, L. (2021). Graphene oxide prevents lateral amygdala dysfunctional synaptic plasticity and reverts long lasting anxiety behavior in rats. *Biomaterials*, *271*. https://doi.org/10.1016/j.biomaterials.2021.120749

Franco, M., Alves, R., Perinka, N., Tubio, C., Costa, P. & Lanceros-Mendéz, S. (2020). Water-Based Graphene Inks for All-Printed Temperature and Deformation Sensors. *ACS Applied Electronic Materials*, *2*(9), 2857–2867. https://doi.org/10.1021/acsaelm.0c00508

Grimm, K. B., Oberleithner, H. & Fels, J. (2014). Fixed endothelial cells exhibit physiologically relevant nanomechanics of the cortical actin web. *Nanotechnology*, *25*(21). https://doi.org/10.1088/0957-4484/25/21/215101

Grishagin, I. V. (2015). Automatic cell counting with ImageJ. *Analytical Biochemistry*, *473*(December), 63–65. https://doi.org/10.1016/j.ab.2014.12.007

Gupta, M., Doss, B., Lim, C. T., Voituriez, R. & Ladoux, B. (2016). Single cell rigidity sensing: A complex relationship between focal adhesion dynamics and large-scale actin cytoskeleton remodeling. *Cell Adhesion and Migration*, *10*(5), 554–567. https://doi.org/10.1080/19336918.2016.1173800

Hossain, Z., Walsh, M. A. & Hersam, M. C. (2010). *Hossain_Scanning Tunneling Microscopy, Spectroscopy, and Nanolithography of Epitaxial Graphene Chemically Modified with Aryl Moieties_JACS_2010.pdf*. *29*, 15399–15403.

Jäkel, S. & Dimou, L. (2017). Glial cells and their function in the adult brain: A journey through the history of their ablation. *Frontiers in Cellular Neuroscience*, *11*(February), 1–17. https://doi.org/10.3389/fncel.2017.00024

Jeong, J. T., Choi, M. K., Sim, Y., Lim, J. T., Kim, G. S., Seong, M. J., Hyung, J. H., Kim, K. S., Umar, A. & Lee, S. K. (2016). Effect of graphene oxide ratio on the cell adhesion and growth behavior on a graphene oxide-coated silicon substrate. *Scientific Reports*, *6*(September), 1–10. https://doi.org/10.1038/srep33835

Jiang, F., DC, L., F, H. & NA, L. (2011). Probing Mechanical Adaptation of Neurite Outgrowth on a Hydrogel Material Using Atomic Force Microscopy. *Annals of Biomedical Engineering*, *39*(2), 706–713. https://doi.org/10.1007/s10439-010-0194-0.Probing

Karki, N., Tiwari, H., Tewari, C., Rana, A., Pandey, N., Basak, S. & Sahoo, N. G. (2020). Functionalized graphene oxide as a vehicle for targeted drug delivery and bioimaging applications. *Journal of Materials Chemistry B*, *8*(36), 8116–8148. https://doi.org/10.1039/d0tb01149e

Keselowsky, B. G., Collard, D. M. & García, A. J. (2004). Surface chemistry modulates focal adhesion composition and signaling through changes in integrin binding. *Biomaterials*, *25*(28), 5947–5954. https://doi.org/10.1016/j.biomaterials.2004.01.062

Kitko, K. E., Hong, T., Lazarenko, R. M., Ying, D., Xu, Y. Q. & Zhang, Q. (2018). Membrane cholesterol mediates the cellular effects of monolayer graphene substrates. *Nature Communications*, *9*(1). https://doi.org/10.1038/s41467-018-03185-0

Lee, J. W., Serna, F., Nickels, J. & Schmidt, C. E. (2006). Carboxylic acid-functionalized conductive polypyrrole as a bioactive platform for cell adhesion. *Biomacromolecules*, *7*(6), 1692–1695. https://doi.org/10.1021/bm060220q

Lee, W. C., Lim, C. H. Y. X., Shi, H., Tang, L. A. L., Wang, Y., Lim, C. T. & Loh, K. P. (2011). Origin of enhanced stem cell growth and differentiation on graphene and graphene oxide. *ACS Nano*, *5*(9), 7334–7341. https://doi.org/10.1021/nn202190c

Lessey, E. C., Guilluy, C. & Burridge, K. (2012). From mechanical force to RhoA activation. *Biochemistry*, *51*(38), 7420–7432. https://doi.org/10.1021/bi300758e

Lévy, R. & Maaloum, M. (2002). Measuring the spring constant of atomic force microscope cantilevers: Thermal fluctuations and other methods. *Nanotechnology*, *13*(1), 33–37. https://doi.org/10.1088/0957-4484/13/1/307

Li, N., Zhang, X., Song, Q., Su, R., Zhang, Q., Kong, T., Liu, L., Jin, G., Tang, M. & Cheng, G. (2011). The promotion of neurite sprouting and outgrowth of mouse hippocampal cells in culture by graphene substrates. *Biomaterials*, *32*(35), 9374–9382. https://doi.org/10.1016/j.biomaterials.2011.08.065

Lovat, V., Pantarotto, D., Lagostena, L., Cacciari, B., Grandolfo, M., Righi, M., Spalluto, G., Prato, M. & Ballerini, L. (2005). Carbon nanotube substrates boost neuronal electrical signaling. *Nano Letters*, *5*(6), 1107–1110. https://doi.org/10.1021/nl050637m

Lu, Y., Lyu, H., Richardson, A. G., Lucas, T. H. & Kuzum, D. (2016). Flexible Neural Electrode Array Based-on Porous Graphene for Cortical Microstimulation and Sensing. *Scientific Reports*, *6*(September), 1–9. https://doi.org/10.1038/srep33526

Luo, Q., Kuang, D., Zhang, B. & Song, G. (2016). Cell stiffness determined by atomic force microscopy and its correlation with cell motility. *Biochimica et Biophysica Acta - General Subjects*, *1860*(9), 1953–1960. https://doi.org/10.1016/j.bbagen.2016.06.010

Malard, L. M., Pimenta, M. A., Dresselhaus, G. & Dresselhaus, M. S. (2009). Raman spectroscopy in graphene. *Physics Reports*, *473*(5–6), 51–87. https://doi.org/10.1016/j.physrep.2009.02.003

Megías, M., Emri, Z., Freund, T. F. & Gulyás, A. I. (2001). Total number and distribution of inhibitory and excitatory synapses on hippocampal CA1 pyramidal cells. *Neuroscience*, *102*(3), 527–540. https://doi.org/10.1016/S0306-4522(00)00496-6

Nayak, T. R., Andersen, H., Makam, V. S., Khaw, C., Bae, S., Xu, X., Ee, P. L. R., Ahn, J. H., Hong, B. H., Pastorin, G. & Özyilmaz, B. (2011). Graphene for controlled and accelerated osteogenic differentiation of human mesenchymal stem cells. *ACS Nano*, *5*(6), 4670–4678. https://doi.org/10.1021/nn200500h

Nečas, D. & Klapetek, P. (2012). Gwyddion: An open-source software for SPM data analysis. *Central European Journal of Physics*, *10*(1), 181–188. https://doi.org/10.2478/s11534-011-0096-2

Nguyen, V. T., Le, H. D., Nguyen, V. C., Ngo, T. T. T., Le, D. Q., Nguyen, X. N. & Phan, N. M. (2013). Synthesis of multi-layer graphene films on copper tape by atmospheric pressure chemical vapor deposition method. *Advances in Natural Sciences: Nanoscience and Nanotechnology*, *4*(3). https://doi.org/10.1088/2043-6262/4/3/035012

Pampaloni, N. P., Lottner, M., Giugliano, M., Matruglio, A., D'Amico, F., Prato, M., Garrido, J. A., Ballerini, L. & Scaini, D. (2018). Single-layer graphene modulates neuronal communication and augments membrane ion currents. *Nature Nanotechnology*, *13*(8), 755–764. https://doi.org/10.1038/s41565-018-0163-6

Pampaloni, N., Scaini, D., Perissinotto, F., Bosi, S., Prato, M. & Ballerini, L. (2018). Sculpting neurotransmission during synaptic development by 2D nanostructured interfaces. *Nanomedicine: Nanotechnology, Biology, and Medicine*, *14*(7), 2521–2532. https://doi.org/10.1016/j.nano.2017.01.020

Paulus, G. L. C., Wang, Q. H. & Strano, M. S. (2013). Covalent electron transfer chemistry of graphene with diazonium salts. *Accounts of Chemical Research*, *46*(1), 160–170. https://doi.org/10.1021/ar300119z

Peyton, S. R., Raub, C. B., Keschrumrus, V. P. & Putnam, A. J. (2006). The use of poly(ethylene glycol) hydrogels to investigate the impact of ECM chemistry and mechanics on smooth muscle cells. *Biomaterials*, *27*(28), 4881–4893. https://doi.org/10.1016/j.biomaterials.2006.05.012

Raastad, M., Storm, J. F. & Andersen, P. (1992). Putative Single Quantum and Single Fibre Excitatory Postsynaptic Currents Show Similar Amplitude Range and Variability in Rat Hippocampal Slices. *European Journal of Neuroscience*, *4*(1), 113–117. https://doi.org/10.1111/j.1460-9568.1992.tb00114.x

Rago, I., Rauti, R., Bevilacqua, M., Calaresu, I., Pozzato, A., Cibinel, M., Dalmiglio, M., Tavagnacco, C., Goldoni, A. & Scaini, D. (2019). Carbon Nanotubes, Directly Grown on Supporting Surfaces, Improve Neuronal Activity in Hippocampal Neuronal Networks. *Advanced Biosystems*, *3*(5), 1–13. https://doi.org/10.1002/adbi.201800286

Rajnicek, A. M., Britland, S. & McCaig, C. D. (1997). Contact guidance of CNS neurites on grooved quartz: Influence of groove dimensions, neuronal age and cell type. *Journal of Cell Science*, *110*(23), 2905–2913. https://doi.org/10.1242/jcs.110.23.2905

Randviir, E. P., Brownson, D. A. C. & Banks, C. E. (2014). A decade of graphene research: Production, applications and outlook. *Materials Today*, *17*(9), 426–432. https://doi.org/10.1016/j.mattod.2014.06.001

Rauti, R., Cellot, G., D'Andrea, P., Colliva, A., Scaini, D., Tongiorgi, E. & Ballerini, L. (2020). BDNF impact on synaptic dynamics: Extra or intracellular long-term release differently regulates cultured hippocampal synapses. *Molecular Brain*, *13*(1), 1–16. https://doi.org/10.1186/s13041-020-00582-9

Rauti, R., Secomandi, N., Martín, C., Bosi, S., Severino, F. P. U., Scaini, D., Prato, M., Vázquez, E. & Ballerini, L. (2020). Tuning Neuronal Circuit Formation in 3D Polymeric Scaffolds by Introducing Graphene at the Bio/Material Interface. *Advanced Biosystems*, *4*(4), 1–12. https://doi.org/10.1002/adbi.201900233

Reina, A., Jia, X., Ho, J., Nezich, D., Son, H., Bulovic, V., Dresselhaus, M. S. & Kong, J. (2009). Large Area, Few-Layer Graphene Films on Arbitrary Substrates by Chemical Vapor Deposition. *Nano Letters*, *9*, 30–35.

Reina, G., González-Domínguez, J. M., Criado, A., Vázquez, E., Bianco, A. & Prato, M. (2017). Promises, facts and challenges for graphene in biomedical applications. *Chemical Society Reviews*, *46*(15), 4400–4416. https://doi.org/10.1039/c7cs00363c

Ren, Y. J., Zhang, H., Huang, H., Wang, X. M., Zhou, Z. Y., Cui, F. Z. & An, Y. H. (2009). In vitro behavior of neural stem cells in response to different chemical functional groups. *Biomaterials*, *30*(6), 1036–1044. https://doi.org/10.1016/j.biomaterials.2008.10.028

Ryoo, S., Kim, Y., Kim, M. & Min, D. (2010). Behaviors of NIH-3T3 Fibroblasts on. *ACS Nano*, *4*(11), 6587–6598.

Saphirstein, R. J., Gao, Y. Z., Jensen, M. H., Gallant, C. M., Vetterkind, S., Moore, J. R. & Morgan, K. G. (2013). The Focal Adhesion: A Regulated Component of Aortic Stiffness. *PLoS ONE*, *8*(4). https://doi.org/10.1371/journal.pone.0062461

Sarnat, H. B., Nochlin, D. & Born, D. E. (1998). Neuronal nuclear antigen (NeuN): A marker of neuronal maturation in the early human fetal nervous system. *Brain and Development*, *20*(2), 88–94. https://doi.org/10.1016/S0387-7604(97)00111-3

Schindelin, J., Arganda-Carreras, I., Frise, E., Kaynig, V., Longair, M., Pietzsch, T., Preibisch, S., Rueden, C., Saalfeld, S., Schmid, B., Tinevez, J. Y., White, D. J., Hartenstein, V., Eliceiri, K., Tomancak, P. & Cardona, A. (2012). Fiji: An open-source platform for biological-image analysis. *Nature Methods*, *9*(7), 676–682. https://doi.org/10.1038/nmeth.2019

Shin, S. R., Li, Y. C., Jang, H. L., Khoshakhlagh, P., Akbari, M., Nasajpour, A., Zhang, Y. S., Tamayol, A. & Khademhosseini, A. (2016). Graphene-based materials for tissue engineering. *Advanced Drug Delivery Reviews*, *105*, 255–274. https://doi.org/10.1016/j.addr.2016.03.007

Sneddon, I. N. (1965). The relation between load and penetration in the axisymmetric boussinesq problem for a punch of arbitrary profile. *International Journal of Engineering Science*, *3*(1), 47–57. https://doi.org/10.1016/0020-7225(65)90019-4

Tang, M., Song, Q., Li, N., Jiang, Z., Huang, R. & Cheng, G. (2013). Enhancement of electrical signaling in neural networks on graphene films. *Biomaterials*, *34*(27), 6402–6411. https://doi.org/10.1016/j.biomaterials.2013.05.024

Tee, S. Y., Fu, J., Chen, C. S. & Janmey, P. A. (2011). Cell shape and substrate rigidity both regulate cell stiffness. *Biophysical Journal*, *100*(5), L25–L27. https://doi.org/10.1016/j.bpj.2010.12.3744

Torrisi, F., Hasan, T., Wu, W., Sun, Z., Lombardo, A., Kulmala, T. S., Hsieh, G. W., Jung, S., Bonaccorso, F., Paul, P. J., Chu, D. & Ferrari, A. C. (2012). Inkjet-printed graphene electronics. *ACS Nano*, *6*(4), 2992–3006. https://doi.org/10.1021/nn2044609

Ulloa, L. S., Perissinotto, F., Rago, I., Goldoni, A., Santoro, R., Pesce, M., Casalis, L. & Scaini, D. (2021). *Carbon Nanotubes Substrates Alleviate Pro-Calcific Evolution in Porcine Valve Interstitial Cells*. 1–20.

Xu, M., Zhu, J., Wang, F., Xiong, Y., Wu, Y., Wang, Q., Weng, J., Zhang, Z., Chen, W. & Liu, S. (2016). Improved In Vitro and In Vivo Biocompatibility of Graphene Oxide through Surface Modification: Poly(Acrylic Acid)-Functionalization is Superior to PEGylation. *ACS Nano*, *10*(3), 3267–3281. https://doi.org/10.1021/acsnano.6b00539

Yang, L., Gao, Q., Ge, L., Zhou, Q., Warszawik, E. M., Bron, R., Lai, K. W. C. & Van Rijn, P. (2020). Topography induced stiffness alteration of stem cells influences osteogenic differentiation. *Biomaterials Science*, *8*(9), 2638–2652. https://doi.org/10.1039/d0bm00264j

Zhang, L., Lu, Z., Zhao, Q., Huang, J., Shen, H. & Zhang, Z. (2011). Enhanced chemotherapy efficacy by sequential delivery of siRNA and anticancer drugs using PEI-grafted graphene oxide. *Small*, *7*(4), 460–464. https://doi.org/10.1002/smll.201001522

Zhou, K., Motamed, S., Thouas, G. A., Bernard, C. C., Li, D., Parkington, H. C., Coleman, H. A., Finkelstein, D. I. & Forsythe, J. S. (2016). Graphene functionalized scaffolds reduce the inflammatory response and supports endogenous neuroblast migration when implanted in the Adult Brain. *PLoS ONE*, *11*(3), 1–15. https://doi.org/10.1371/journal.pone.0151589

Zhou, X., Wang, F., Zhu, Y. & Liu, Z. (2011). Graphene modified LiFePO4 cathode materials for high power lithium ion batteries. *Journal of Materials Chemistry*, *21*(10), 3353–3358. https://doi.org/10.1039/c0jm03287e

Figures

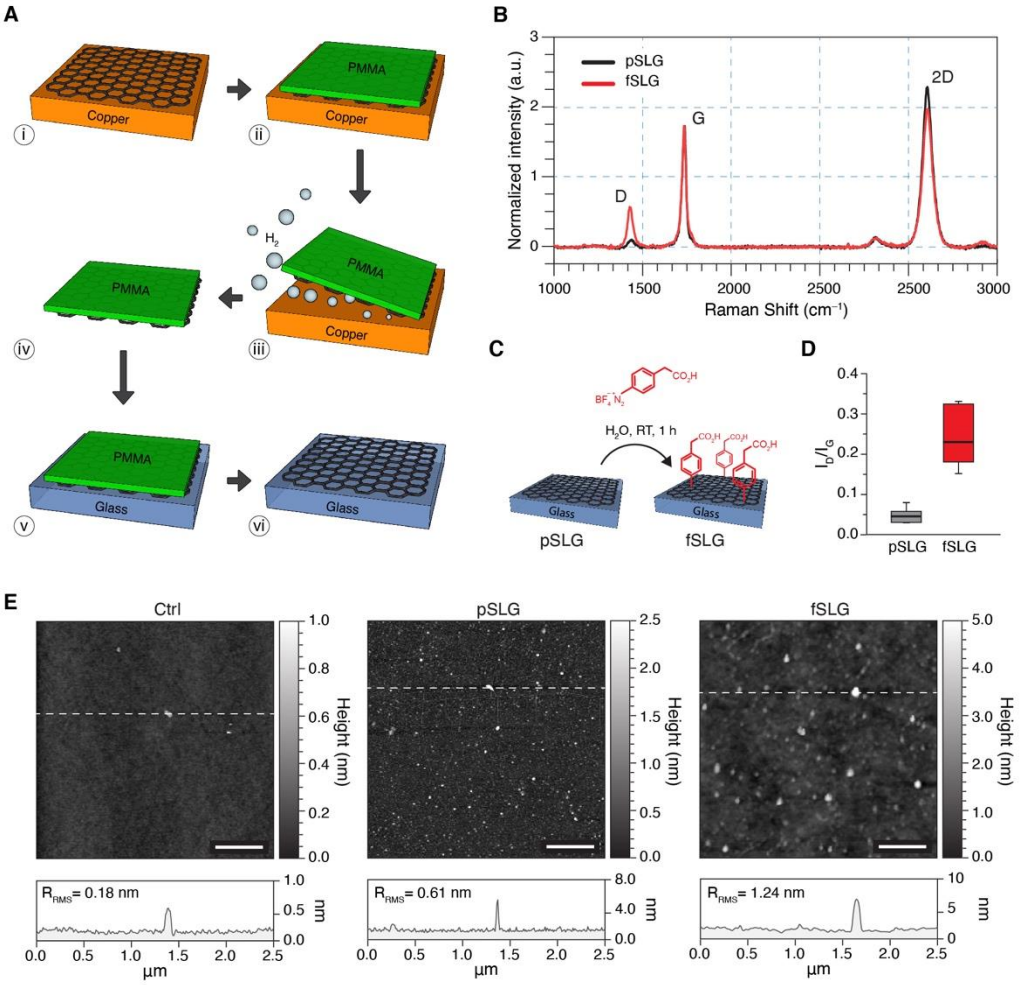

Figure 1. Fabrication and characterization of pSLG and fSLG. A) *Scheme of the graphene transfer process from copper to glass exploiting an electrochemical delamination procedure: (i) CVD-grown single-layer graphene on copper; (ii) deposition of a supportive PMMA film; (iii) electrochemical delamination; (iv) free-standing graphene/PMMA layers; (v) transfer on glass; (vi) dissolution of the sacrificial PMMA layer.* ***B)*** *Average of 20 randomly-acquired Raman spectra of a graphene sample before the chemical functionalization (pSLG, in black) and after (fSLG, in red) exhibiting the typical bands of CVD graphene in both conditions (□I_D/I_G of about 0.29). It is worth noting that peaks' shape was impacted by the sporadic presence of double layer nucleation sites.* ***C)*** *Schematic of the diazonium coupling onto pSLG by using 4-(carboxymethyl)benzene diazonium tetrafluoroborate to obtain fSLG.* ***D)*** *Box plot of the I_D/I_G ratio for pSLG and fSLG. The plot showed a significant change after functionalization reaction which confirms the covalent modification of graphene.* ***E)*** *AFM topographic images of glass (left), pSLG (middle), and fSLG (right) surfaces before cell plating. Below, the representative topographic profiles relative to the highlighted lines in the images are shown.*

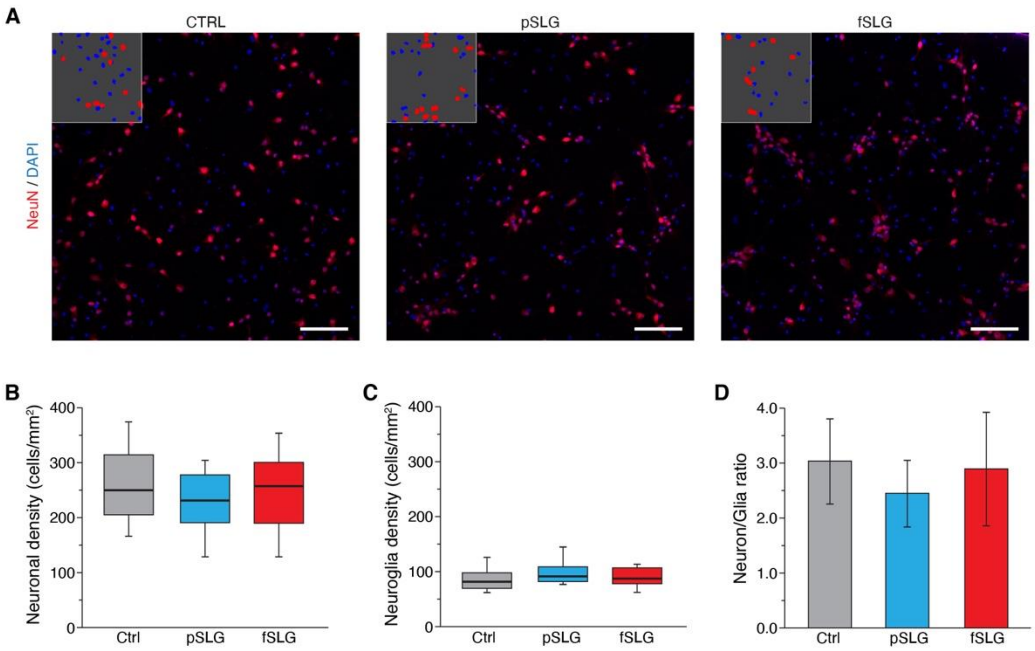

Figure 2. Graphene-based substrates does not affect the cell density. A) *Representative fluorescence images of hippocampal cells on glass control (left), pSLG (middle) and fSLG (right). Cells were stained for NeuN (red) and DAPI (blue). Insets show representative portions of the images after the binarization and segmentation procedure highlighting DAPI-positive regions and NeuN-positive ones. Scale bars: 100µm.* ***B)*** *Box plot of neuronal cells densities showing no significant difference across the three conditions (p>0.05).* ***C)*** *Box plot of glial cells density. No statistically significant differences were found between experimental groups (p>0.05).* ***D)*** *Bars plot highlighting the consistency of the neuronal/glial cells density ratio across the three conditions (p>0.05).*

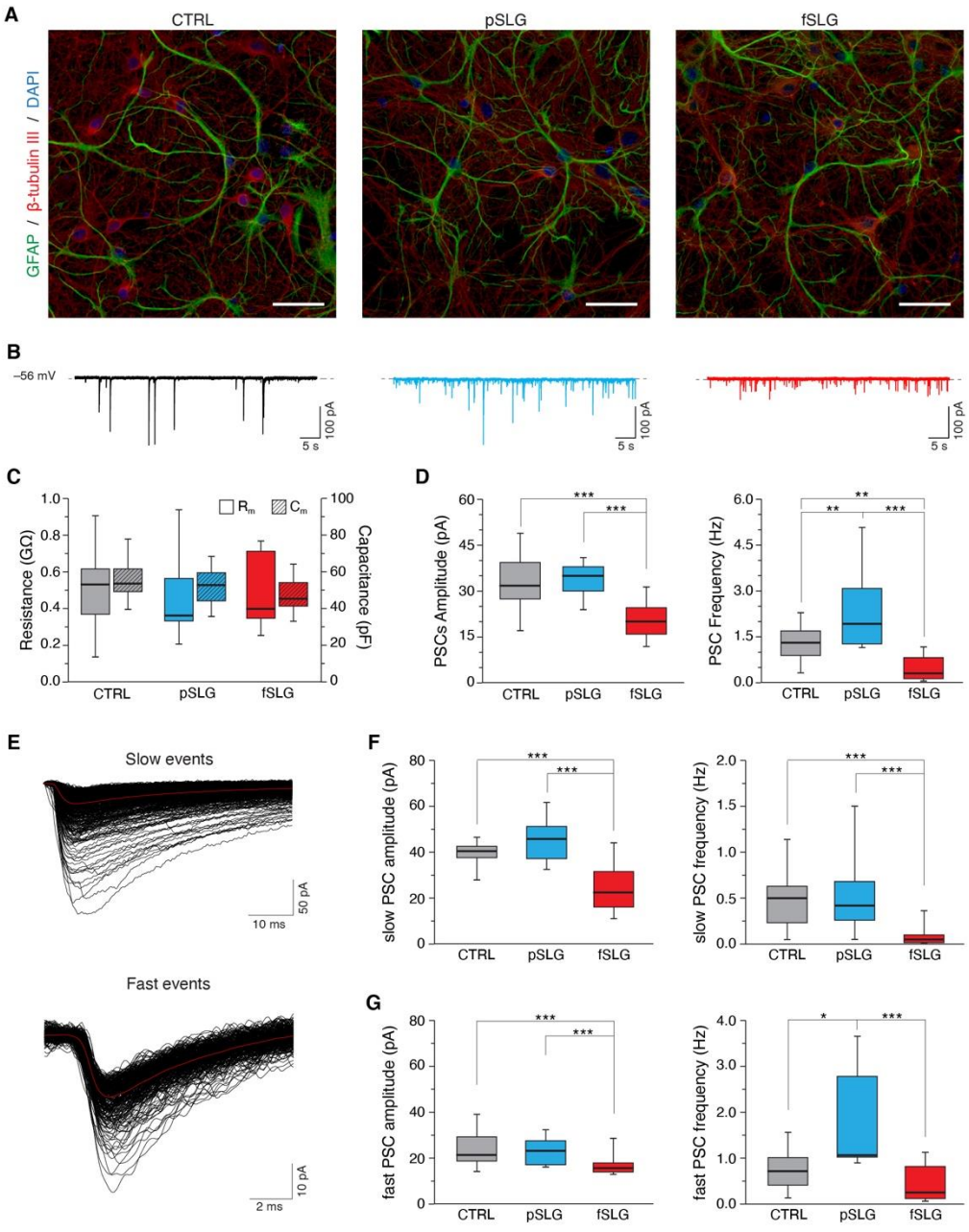

Figure 3. Graphene-based substrates modulate neuronal network activity. A) *Representative confocal micrographs of hippocampal cells grown on glass control, pSLG and fSLG***.** *Neurons were labeled against β-tubulin III (red), astrocytes against GFAP (green) and nuclei with DAPI (blue). Scale bars: 40μm.* ***B)*** *Representative voltage-clamp current traces for controls (in black, on the left), pSLG (in blue, on the middle) and fSLG (in red, on the right).* ***C)*** *Box plot summarizing neuronal cell membrane resistances (R_m, plain boxes) and capacitances (R_c, striped boxes) across the three supporting substrates.* ***D)*** *Boxplot of PSCs amplitudes (left) and frequencies (right). A significant difference was detected only in fSLG PSCs amplitudes, while pSLG and fSLG oppositely modulated neuronal PSCs frequencies (up-regulating and down-regulating, respectively).* ***E)*** *Representative PSCs traces of slow (top) and fast (bottom) events, identified on the basis of*

their decay time (τ = 22.3±6.64 ms and τ = 3.79±1.31 ms, respectively; n=40, in red the averaged events). ***F)*** *Box plots of slow PSCs amplitudes (left) and frequencies (right) highlighting a significant reduction of both by the fSLG.* ***G)*** *Box plots of fast PSCs amplitudes (left) and frequencies (right) highlighting a significant reduction in both amplitude and frequency by the fSLG, but an enhanced frequency of PSC activity in pSLG interfaced neurons.*

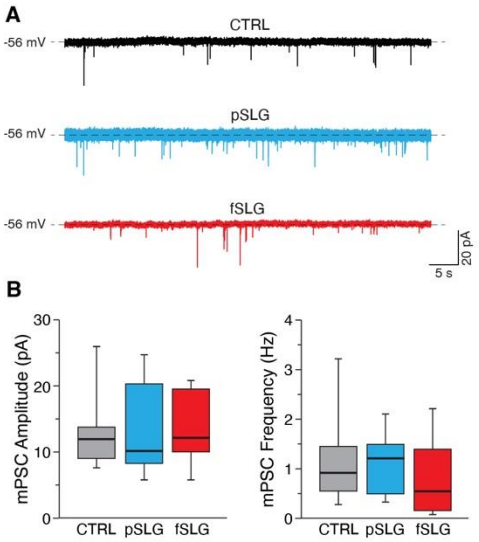

Figure 4. Graphene-based substrates do not alter structural functionality of synapses at pre- and post-synaptic level. ***A)*** *Representative traces of mPSCs for the three conditions under investigation.* ***B)*** *Box plots of mPSCs amplitudes (left) and frequencies (right) measured from neuronal networks developed above glass, pSLG and fSLG substrates. No significant differences were detected across the three experimental groups in terms of both mPSCs amplitudes nor frequencies (p>0.05).*

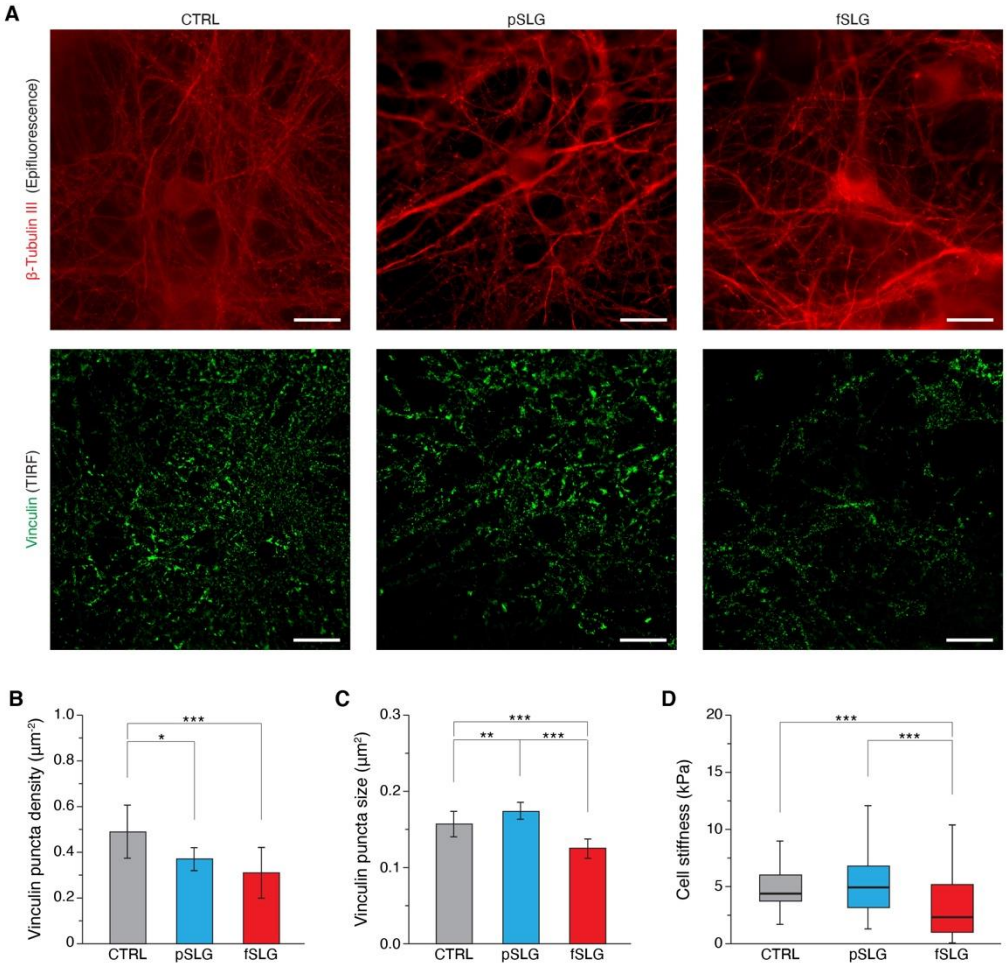

Figure 5. Focal adhesion distribution and cell stiffness. A) *TIRF-based investigation of hippocampal cells on glass control (left column), pSLG (central column) and fSLG (right column). Micrographs in the first row show cells stained against β-tubulin III (in red, acquired as an epi-fluorescence signal), those in the second row show cells labelled against vinculin (in green, acquired as a TIRF signal). Scale bars: 20 μm.* ***B)*** *Bar plot summarizing vinculin puncta density across the three conditions. Significant differences were detected.* ***C)*** *Bar plot showing vinculin-positive puncta size. Statistically significant differences emerged between the three experimental groups.* ***D)*** *Box plot depicting cell stiffnesses measured on neurons grown above the three examined substrates. A significant reduction in cell stiffness was found in the case of fSLG-interfaced cells.*

Table S1

Sample	I_D/I_G		$\Delta I_D/I_G$	*nD* (cm^{-2})
	pSLG	pSLG		
1	0.04	0.33	0.29	6.52×10^{10}
2	0.05	0.23	0.18	4.04×10^{10}
3	0.03	0.19	0.16	3.60×10^{10}
4	0.03	0.23	0.20	4.49×10^{10}
5	0.08	0.15	0.07	1.57×10^{10}
6	0.05	0.32	0.27	6.07×10^{10}

Table S1. *The table summarizes the I_D/I_G ratio for pSLG and fSLG, and defect density for fSLG. Values are relative of six graphene samples and represent measurements performed before the chemical functionalization (pSLG, gray column) and after (fSLG, red column).*

3.3 PEG-functionalized DWCNT 3D foams promote the formation of neuronal hippocampal networks

Introduction

In the attempt to evaluate the synergic contribution of extra-cellular matrix mechanical and chemical cues, primary hippocampal neurons were grown on three-dimensional carbon nanotubes (CNTs) foams where specific chemical functionalizations were introduced with the intent to modify substrate stiffness and introduce neuronal-specific responses in the interfaced networks. In these preliminary experiments, we evaluated the neuronal network morphology uncovering a significantly different adaptation induced by pristine and functionalized CNTs foams in the form of cell distribution, elongation and orientation. Furthermore, from a functional point of view, the neuronal functionality was monitored in terms of spontaneous calcium oscillations. It was highlighted an increased calcium activity in cells developed above the stiffer functionalized CNTs compared to the pristine ones.

Experimental procedures

We attempted to investigate the synergic contribution of surface morphology, chemical functionalization and substrate stiffness in modulating neuronal network adaptation from both morphological and functional perspectives. To accomplish this task, we exploited double-walled carbon nanotubes (DWCNTs). Three-dimensional foams were produced starting from two different types of carbon nanotubes: pristine DWCNTs and functionalized DWCNTs (Figure 3.1A). Specifically, to obtain the functionalized nanotubes, pristine DWCNTs samples underwent a process of PEGylation, where polyethylene glycol (PEG) chains cross-link the DWCNTs. The choice of PEG derivatives for the chemical modification of the DWCNT surface was made based on the well-demonstrated ability of this synthetic material to inhibit inflammatory responses and improve axonal repair and regeneration into the lesion cavity after a spinal cord injury (Kong et al., 2017; Roman et al., 2011). Three-dimensional foams were obtained following a template-dissolution approach. In

brief, 15 mg of pristine or functionalized DWCNTs powder was sonicated for 15 minutes in THF and subsequently mixed with 150 mg of NaCl crystals of about 100–250 μm in side size. CNT/NaCl agglomerates were let drying in an oven at 60 °C for 6 hours and, subsequently, the NaCl phase was dissolved by a 48 hours water immersion. The resulting foams were characterized by macroscopic dimensions and very low volume-to-cavity ratio (Figure 3.1B). Scanning electron micrographs revealed that the microscopic surface of such foams is constituted by a continuous thin film of interconnected DWCNT (Figure 3.1C). The mechanical properties of the foams obtained from pristine DWCNTs and functionalized DWCNTs were investigated in the laboratory of Juan Jose Vilatela at IMDEA Materials Institute, Madrid, ES. Tensile tests revealed that the chemical functionalization, and the consequent DWCNT cross-linkage, gave rise to a more robust foam structures with significantly enhanced stiffness when compared to the one made by pristine DWCNTs (Figure 3.1D, red and black traces, respectively). Cross-linked foams are almost five times stronger than pristine samples, with a sample specific tensile strength of about 4.289 MPa (Figure 3.1E). Comparing the specific stiffness values (about 382.11 MPa for functionalized DWCNT and 37.23 MPa for pristine ones), we may assume that these notable changes in the mechanical performance are not associated with a simple gain in density of the material, but with a more efficient stress transfer by the PEG-chains between cross-linked CNTs. From this point on we will refer to pristine and functionalized DWCNTs foams as CNTs and fCNTs, respectively. All materials were prepared and provided by the team of Professor Maurizio Prato at the laboratories in CIC biomaGUNE, San Sebastian (ES), and the corresponding characterization were performed or coordinated there.

CNTs and fCNTs samples were interfaced with mammalian neurons and glial cells isolated from the neonatal rat hippocampus and compared to cultures let to develop on glass controls (see Methods section - Cell culture preparation, page 66). Immunofluorescence confocal microscopy allowed us to identify neurons and astrocytes, labelled with β-tubulin III and glial fibrillary acidic protein (GFAP), respectively (see Methods section – immunofluorescence, page 68). Furthermore, in order to visualize foams' structure confocal under reflection mode was used.

By taking advantage of live calcium imaging, we monitored synaptic activity focused, in particular, assessing if the chemical functionalization of DWCNTs and subsequent cross-linking may control the formation of connected networks characterized by the emergence of spontaneous network activities. In brief, hippocampal cultures were incubated with 4 μM Ca^{2+} dye Oregon Green 488 BAPTA-1 AM (Molecular Probes) for 40 min at 37 °C, 5% CO2. The Petri dish containing the sample was then mounted in a fixed-stage upright microscope (Eclipse FN1, Nikon). Cultures were continuously perfused at 5 mL/min rate at room temperature (RT) with extracellular saline solution, which is composed of (in mM): 150 NaCl, 4 KCl, 2 $CaCl_2$, 1 $MgCl_2$, 10 HEPES, 10 glucose (all Sigma), pH 7.4. Ca^{2+} dye was excited at 488 nm with a mercury lamp; excitation light was separated from the light emitted from the sample using a 505 nm dichroic mirror and ND filter (1/32). Spontaneous calcium transients were recorded with a 20× water immersion objective (Fluor, 0.50W NA, Nikon) using an EMCCD camera (iXon Ultra 897, AndorTM, Oxford Instruments) controlled by a computer through NIS-elements D (Nikon) software. Images were acquired each 150 ms at 10 MHz readout compensating the read noise with ×300 EM gain. Spontaneous activity was therefore recorded. In order to induce rhythmic bursts 5 μM gabazine (Sigma-Aldrich), diluted in the saline solution, was added after 10 min of recording. Finally, 1 μM tetrodotoxin (TTX, Latoxan), which is a voltage-gated fast Na+ channel blocker, was added to confirm the neuronal nature of the recorded signals. Recorded images were analyzed off-line with Fiji (selecting region of interest, ROI, around cell bodies) and Clampfit (pClamp software, 11.0.3 version; Axon Instruments). Intracellular Ca^{2+} transients were detected as signals that exceed at least five times the standard deviation of the noise and were expressed as fractional amplitude increase ($\Delta F/F0$, where $F0$ is the baseline fluorescence level and ΔF is the rise over baseline). The inter events interval (IEI), time between the onset of consecutive Ca^{2+} events, was then calculated. IEI values recorded under the same experimental conditions were pooled together and averaged for further comparison. The correlation between the Ca^{2+} events among all cells recorded from the same field was assessed by cross-correlation analysis, as previously described (Bosi et al., 2015).

Results

We identified neurons and astrocytes by immunofluorescence microscopy targeting, respectively, β-tubulin III and GFAP, two widely used cytoskeletal markers specifying the two cellular phenotypes. In Figure 3.2A the number of neurons (in red) and GFAP-positive astrocytes (in green) were displayed for cultures interfaced to both CNT-foams. The fact that both materials allowed effective cell adhesion and survival is supportive of the idea of CNT and fCNT cytocompatibility. Anyhow, some qualitative differences emerged by comparing the morphology of cells interfaced with the two substrates, as revealed also by Figure 3.2B, where the foams are clearly visible by visualizing them in confocal reflection mode (in grey). Specifically, neurons adherent to CNT developed a network mostly constituted by sparse cells with only a partial superimposition with stellate glial cells while, on the other hand, fCNT-interfaced neurons are organized in small tightly interconnected clusters, mostly adherent on large and flat glial cells. Interestingly, on fCNT-foam, cellular networks followed the curved surface of the foam giving rise, apparently, to a higher cell colonization of the material.

To investigate the impact of CNT and fCNT foams on network functionality, we live-monitored the network activity emerging from a small sub-group of neurons by fluorescence calcium imaging. This analysis has the advantage to combine in a single measurement the evaluation of both the morphology and calcium-signaling of the interfaced cellular assemblies. Consistent with data we obtained from the confocal microscopy investigation, fluorescent fCNTs neurons visualized by loading them with the calcium dye Oregon Green 488-BAPTA-1 AM appeared distributed on a larger area when compared to those grown on CNT (as shown in the snapshots in figure 3.3A).

The acquired fields of view (409.6 µm × 409.6 µm) enabled to clearly identify and monitor small clusters of cells and neurons simultaneously (in each field of view analyzed we detected 8 ± 2 cells in CNT and 12 ± 3 in fCNT; 3 different culture series). Figure 3.3B reports some representative fluorescent tracings of spontaneous calcium activity recorded in CNT-interfaced cells (grey) and in fCNT (black). As previously reported in our previous works, in hippocampal neurons the spontaneous activity appears as the occurrence of transient episodes of calcium concentration elevation (Bosi et al., 2015; Rago et al., 2019; Rauti et al., 2020). We measured the occurrence of spontaneous calcium events in neurons by calculating the inter events interval (IEI). Neurons cultured on fCNT displayed an IEI of 19.5 ± 1 s, a value significantly lower when compared to neurons cultured on CNT (102.2 ± 19.8 s), as shown in Figure 3.3C (left) cumulative distributions (n=24 cells for CNT and n=39 cells for fCNT; Kolmogorov-Smirnov test, $p<0.0001$). The lower IEI in fCNTs was in fact accompanied by higher calcium events frequency in fCNT compared to CNT (Figure 3.3C right; n=24 cells 0.006 ± 0.001 Hz in CNT and n=39 cells 0.027 ± 0.003 Hz for fCNT, no parametric data, Mann Whitney test, $p<0.0001$). These data suggested that fCNTs-foams enhanced the formation of small clusters of neurons, increasing the colonization of cells following the curves of foam surfaces, and this results in higher network outputs. To gain insights into the dynamics of the two different foam-networks constructs, we pharmacologically blocked synaptic inhibition by application of the $GABA_A$ receptors antagonist gabazine (5 µM), a manipulation known to induce network activity patterns of synchronized neuronal activity (Sokal et al., 2000). In both CNT and fCNT groups, in respect to spontaneous activity, the removal of synaptic inhibition induced the appearance of regular calcium oscillations with a similar pace in the two conditions, measured as IEI (35.5 ± 3 s for CNT and 37 ± 1.6 s for fCNT, no parametric data, Kolmogorov-Smirnov test, $p=0.07$) and frequency (0.025 ± 0.003 Hz for CNT and 0.026 ± 0.001 Hz for fCNT, no parametric data, Mann-Whitney test, $p=0.14$), as shown in Figure 3.3D. This suggests that above the two foams diverse networks developed and that, in opposition to sparse neuronal networks, the activity in clustered network organizations is differently shaped by the synaptic inhibition. Interestingly, when tetrodotoxin (TTX, 1 µM) is

applied, a known blocker of action potential mediated-synaptic activity (Jal & Khora, 2015; Narahashi, 2008); we completely suppressed network activity (Figure 3.3B, right traces) unmasking glial cells sole spontaneous calcium signaling (Figure 3.3E). This activity is very different in its kinetic from the neuronal one, and appeared as a sequence of calcium events, significantly slower on CNT samples compared to fCNT ones (13.5±5 s for CNT and 10.1±2.6 s for fCNT, no parametric data, Mann-Whitney test, p=0.02), as reported in the box plots of Figure 3.3F. Furthermore, pristine CNT display a higher glial activity, expressed in terms of frequency, compared to fCNT (n=8 cells $8 \cdot 10^{-3} \pm 1 \cdot 10^{-3}$ Hz for CNT and n=7 cells $2 \cdot 10^{-3} \pm 0.3 \cdot 10^{-3}$ Hz for fCNT).

In a different set of experiments, we further investigated the emergence in CNT and fCNT interfaced networks of synchronization in the spontaneous calcium episodes. We evaluated the synchronization just between the cells located within the same field of view, and we quantified it computing the cell-to-cell signal cross-correlation function (CCF). Figure 3.4A shows sample traces taken from distant cells within the same recording field. We subsequently pooled together data highlighting the fact that cells appeared significantly more correlated on fCNT foams (CCF 0.6 ± 0.01) when compared to CNT ones (CCF 0.1 ± 0.01). Results are summarized in the box plots of Figure 3.4B (no parametric data, Mann Whitney test, $p<0.0001$). Thus, we can conclude that fCNT foams were able to effectively affect both neuronal network morphology and activity. Finally, to verify whether the differences in the calcium events were due to different organization of the cytoskeleton actin filaments, directly involved in cellular mechanosensing, we performed immunofluorescence for phalloidin, a marker of polymerized F-actin. Anyhow, as shown by the representative confocal micrographs in Figure 3.4C, no apparent changes emerged in this respect.

Conclusions

The preliminary investigation we have conducted have demonstrated the possibility to exploit a PEG-functionalization on DWCNT to tune the electrical and mechanical properties of a three-dimensional, foam-like, hybrid structure. Specifically, the functionalized foam is characterized by a higher rigidity

compared to a pristine one. Interestingly, this increase in stiffness seems to impact the development of neuronal cells interfaced with the foam in terms of network topology and neuronal network activity. Regarding the latter aspect, neuronal networks let to develop above functionalized foam shown an enhanced activity when compared to networks interfaced to pristine DWCNT-foams. On the other hand, we have highlighted also an altered regulation of glial cells calcium activity, concretizing in more pronounced calcium waves above pristine DWCNTs samples. We cannot exclude that the phenomenon could play a role in shaping the final pattern of activity characterizing the neuronal cells. As a conclusive remark, we can hypothesize that the different chemical, mechanical and topographical cues associable to our DWCNT-foams synergically cooperate to regulate the cellular network topology and functionality, presumably impacting both cellular phenotypes constituting our cultures: neuronal and glial cells. The work we have conducted until now, despite still being a work in progress, contributed to shed some light on the neuromodulation capabilities of functionalized CNT-foams. Anyhow, further investigations are needed in order to clearly identify the mechanisms responsible for the functional adaptation observed in hippocampal cells interfaced with this new class of carbon materials.

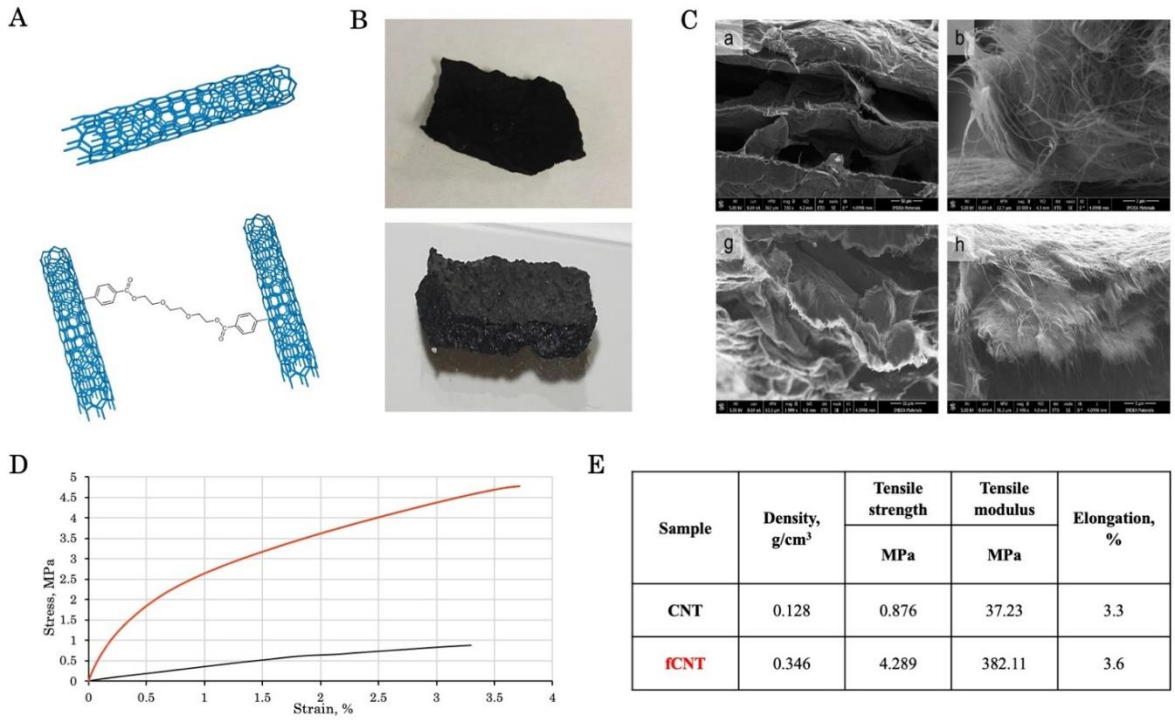

E

Sample	Density, g/cm³	Tensile strength	Tensile modulus	Elongation, %
		MPa	MPa	
CNT	0.128	0.876	37.23	3.3
fCNT	0.346	4.289	382.11	3.6

Figure 3.1. Primary hippocampal cultures on carbon nanotubes foams. *A) Cartoons depicting the structure of pristine DWCANTs (top), and PEGylated ones (bottom), the latter functionalization induces effective cross-linking between nanotubes impacting both cellular reactivity and the mechanical properties of the resulting aggregate. B) An example of a macroscopic CNTs-foam (top) and a fCNTs one (bottom), Both foams were about 5 mm in their longer side. C) Scanning electron micrographs revealing micro- and nano-structures of CNTs (top) and fCNTs (bottom) foams. D) Stress-strain plot from a tensile mechanical test revealing the better mechanical properties characterizing the fCNTs foam (red trace) when compared to a CNTs one (black trace). E) A table summarizing the main physical and mechanical properties characterizing CNTs and fCNTs samples.*

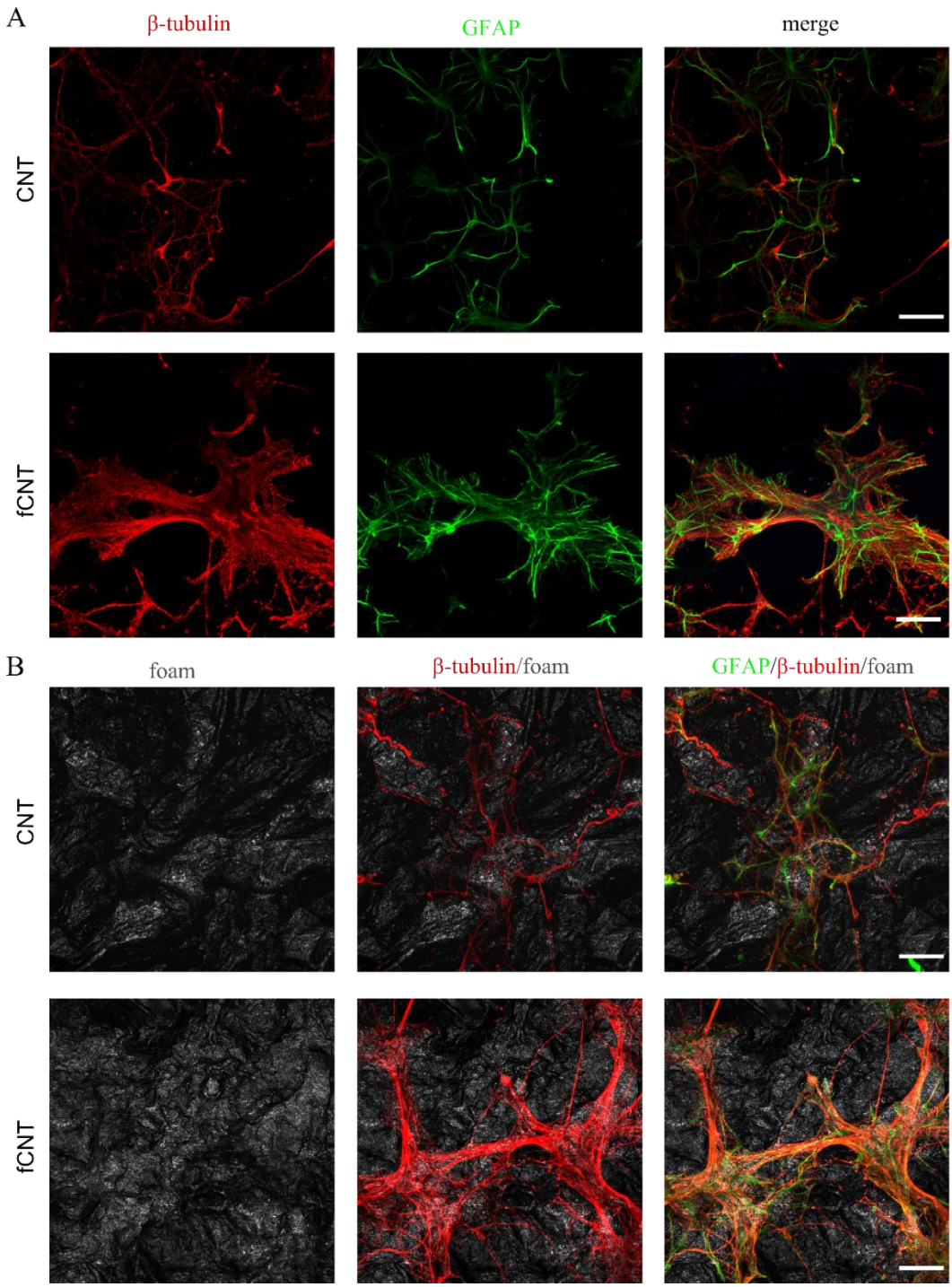

Figure 3.2 Primary hippocampal cultures on carbon nanotubes foams. *A) Confocal micrographs show hippocampal cultures grown (8 DIV) on CNT (top) and fCNT (bottom) immune-stained for β-Tubulin III (in red) and GFAP (green), scale bars 50 µm. B) Confocal reconstruction of CNT and fCNT foam (the foam was visualized by confocal microscopy in reflection acquisition mode, in grey in the images); neurons (red) grow both on CNT and fCNT using glial cells as support (green). From a qualitative point of view, fCNTs neurons appear more interconnected than CNTs-interfaced ones. Scale bars 50 µm.*

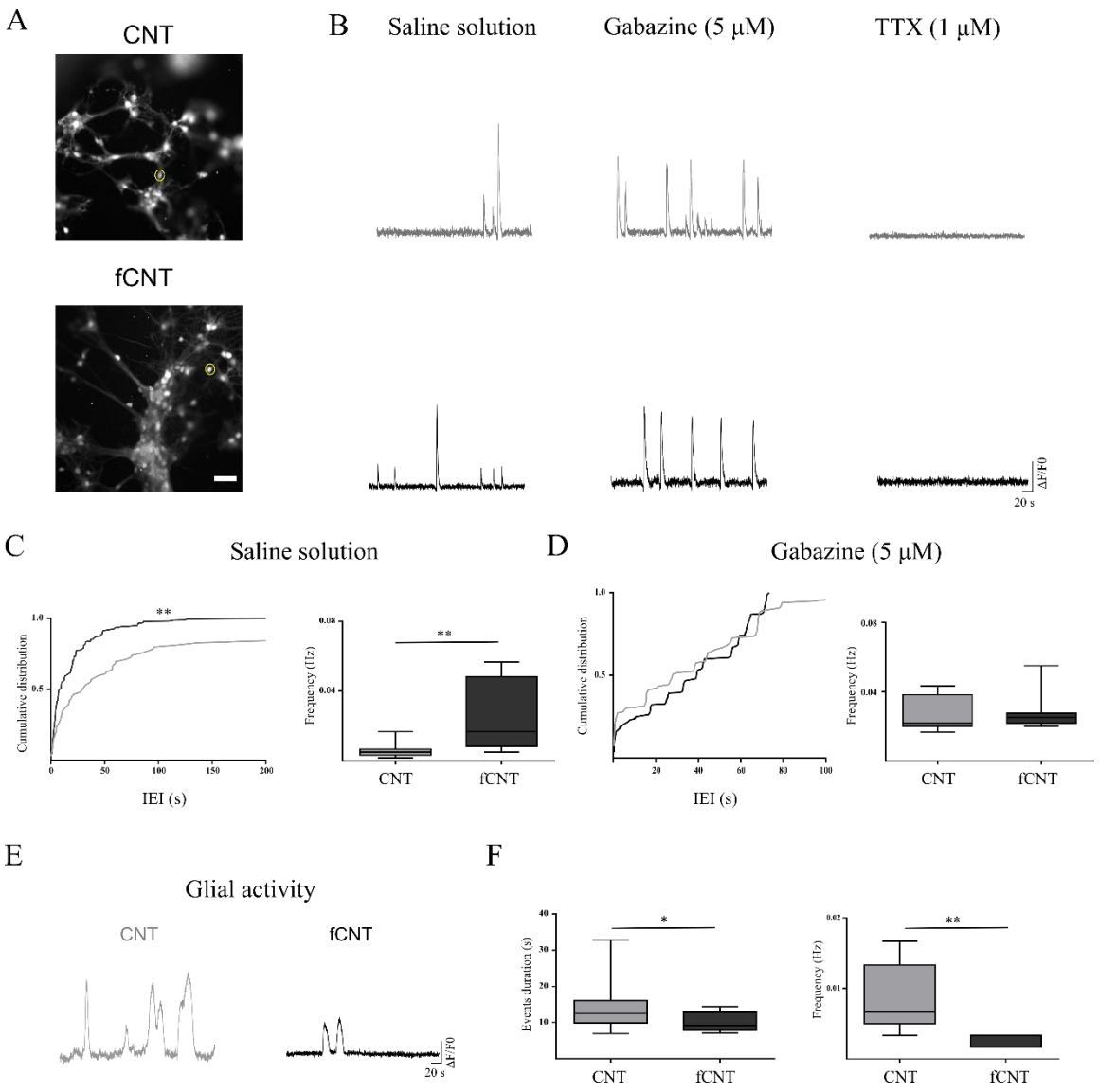

Figure 3.3 Network activity in CNT foams. *A) Snapshots of representative fields of neuronal cultures at 8-10 DIV grown on CNT (top) and fCNT (bottom) samples stained with the Oregon Green 488-BAPTA-1 AM. Dashed lines indicate the selected regions of interest (ROI). Scale bar: 50 µm. B) Representative traces of Ca^{2+} events recorded on CNT (grey) and fCNT (black) spontaneously in saline solution and in gabazine. Traces in TTX confirm neuronal activity. C) On the left, the graph of cumulative distribution of inter events interval (IEI), on the right, the box plot summarizes the events frequencies between two groups in spontaneous activity. D) On the left, the graph of cumulative distribution of inter events interval (IEI), on the right, the box plot summarizes the events frequencies between two groups in gabazine activity. E) Representative traces of Ca^{2+} events recorded in glial cells on CNT (grey) and fCNT (black) in TTX solution. D) On the left the box plot depicts Ca^{2+} events duration, on the right the plot illustrates the events frequencies in glial cells.*

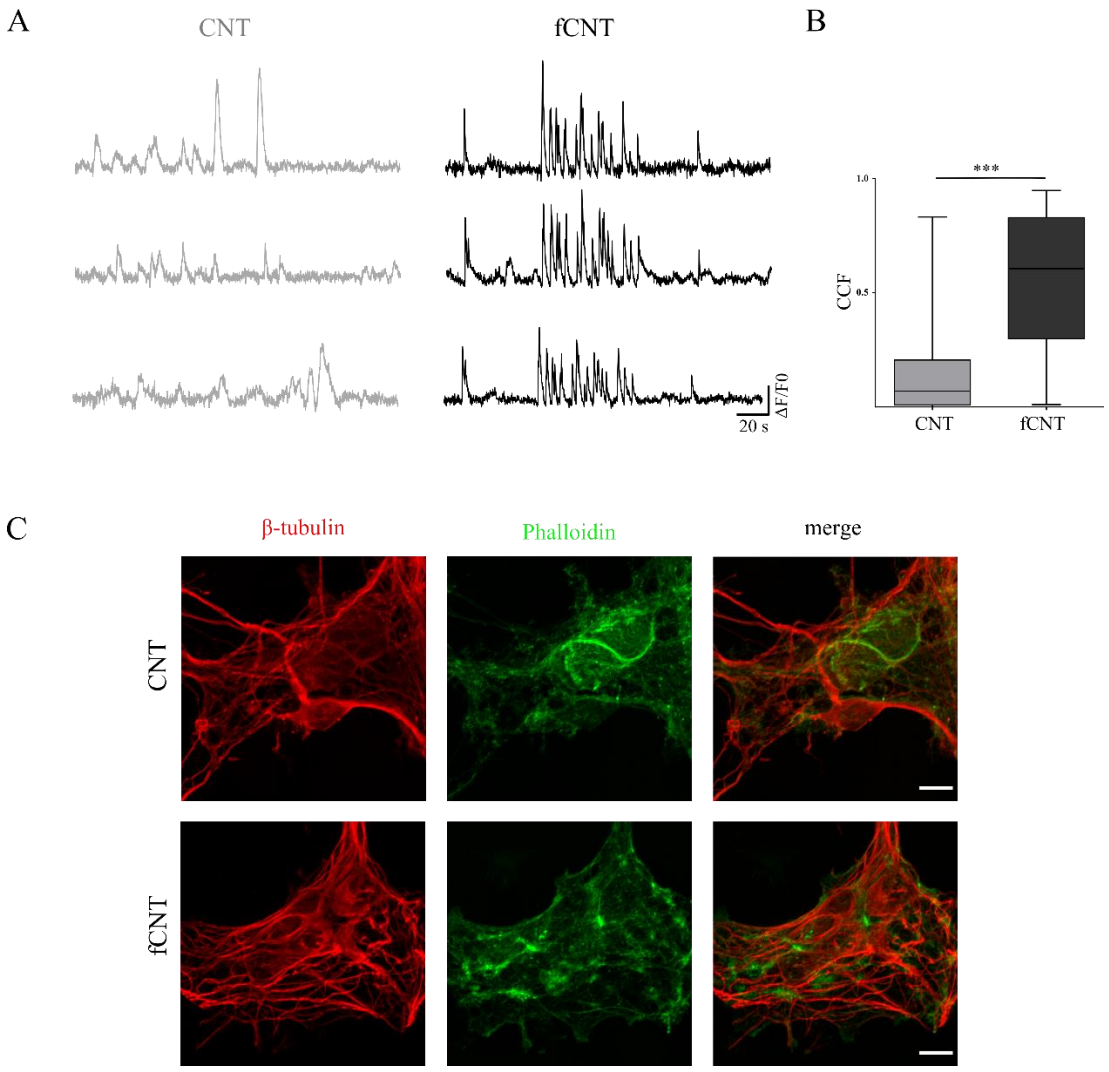

Figure 3.4 Functionalized carbon nanotubes increase the cross correlation of spontaneous Ca^{2+} events. *A) Representative traces of spontaneous Ca^{2+} events of neurons grown on CNT (grey) and fCNT (black). B) The box plot summarizes the cross-correlation factor between the two data sets. C) Confocal images show actin filaments stained with phalloidin (green) and neurons with β-tubulin III (red). Scale bars 10 µm.*

References

Bosi, S., Rauti, R., Laishram, J., Turco, A., Lonardoni, D., Nieus, T., Prato, M., Scaini, D. & Ballerini, L. (2015). From 2D to 3D: Novel nanostructured scaffolds to investigate signalling in reconstructed neuronal networks. *Scientific Reports*, *5*, 1–11. https://doi.org/10.1038/srep09562

Jal, S. & Khora, S. S. (2015). An overview on the origin and production of tetrodotoxin, a potent neurotoxin. *Journal of Applied Microbiology*, *119*(4), 907–916. https://doi.org/10.1111/jam.12896

Kong, X. Bin, Tang, Q. Y., Chen, X. Y., Tu, Y., Sun, S. Z. & Sun, Z. L. (2017). Polyethylene glycol as a promising synthetic material for repair of spinal cord injury. *Neural Regeneration Research*, *12*(6), 1003–1008. https://doi.org/10.4103/1673-5374.208597

Narahashi, T. (2008). Tetrodotoxin - A brief history. *Proceedings of the Japan Academy Series B: Physical and Biological Sciences*, *84*(5), 147–154. https://doi.org/10.2183/pjab.84.147

Rago, I., Rauti, R., Bevilacqua, M., Calaresu, I., Pozzato, A., Cibinel, M., Dalmiglio, M., Tavagnacco, C., Goldoni, A. & Scaini, D. (2019). Carbon Nanotubes, Directly Grown on Supporting Surfaces, Improve Neuronal Activity in Hippocampal Neuronal Networks. *Advanced Biosystems*, *3*(5), 1–13. https://doi.org/10.1002/adbi.201800286

Rauti, R., Secomandi, N., Martín, C., Bosi, S., Severino, F. P. U., Scaini, D., Prato, M., Vázquez, E. & Ballerini, L. (2020). Tuning Neuronal Circuit Formation in 3D Polymeric Scaffolds by Introducing Graphene at the Bio/Material Interface. *Advanced Biosystems*, *4*(4). https://doi.org/10.1002/adbi.201900233

Roman, J. A., Niedzielko, T. L., Haddon, R. C., Parpura, V. & Floyd, C. L. (2011). Single-walled carbon nanotubes chemically functionalized with polyethylene glycol promote tissue repair in a rat model of spinal cord injury. *Journal of Neurotrauma*, *28*(11), 2349–2362. https://doi.org/10.1089/neu.2010.1409

Sokal, D. M., Mason, R. & Parker, T. L. (2000). Multi-neuronal recordings reveal a differential effect of thapsigargin on bicuculline- or gabazine-induced epileptiform excitability in rat hippocampal neuronal networks. *Neuropharmacology*, *39*(12), 2408–2417. https://doi.org/10.1016/S0028-3908(00)00095-2

4. Final remarks

It is nowadays well known that cells are embedded in a microenvironment that is not a passive space ensuring just proper spatial confinement and position but, instead, is full of biological relevant cues (Frantz et al., 2010). In a mutual relation, the origin and target of this vast range of biochemical, morphological, and mechanical stimuli are cells and the extracellular matrix. Neuronal cells do not represent an exception in this picture. While the role of biochemical and morphological stimuli in driving and shaping neuronal development has been extensively studied in the past, the elusive contribution of mechanical cues, such as active cell-to-cell forces or passive properties such as environmental stiffness, has received far less attention. Only recently, mechanical cues have been recognized as key players in governing multiple processes, such as regulating the proliferation and differentiation of neural stem cells, the migration of cells, and the formation and maturation of neuronal circuits. In this scenario, the newborn research field of neuromechanobiology is taking its first steps to unravel the contribution of mechanics in modulating morphological and functional aspects of neuronal systems. In this regard, one of its final aims is to shed light on the molecular basis involved in the neuronal mechanosensing process within the central nervous system (CNS) (Tyler, 2018).

Although several neuroscience laboratories have started to deal with this fascinating topic, many discrepancies emerged in the experimental outcomes. Indeed, many questions remain still open or not univocally addressed. For example, can mechanical cues actively modulate the overall functionality of a nervous system? If so, how does it occur? Which are the molecular mechanisms involved in CNS-cells mechano-adaptation? How can different environments, characterized by a diverse range of mechanical and/or chemical cues, alter neuronal mechanical properties and their pattern of electrical activity? To address these questions and shed some light on the effective impact of matrix mechanical properties on CNS neurons, we investigated the behaviour of rat primary hippocampal

cells grown and developed on culture supports with different stiffness. Moreover, we have extended the study exploring the impact of chemical functionalization on the mechanoadaptation process.

We demonstrated that neuronal cells, when cultured on polyacrylamide (PAA) hydrogels characterized by stiffnesses in the physiological range from 50 kPa to 1 kPa, grow and develop well, giving rise to neuronal networks similar in both morphology and cellular composition when compared to control cultures developed above (stiff) glass controls. On the other hand, interestingly, a morphological study highlighted that compliant substrates determine a less complex arborization of the neuronal processes tree. Moreover, we revealed how soft gels induce a drastic and significant reduction in spontaneous postsynaptic currents compared to glass controls. These data suggested that a decrease in stiffness is accompanied by a decrease in synaptic activity. In order to better understand the reasons for the observed decrease in the spontaneous network activity, we probed miniature postsynaptic currents finding out no difference. This allowed us to rule out an involvement of structural changes in the number or properties of the synaptic connections. Conversely, investigating cell excitability, we observed a significant difference in excitable properties of neurons cultured on soft supports. We recapitulated all these results hypothesizing that a change of the composition at the plasma membrane level occurs in gel-interfaced cells. In this regard, many studies reported that cholesterol can influence the plasma membrane structure in multiple ways. It regulates membrane fluidity, permeability, thickness, and the tensional states of the lipidic bilayer (Al-Rekabi & Contera, 2018; Yang et al., 2017). Furthermore, cholesterol can induce conformational changes in membrane-embedded proteins (Niu et al., 2002) and modulate the kinetic of many ion channels (Levitan et al., 2000; Li et al., 2007). We investigated if an alteration in cholesterol levels occurs in gel-interfaced neurons and, surprisingly, we detected a significant alteration in its levels. Hippocampal cultures were characterized by a higher amount of cholesterol when grown in a soft environment with respect to a stiff one. We speculated that this dysregulation in cholesterol levels could be responsible for the different electrical activity observed on soft substrates by the fact they induced an altered membrane rigidity and, consequently, altered ionic channels activity. Noteworthy, another critical aspect

investigated concerns the correlation between substrate stiffness and the mechanosensing pathway. The latter involves components at different levels: the membrane (focal adhesions reorganization), the cytoskeleton (stress fibres formation) and the nucleus (transcription factors activation) (Martino et al., 2018). In particular, we focused on actomyosin assemblies that can organize in a specific matter upon variations in environmental stiffness (Ingber, 2008). Indeed, we demonstrated that the contractility of actomyosin cytoskeletal bundles plays a crucial role in stiffness sensing and its inhibition through specific molecules is sufficient to recapitulate the reduction in electrical activity observed in neurons grown above soft substrates. These results contribute to clarifying some aspects of the mechanisms linking together compliance-mediated mechanical and electrical adaptation.

Additionally, we investigated how chemical cues, in the form of chemically modified surfaces, can impact neuronal mechanoadaptation leading to unveiling how hippocampal neurons regulate their own stiffness not only in response to environmental stiffness changes. Several studies in the literature have demonstrated that cells initiate different cellular responses and adopt different behaviours to substrates characterized by different surface chemistries (Allen et al., 2003; Brodbeck et al., 2002). Our side study found that neuronal electrical activity could be modulated by interfacing neuronal cells with pristine or carboxyl-functionalized graphene substrates, potentiating or depressing networks, respectively. Specifically, the functionalization causes a decrease in synaptic activity accompanied by a decrease in cellular stiffness. This phenomenon may be accounted for by the synergic contribution of perturbed electrical properties induced in the graphene by the chemical functionalization and the presence of negative charges introduced by the carboxyl chemical groups. This effect could lead to the suppression of the intrinsic electro-enhancing effect of pristine graphene coupled to an impaired ability of the cell to perceive the substrate stiffness through a dysregulated assembly and distribution of focal adhesions. Again, the resulting picture shows a concomitant alteration in mechanical and electrical properties of interfaced neuronal cells.

Furthermore, we attempted to evaluate the coordinate effect of mechanical and chemical contributions exploiting a more complex system where hippocampal neurons have been cultured on three-dimensional double-walled carbon nanotubes (DWCNTs) foams endowing a multipurpose functionalization. According to the preliminary data we have collected, we highlighted that stiffer substrates, represented in this study by functionalized CNTs, alter neuronal network topology and enhance the overall electrical activity.

In conclusion, by combining multiple experimental approaches ranging from electrophysiology to live imaging and atomic force microscopy, our studies highlighted the relevance of mechanical cues in modulating the development and functionality of CNS nerve cells. In particular, the primary purpose of this thesis work was to evaluate the contribution of the substrate stiffness in neuromodulation, an aspect extremely relevant by the fact that abnormal variations in environmental stiffness are associated with neurodegenerative diseases and ageing. A deeper understanding of how neurons and glial cells perceive mechanical inputs and integrate them with chemical and morphological cues is fundamental to disclose how environmental properties translate to specific cellular responses. This knowledge will help develop novel strategies for neural tissue engineering, such as neuronal scaffolds or neuroprosthetic devices where all these properties are accurately controlled and finely tuned to be exploited to repair damaged portions of the CNS. Furthermore, a deeper comprehension of mechanical impact on nerve cells of CNS and of the involved molecular pathway of mechanosensing could be exploited to design and develop drug compounds targeting the cell mechanosensation and tuning thus neuronal behavior. This could be relevant especially during neuropathologies development where mechanical and chemical components play crucial roles. Despite the limitations of our *in vitro* studies, they are steps towards a better understanding of the mechanisms correlating physical and chemical cues and brain physiology in the future perspective to investigate neuronal circuits in a more complex three-dimensional environment.

5. Appendix

5.1 Impact of polycaprolactone (PCL) scaffolds on the development and activity of primary hippocampal cells

Extracellular environment is an important source of a plethora of biophysical cues. In addition to the stiffness, another ECM feature able to actively modulate cell behavior is the topography (e.g., architecture, geometry, size and organization of matrix fibers) (Bettinger et al., 2009). In this side project, carried out in collaboration with Professor Gianluca Turco (University of Trieste), we investigated the growth and activity, in terms of calcium signals, of rat primary hippocampal cells cultured on three-dimensional (3D) polycaprolactone (PCL) scaffolds, taking advantage of electrospinning technique in order to fabricate fibrous membranes, and on bi-dimensional (2D) PCL thin layer, deposited on glass coverslips. The main goal of this study was to evaluate the topographical contribution to neuronal network development.

Materials and Methods

Dissociated hippocampal cells were obtained from rat pups (P1-P4), as previously described (see chapter 3, Methods section – Cell culture preparation, page 66). Neuronal cells were seeded and grown on poly-L-ornithine-coated glass coverslips, PCL flat substrates and PCL electrospun membranes, the latter two were prepared according to literature (Pham et al 2016) and provided by the team of Professor Gianluca Turco (University of Trieste). Before cell plating, PCL-based support underwent air plasma treatment and were sterilized by UV exposure. Neurons and astrocytes were identified by labeling the cytoskeletal components, β-tubulin-III and GFAP respectively, as described in the section Methods section (chapter 3, page 68). Cell density, morphology and membrane

colonization were evaluated taking images at confocal microscope (Nikon A1R). Neuronal activity was measured by performing calcium imaging experiments at 8-10 DIV. Specifically, hippocampal cultures were loaded with cell permeable Ca^{2+} dye Oregon Green 488 BAPTA-1 AM (Molecular Probes) at final concentration of 4 μM for 40 min at 37 °C, 5% CO_2. Samples were then positioned in a fixed-stage upright microscope (Eclipse FN1, Nikon), where they were continuously perfused at 5 mL/min rate at room temperature (RT) with saline solution composed of (in mM): 150 NaCl, 4 KCl, 1 $MgCl_2$, 2 $CaCl_2$, 1 $MgCl_2$, 10 HEPES, 10 glucose (all Sigma), pH 7.4. Dye-loaded cells were observed with a 40× water immersion objective (Fluor, 0.80W NA, Nikon) exciting the Ca2+ dye at 488 nm wavelength by means of a fluorescence cube filter set (Ex = 480/20 nm, Em = 520/40 nm, Dic = 500–510 nm) coupled to a high-pressure Hg lamp (Nikon). Images were acquired each 150 ms at 10 MHz readout compensating the read noise with ×300 EM gain using an EMCCD camera (IXon Ultra 897, AndorTM, Oxford Instruments) controlled by a computer through NIS-elements D (Nikon) software. Spontaneous activity was therefore recorded for 10 minutes. In order to induce rythimic bursts 10 μM bicuculline (Sigma-Aldrich), which is a GABAA antagonist, was added to the perfusion. Finally, 1 μM tetrodotoxin (TTX, Latoxan), which is a voltage-gated fast Na+ channel blocker, was added to confirm the neuronal nature of the recorded signals. Recorded images were analyzed off-line by Fiji ImageJ (version 2.0) selecting regions of interest (ROI) around the cell bodies; traces were analyzed by Clampfit 10.7 version; Axon Instruments) software. Ca^{2+} transients were expressed as fractional amplitude increase ($\Delta F/F_0$, where F_0 is the baseline fluorescence level and ΔF is the rise over baseline); the onset time of neuronal activation was determined by detecting those events in the fluorescence signal that exceeded at least five times the standard deviation of the noise. In particular, we calculated the inter event interval (IEI), that is the time (expressed in seconds) elapsed between two consecutive onsets of intracellular calcium transients. In this analysis, “n” represents the number of cells.

Results and Discussion

In this study we explored the ability of polymeric fibrous scaffolds to affect the behavior of neuronal network from morphological and functional point of view. In order to evaluate the contribution of substrate topography and to rule out the that one of the chemical component, dissociated hippocampal cells were grown on 3D PCL electrospun membranes and on PCL thin layers used as flat substrates. Topographical differences were pointed out by SEM micrographs, kindly provided by Dr Davide Porrelli (University of Trieste). PCL flat substrates are characterized by homogeneous surface lacking of patterned architecture (figure 5.1A on the left). The high magnification reveals the presence of

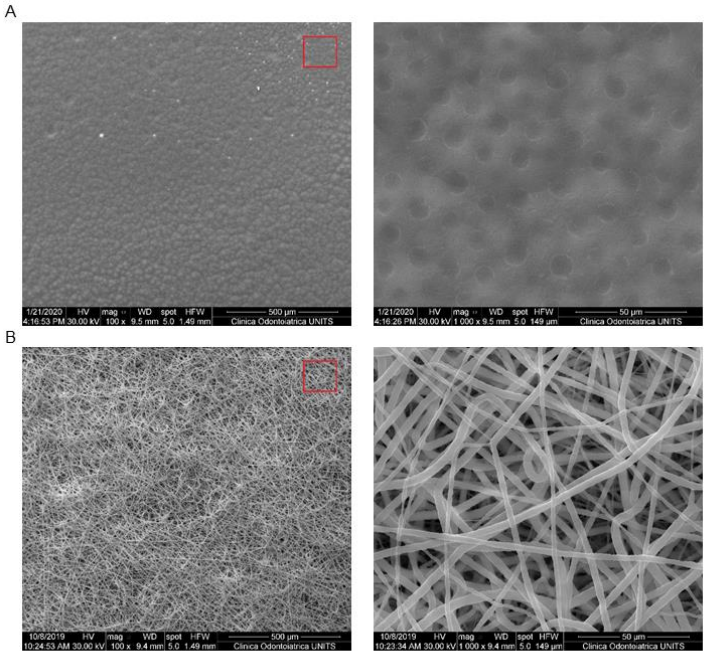

Figure 5.15 PCL substrates*. A) Representative SEM micrographs of PCL flat substrates. Scalebar: 500 µm (left) and 50 µm (right). B) Representative SEM micrographs of a PCL electrospun membrane. Scalebar: 500 µm (left) and 50 µm (right).*

some cavities due to solvent evaporation during deposition, whose impact on cell network organization may be considered irrelevant for the purpose of this study (figure 5.1A on the right). Conversely, 3D PCL membranes present a mesh of random oriented fibers (figure 5.1B), an unique feature that allows to have a high surface-to-volume ratio, facilitating cell adhesion and colonization of the scaffold.

We performed immunofluorescence experiments to compare neuronal cells grown on PCL flat, 3D PCL membranes and on glass coverslips. We investigated cell density and we found any significant difference in terms of neuronal density highlighting that PCL material does not affect neurons network formation; by contrast we observed a significant decrease in astrocytes number in 3D PCL substrates compared to the other two conditions (see figure 5.2A, D and E). These encouraging data make the electrospun membranes ideal to be applicated as neuroprosthesis because the astrocyte reduction is an index of reduced inflammatory response (González-Reyes et al., 2017; Raposo & Schwartz, 2014). To prove the colonization of 3D supports, we used confocal reconstructions at 0.75 μm steps (60× oil-immersion objective, 1.40 NA). Cells are able to migrate approximately until 40 μm in z direction when grown on PCL electrospun membranes (total thickness of the sample ≈400 μm); conversely cultures on glass coverslips and on PCL flat supports adopt a traditional planar distribution arranging as a monolayer (figure 5.2B). To further study neuronal migration within 3D scaffolds we visualized single neurons transfected with eGFP-expressing vectors by calcium phosphate method (see chapter 3, Methods section, page 69). Figure 5.2C shows confocal reconstructions that confirm previous observations. Our 3D culture systems are revealed suitable to the formation and development of hippocampal networks promoting cell migration and processes elongation in all three directions.

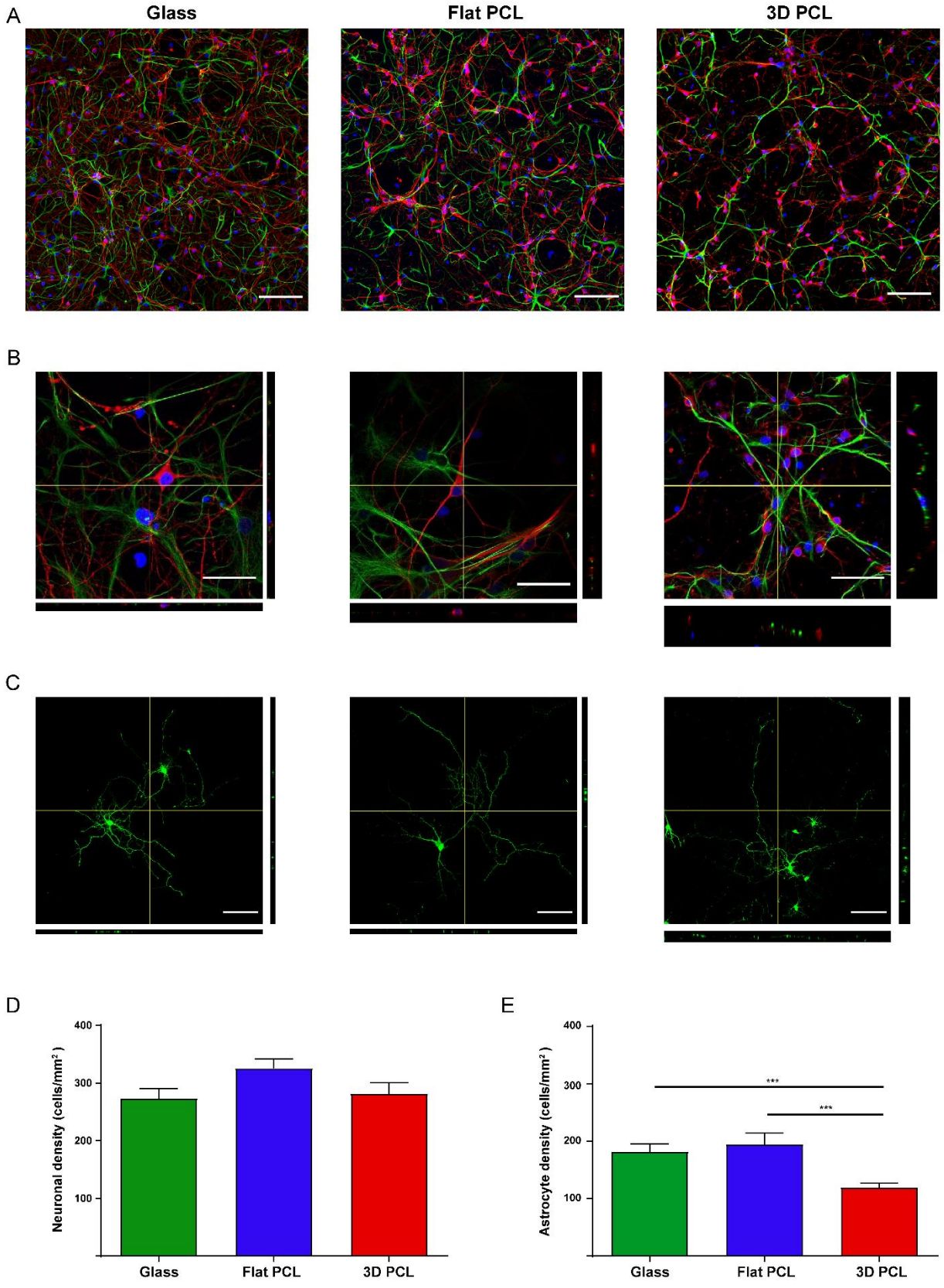
A
Glass
Flat PCL
3D PCL
B
C
D
Neuronal density (cells/mm²)
400
300
200
100
Glass
Flat PCL
3D PCL
E
Astrocyte density (cells/mm²)
400
300
200
100
***
***
Glass
Flat PCL
3D PCL

Figure 5.2 Growth and development of hippocampal network in 2D and 3D substrates. *A) Immunofluorescence micrographs of hippocampal cells cultured on glass (left), flat PCL (middle), and 3D PCL (right). Scalebar: 100 μm. B) Representative confocal reconstructions of hippocampal cells grown on glass (left), flat PCL (middle), and 3D PCL (right). Orthogonal projections show 3D cell organization within PCL membranes, as opposed to 2D organization on flat substrates. Scalebar (maintained in the orthogonal views): 50 μm; z-step: 0.75 μm. C) Representative confocal reconstructions of GFP-transfected neurons grown on glass (left), flat PCL (middle), and 3D PCL (right). Orthogonal projections show 3D organization within electrospun membranes, as opposed to 2D organization on flat substrates. Scalebar (maintained in the orthogonal views): 100 μm; z-step: 1.75 μm. D) The bar plot illustrates neuronal density (273 ± 17 cells/mm^2, n=11 visual fields for glass; 325 ± 16 cells/mm^2, n=11 for flat PCL; 281 ± 19 cells/mm^2, n=14 for 3D PCL). E) The bar plot depicts astrocytes density (182 ± 13 cells/mm^2, n=11 for glass; 195 ± 20 cells/mm^2, n=11 for flat PCL; 120 ± 7 cells/mm^2, n=14 for 3D PCL; *** p =0.0006; One-Way ANOVA).*

Neuronal activity was indirectly monitored in terms of calcium oscillations by calcium imaging technique. On average 20 ± 4 cells were analyzed in each field (204.8 x 204.8 μm^2). The occurrence of spontaneous calcium episodes in single neuron was evaluated by measuring the IEI parameter (figure 5.3). Regarding spontaneous activity, IEIs are significantly shorter in cultures grown on PCL electrospun membranes compared to other two control conditions, as shown in the graph 5.3C. Electrical activity was also measured upon application of bicuculline (10 μM) in order to block GABAA receptors and to disinhibit the network. We found a further decrease in IEI when neurons grown on 3D PCL membrane and also on PCL flat compared to those cultured on glass coverslips, as depicted in figure 5.3D. At the end of each experiment, TTX (1 μM) was added for 10 minutes before recording in order to discriminate neuronal signals from glial ones. Overall, our results reveal an increased neuronal activity on 3D fibrous membranes, suggesting that a specific topography has an important impact on cell adhesion, spreading, and activity.

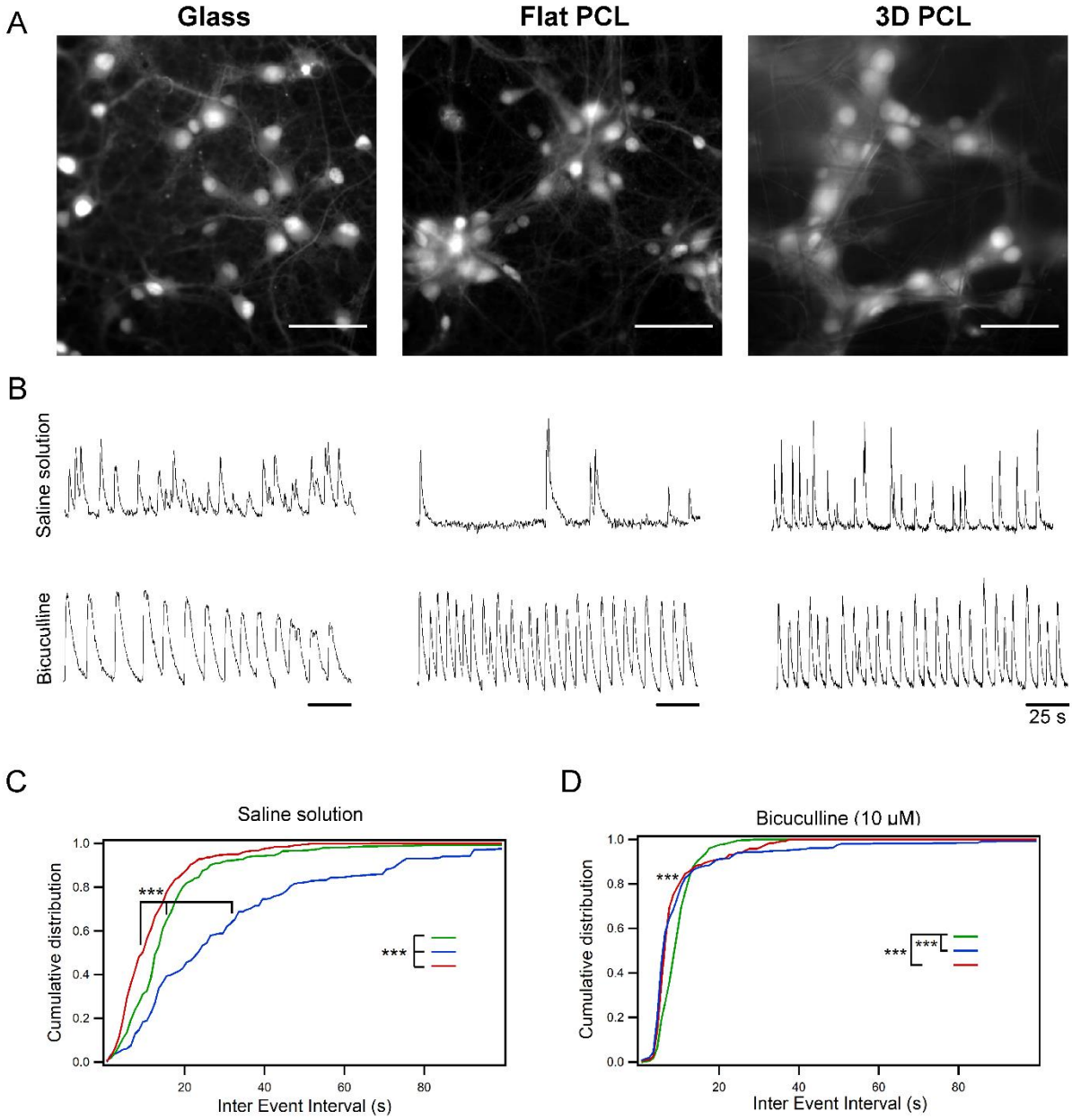

Figure 5.3 Network activity in 2D and 3D substrates. *A) Representative snapshots of recorded fields glass (left), flat PCL (middle), and 3D PCL (right). B) Representative traces recorded in the presence of saline solution (top) or bicuculline 10 μM (bottom). C) The graph of cumulative distribution of inter events interval (IEI), in saline solution (16.4±16.3 s, n=55 cells for glass; 32.5±30.6 s, n=73 cells for flat PCL; 11.9±9.2 s, n=71 cells for 3D PCL; *** = p < 0.0001; Kruskal-Wallis test followed by Dunn's multiple comparisons test). D)The graph of cumulative distribution of IEIs upon application of bicuculline (9.7±4.1 s for glass; 11±15.5 s for flat PCL; 9.1±6.9 s for 3D PCL; *** = p < 0.0001; Kruskal-Wallis test followed by Dunn's multiple comparisons test). Data are expressed as mean± standard deviation.*

6. References

Abbott, J. N. (1985). Are glial cells excitable after all? *Elsevier Science Publishers*. https://doi.org/10.1016/0166-2236(85)90057-8

Abraira, V. E. & Ginty, D. D. (2013). The sensory neurons of touch. *Neuron*, *79*(4), 618–639. https://doi.org/10.1016/j.neuron.2013.07.051

Agulhon, C., Petravicz, J., Mcmullen, A. B., Sweger, E. J., Minton, S. K., Taves, S. R., Casper, K. B., Fiacco, T. A. & Mccarthy, K. D. (2008). What Is the Role of Astrocyte Calcium in Neurophysiology? Glia: From Passive Glue to Excitable Cells. *Neuron*, *59*(6), 932–946. https://doi.org/10.1016/j.neuron.2008.09.004.What

Al-Rekabi, Z. & Contera, S. (2018). Multifrequency AFM reveals lipid membrane mechanical properties and the effect of cholesterol in modulating viscoelasticity. *Proceedings of the National Academy of Sciences of the United States of America*, *115*(11), 2658–2663. https://doi.org/10.1073/pnas.1719065115

Allen, L. T., Fox, E. J. P., Blute, I., Kelly, Z. D., Rochev, Y., Keenan, A. K., Dawson, K. A. & Gallagher, W. M. (2003). Interaction of soft condensed materials with living cells: Phenotype/transcriptome correlations for the hydrophobic effect. *Proceedings of the National Academy of Sciences of the United States of America*, *100*(11), 6331–6336. https://doi.org/10.1073/pnas.1031426100

Allen, N. J. (2014). Astrocyte regulation of synaptic behavior. *Annual Review of Cell and Developmental Biology*, *30*(1), 439–463. https://doi.org/10.1146/annurev-cellbio-100913-013053

Alonso, J. L. & Goldmann, W. H. (2016). Cellular mechanotransduction. *AIMS Biophysics*, *3*(1), 50–62. https://doi.org/10.3934/biophy.2016.1.50

Amano, M., Ito, M., Kimura, K., Fukata, Y., Chihara, K., Nakano, T., Matsuura, Y. & Kaibuchi, K. (1996). Phosphorylation and activation of myosin by Rho-associated kinase (Rho- kinase). *Journal of Biological Chemistry*, *271*(34), 20246–20249. https://doi.org/10.1074/jbc.271.34.20246

Amaral, D. & Lavenex, P. (2007). The Hippocampus Book - Hippocampal Neuroanatomy - chapter 3. In *The Hippocampus Book*. https://doi.org/10.1093/acprof:oso/9780195100273.003.0014

Anand, K. & Dhikav, V. (2012). Hippocampus in health and disease: An overview. *Annals of Indian Academy of Neurology*, *15*(4), 239–246. https://doi.org/10.4103/0972-2327.104323

Attwell, D., Buchan, A. M., Charpak, S., Lauritzen, M., MacVicar, B. A. & Newman, E. A. (2010). Glial and neuronal control of brain blood flow. *Nature*, *468*(7321), 232–243. https://doi.org/10.1038/nature09613

Ayala, Y. A., Pontes, B., Ether, D. S., Pires, L. B., Araujo, G. R., Frases, S., Romão, L. F., Farina, M., Moura-Neto, V., Viana, N. B. & Moysés Nussenzveig, H. (2016). Rheological properties of cells measured by optical tweezers. *BMC Biophysics*, *9*(1), 1–11. https://doi.org/10.1186/s13628-016-0031-4

Banker, G. A. & Cowan, W. M. (1977). Rat hippocampal neurons in dispersed cell culture. *Brain Research*, *126*(3), 397–425. https://doi.org/10.1016/0006-8993(77)90594-7

Barnes, J. M., Przybyla, L. & Weaver, V. M. (2017). Tissue mechanics regulate brain development, homeostasis and disease. *Journal of Cell Science*, *130*(1), 71–82. https://doi.org/10.1242/jcs.191742

Baumgart, F. & Cordey, J. (2001). Stiffness - An unknown world of mechanical science? *Injury*, *32*, 14–23. https://doi.org/10.1016/S0020-1383(01)00057-2

Berg, D. (2011). Hyperechogenicity of the substantia nigra: pitfalls in assessment and specificity for

Parkinson's disease. *Journal of Neural Transmission (Vienna, Austria : 1996)*, *118*(3), 453–461. https://doi.org/10.1007/s00702-010-0469-5

Berger, S. L., Leo-Macias, A., Yuen, S., Khatri, L., Pfennig, S., Zhang, Y., Agullo-Pascual, E., Caillol, G., Zhu, M., Rothenberg, E., Melendez-Vasquez, C. V., Delmar, M., Leterrier, C. & Salzer, J. L. (2019). Localized myosin II activity regulates assembly and plasticity of the axon initial segment. *Neuron*, *97*(3), 555–570. https://doi.org/10.1016/j.neuron.2017.12.039.Localized

Bettinger, C. J., Langer, R. & Borenstein, J. T. (2009). Engineering substrate topography at the Micro- and nanoscale to control cell function. *Angewandte Chemie - International Edition*, *48*(30), 5406–5415. https://doi.org/10.1002/anie.200805179

Betz, T., Koch, D., Lu, Y. B., Franze, K. & Käs, J. A. (2011). Growth cones as soft and weak force generators. *Proceedings of the National Academy of Sciences of the United States of America*, *108*(33), 13420–13425. https://doi.org/10.1073/pnas.1106145108

Blair, C. A. & Pruitt, B. L. (2020). Mechanobiology Assays with Applications in Cardiomyocyte Biology and Cardiotoxicity. *Advanced Healthcare Materials*, *9*(8), 1–14. https://doi.org/10.1002/adhm.201901656

Bradford, A. B. (2015). Importance of being Nernst: Synaptic activity and functional relevance in stem cell-derived neurons. *World Journal of Stem Cells*, *7*(6), 899. https://doi.org/10.4252/wjsc.v7.i6.899

Brian D. Clark, Goldberg, E. M. & Rudy, B. (2009). Electrogenic Tuning of the Axon Initial Segment Brian. *Neuroscientist*, *15*(6), 651–668. https://doi.org/10.1177/1073858409341973.Electrogenic

Brodal, A. (1947). The hippocampus and the sense of smell: A review. *Brain*, *70*(2), 179–222. https://doi.org/10.1093/brain/70.2.179

Brodbeck, W. G., Patel, J., Voskerician, G., Christenson, E., Shive, M. S., Nakayama, Y., Matsuda, T., Ziats, N. P. & Anderson, J. M. (2002). Biomaterial adherent macrophage apoptosis is increased by hydrophilic and anionic substrates in vivo. *Proceedings of the National Academy of Sciences of the United States of America*, *99*(16), 10287–10292. https://doi.org/10.1073/pnas.162124199

Budday, S., Ovaert, T. C., Holzapfel, G. A., Steinmann, P. & Kuhl, E. (2019). Fifty Shades of Brain: A Review on the Mechanical Testing and Modeling of Brain Tissue. In *Archives of Computational Methods in Engineering* (Vol. 27, Issue 4). Springer Netherlands. https://doi.org/10.1007/s11831-019-09352-w

Bugyi, B. & Carlier, M. F. (2010). Control of actin filament treadmilling in cell motility. *Annual Review of Biophysics*, *39*(1), 449–470. https://doi.org/10.1146/annurev-biophys-051309-103849

Burridge, K. & Chrzanowska-Wodnicka, M. (1996). Focal adhesions, contractility, and signaling. *Annual Review of Cell and Developmental Biology*, *12*, 463–519. https://doi.org/10.1146/annurev.cellbio.12.1.463

Burridge, K. & Wittchen, E. S. (2013). The tension mounts: Stress fibers as force-generating mechanotransducers. *Journal of Cell Biology*, *200*(1), 9–19. https://doi.org/10.1083/jcb.201210090

Cai, Y., Biais, N., Giannone, G., Tanase, M., Jiang, G., Hofman, J. M., Wiggins, C. H., Silberzan, P., Buguin, A., Ladoux, B. & Sheetz, M. P. (2006). Nonmuscle myosin IIA-dependent force inhibits cell spreading and drives F-actin flow. *Biophysical Journal*, *91*(10), 3907–3920. https://doi.org/10.1529/biophysj.106.084806

Caliari, S. R. & Burdick, J. A. (2016). A practical guide to hydrogels for cell culture. *Nature Methods*, *13*(5), 405–414. https://doi.org/10.1038/nmeth.3839

Chalfie, M. (2009). Neurosensory mechanotransduction. *Nature Reviews Molecular Cell Biology*, *10*(1), 44–52. https://doi.org/10.1038/nrm2595

Chan, C. E. & Odde, D. J. (2008). Traction dynamics of filopodia on compliant substrates. *Science*, *322*(5908), 1687–1691. https://doi.org/10.1126/science.1163595

Chighizola, M., Dini, T., Lenardi, C., Milani, P., Podestà, A. & Schulte, C. (2019). Mechanotransduction in neuronal cell development and functioning. *Biophysical Reviews*, *11*(5), 701–720. https://doi.org/10.1007/s12551-019-00587-2

Clarke, L. E. & Barres, B. A. (2013). Emerging roles of astrocytes in neural circuit development. *Nature Reviews Neuroscience*, *14*(5), 311–321. https://doi.org/10.1038/nrn3484

Cobo, R., García-Piqueras, J., García-Mesa, Y., Feito, J., García-Suárez, O. & Vega, J. A. (2020). Peripheral mechanobiology of touch—studies on vertebrate cutaneous sensory corpuscles. *International Journal of Molecular Sciences*, *21*(17), 1–17. https://doi.org/10.3390/ijms21176221

Compston, A. (2010). The hippocampus and the sense of smell. A review, by Alf Brodal. Brain 1947: 70; 179-222. *Brain : A Journal of Neurology*, *133*(9), 2509–2513. https://doi.org/10.1093/brain/awq242

Correale, J. & Villa, A. (2009). Cellular elements of the blood-brain barrier. *Neurochemical Research*, *34*(12), 2067–2077. https://doi.org/10.1007/s11064-009-0081-y

Das, A., Fischer, R. S., Pan, D. & Waterman, C. M. (2016). YAP nuclear localization in the absence of cell-cell contact is mediated by a filamentous actin-dependent, Myosin IIand Phospho-YAP-independent pathway during extracellular matrix mechanosensing. *Journal of Biological Chemistry*, *291*(12), 6096–6110. https://doi.org/10.1074/jbc.M115.708313

Dent, E. W. & Baas, P. W. (2014). Microtubules in neurons as information carriers. *Journal of Neurochemistry*, *129*(2), 235–239. https://doi.org/10.1111/jnc.12621

Dent, E. W., Gupton, S. L. & Gertler, F. B. (2011). The Growth Cone Cytoskeleton in Axon. *Cold Spring Harb Perspect Biol*, *3*, a001800.

DuChez, B. J., Doyle, A. D., Dimitriadis, E. K. & Yamada, K. M. (2019). Durotaxis by Human Cancer Cells. *Biophysical Journal*, *116*(4), 670–683. https://doi.org/10.1016/j.bpj.2019.01.009

Dudek, S. M., Alexander, G. M. & Farris, S. (2016). Rediscovering area CA2: Unique properties and functions. *Nature Reviews Neuroscience*, *17*(2), 89–102. https://doi.org/10.1038/nrn.2015.22

Dupont, S., Morsut, L., Aragona, M., Enzo, E., Giulitti, S., Cordenonsi, M., Zanconato, F., Le Digabel, J., Forcato, M., Bicciato, S., Elvassore, N. & Piccolo, S. (2011). Role of YAP/TAZ in mechanotransduction. *Nature*, *474*(7350), 179–184. https://doi.org/10.1038/nature10137

Eichenbaum, H. (2017). The role of the hippocampus in navigation is memory. *Journal of Neurophysiology*, *117*(4), 1785–1796. https://doi.org/10.1152/jn.00005.2017

Elkin, B. S., Azeloglu, E. U., Costa, K. D. & Morrison, B. (2007). Mechanical heterogeneity of the rat hippocampus measured by atomic force microscope indentation. *Journal of Neurotrauma*, *24*(5), 812–822. https://doi.org/10.1089/neu.2006.0169

Emon, B., Bauer, J., Jain, Y., Jung, B. & Saif, T. (2018). Biophysics of Tumor Microenvironment and Cancer Metastasis - A Mini Review. *Computational and Structural Biotechnology Journal*, *16*, 279–287. https://doi.org/10.1016/j.csbj.2018.07.003

Engler, A. J., Sen, S., Sweeney, H. L. & Discher, D. E. (2006). Matrix Elasticity Directs Stem Cell Lineage

Specification. *Cell*, *126*(4), 677–689. https://doi.org/10.1016/j.cell.2006.06.044

Evans, M. D., Tufo, C., Dumitrescu, A. S. & Grubb, M. S. (2017). Myosin II activity is required for structural plasticity at the axon initial segment. *European Journal of Neuroscience*, *46*(2), 1751–1757. https://doi.org/10.1111/ejn.13597

Färber, K. & Kettenmann, H. (2005). Physiology of microglial cells. *Brain Research Reviews*, *48*(2), 133–143. https://doi.org/10.1016/j.brainresrev.2004.12.003

Fields, R. D. & Stevens-Graham, B. (2002). Neuroscience: New insights into neuron-glia communication. *Science*, *298*(5593), 556–562. https://doi.org/10.1126/science.298.5593.556

Fletcher, D. A. & Mullins, R. D. (2010). Cell mechanics and the cytoskeleton. *Nature*, *463*(7280), 485–492. https://doi.org/10.1038/nature08908

Frantz, C., Stewart, K. M. & Weaver, V. M. (2010). The extracellular matrix at a glance. *Journal of Cell Science*, *123*(24), 4195–4200. https://doi.org/10.1242/jcs.023820

Franze, K., Gerdelmann, J., Weick, M., Betz, T., Pawlizak, S., Lakadamyali, M., Bayer, J., Rillich, K., Gögler, M., Lu, Y. B., Reichenbach, A., Janmey, P. & Käs, J. (2009). Neurite branch retraction is caused by a threshold-dependent mechanical impact. *Biophysical Journal*, *97*(7), 1883–1890. https://doi.org/10.1016/j.bpj.2009.07.033

Franze, K., Janmey, P. A. & Guck, J. (2013). Mechanics in neuronal development and repair. *Annual Review of Biomedical Engineering*, *15*, 227–251. https://doi.org/10.1146/annurev-bioeng-071811-150045

Fukata, Y., Kaibuchi, K., Amano, M. & Kaibuchi, K. (2001). Rho-Rho-kinase pathway in smooth muscle contraction and cytoskeletal reorganization of non-muscle cells. *Trends in Pharmacological Sciences*, *22*(1), 32–39. https://doi.org/10.1016/S0165-6147(00)01596-0

Georges, P. C., Miller, W. J., Meaney, D. F., Sawyer, E. S. & Janmey, P. A. (2006). Matrices with compliance comparable to that of brain tissue select neuronal over glial growth in mixed cortical cultures. *Biophysical Journal*, *90*(8), 3012–3018. https://doi.org/10.1529/biophysj.105.073114

González-Reyes, R. E., Nava-Mesa, M. O., Vargas-Sánchez, K., Ariza-Salamanca, D. & Mora-Muñoz, L. (2017). Involvement of astrocytes in Alzheimer's disease from a neuroinflammatory and oxidative stress perspective. *Frontiers in Molecular Neuroscience*, *10*(December), 1–20. https://doi.org/10.3389/fnmol.2017.00427

Gottardi, C. J., Arpin, M., Fanning, A. S. & Louvard, D. (1996). The junction-associated protein, zonula occludens-1, localizes to the nucleus before the maturation and during the remodeling of cell-cell contacts. *Proceedings of the National Academy of Sciences of the United States of America*, *93*(20), 10779–10784. https://doi.org/10.1073/pnas.93.20.10779

Grevesse, T., Dabiri, B. E., Parker, K. K. & Gabriele, S. (2015). Opposite rheological properties of neuronal microcompartments predict axonal vulnerability in brain injury. *Scientific Reports*, *5*, 1–10. https://doi.org/10.1038/srep09475

Gupta, M., Kocgozlu, L., Sarangi, B. R., Margadant, F., Ashraf, M. & Ladoux, B. (2015). Micropillar substrates: A tool for studying cell mechanobiology. In *Methods in Cell Biology* (Vol. 125). Elsevier Ltd. https://doi.org/10.1016/bs.mcb.2014.10.009

Haddad-Tóvolli, R., Dragano, N. R. V., Ramalho, A. F. S. & Velloso, L. A. (2017). Development and function of the blood-brain barrier in the context of metabolic control. *Frontiers in Neuroscience*, *11*(APR), 1–12. https://doi.org/10.3389/fnins.2017.00224

Halder, G., Dupont, S. & Piccolo, S. (2012). Transduction of mechanical and cytoskeletal cues by YAP and TAZ. *Nature Reviews Molecular Cell Biology*, *13*(9), 591–600. https://doi.org/10.1038/nrm3416

Handorf, A. M., Zhou, Y., Halanski, M. A. & Li, W. J. (2015). Tissue stiffness dictates development, homeostasis, and disease progression. *Organogenesis*, *11*(1), 1–15. https://doi.org/10.1080/15476278.2015.1019687

Haws, H. J., Mcneil, M. A. & Hansen, M. D. H. (2016). Control of cell mechanics by RhoA and calcium fl uxes during epithelial scattering. *Tissue Barriers*, *4*(3), 1–15. https://doi.org/10.1080/21688370.2016.1187326

Hayakawa, K., Tatsumi, H. & Sokabe, M. (2011). Actin filaments function as a tension sensor by tension-dependent binding of cofilin to the filament. *Journal of Cell Biology*, *195*(5), 721–727. https://doi.org/10.1083/jcb.201102039

Hohmann & Dehghani. (2019). The Cytoskeleton—A Complex Interacting Meshwork. *Cells*, *8*(4), 362. https://doi.org/10.3390/cells8040362

Huber, O., Korn, R., McLaughlin, J., Ohsugi, M., Herrmann, B. G. & Kemler, R. (1996). Nuclear localization of β-catenin by interaction with transcription factor LEF-1. *Mechanisms of Development*, *59*(1), 3–10. https://doi.org/10.1016/0925-4773(96)00597-7

Hwang, J. H., Byun, M. R., Kim, A. R., Kim, K. M., Cho, H. J., Lee, Y. H., Kim, J., Jeong, M. G., Hwang, E. S. & Hong, J. H. (2015). Extracellular matrix stiffness regulates osteogenic differentiation through MAPK activation. *PLoS ONE*, *10*(8), 1–16. https://doi.org/10.1371/journal.pone.0135519

Ingber, D. E. (2008). Tensegrity-Based Mechanosensing from Macro to Micro DonaldNIH Public Access. *PathologyProg Biophys Mol Biol*, *97*(2–3), 163–179. https://doi.org/10.1016/j.pbiomolbio.2008.02.005.Tensegrity-Based

Ishihara, S., Yasuda, M., Harada, I., Mizutani, T., Kawabata, K. & Haga, H. (2013). Substrate stiffness regulates temporary NF-κB activation via actomyosin contractions. *Experimental Cell Research*, *319*(19), 2916–2927. https://doi.org/10.1016/j.yexcr.2013.09.018

Iwasa, K. & Tasaki, I. (1980). MECHANICAL CHANGES IN SQUID GIANT AXONS ASSOCIATED WITH PRODUCTION OF ACTION POTENTIALS K. *Biochemical and Biophysical Research Communications*, *95*(3), 1328–1331.

Jansen, K. A., Donato, D. M., Balcioglu, H. E., Schmidt, T., Danen, E. H. J. & Koenderink, G. H. (2015). A guide to mechanobiology: Where biology and physics meet. *Biochimica et Biophysica Acta - Molecular Cell Research*, *1853*(11), 3043–3052. https://doi.org/10.1016/j.bbamcr.2015.05.007

Janzer, R. C. & Raff, M. C. (1987). Astrocytes induce blood-brain barrier properties in endothelial cells. *Nature*, *325*, 253–257. https://doi.org/10.1097/00001756-199904260-00035

Jerusalem, A., Al-Rekabi, Z., Chen, H., Ercole, A., Malboubi, M., Tamayo-Elizalde, M., Verhagen, L. & Contera, S. (2019). Electrophysiological-mechanical coupling in the neuronal membrane and its role in ultrasound neuromodulation and general anaesthesia. *Acta Biomaterialia*, *97*, 116–140. https://doi.org/10.1016/j.actbio.2019.07.041

Johnson, L. A., Rodansky, E. S., Haak, A. J., Larsen, S. D., Neubig, R. R. & Higgins, P. D. R. (2014). Novel Rho/MRTF/SRF Inhibitors Block Matrix-stiffness and TGF- β–Induced Fibrogenesis in Human Colonic Myofibroblasts. *Inflamm Bowel Dis.*, *20*(1), 154–165. https://doi.org/10.1097/01.MIB.0000437615.98881.31.Novel

Kamkin, A. & Kiseleva, I. (2009). *Mechanosensitivity of the Nervous System Mechanosensitivity in Cells and Tissues*.

Kanoldt, V., Fischer, L. & Grashoff, C. (2019). Unforgettable force-crosstalk and memory of mechanosensitive structures. *Biological Chemistry*, *400*(6), 687–698. https://doi.org/10.1515/hsz-2018-0328

Kilinc, D. (2018). The emerging role of mechanics in synapse formation and plasticity. *Frontiers in Cellular Neuroscience*, *12*(December), 1–9. https://doi.org/10.3389/fncel.2018.00483

Killian, J. L., Ye, F. & Wang, M. D. (2018). Optical Tweezers: A Force to Be Reckoned With. *Cell*, *175*(6), 1445–1448. https://doi.org/10.1016/j.cell.2018.11.019

Kim, J. H., Lee, G., Won, Y., Lee, M., Kwak, J. S., Chun, C. H. & Chun, J. S. (2015). Matrix cross-linking-mediated mechanotransduction promotes posttraumatic osteoarthritis. *Proceedings of the National Academy of Sciences of the United States of America*, *112*(30), 9424–9429. https://doi.org/10.1073/pnas.1505700112

Kofuji, P. & Newman, E. A. (2004). Potassium buffering in the central nervous system. *Neuroscience*, *129*(4), 1043–1054. https://doi.org/10.1016/j.neuroscience.2004.06.008

Kuo, C. H. R., Xian, J., Brenton, J. D., Franze, K. & Sivaniah, E. (2012). Complex stiffness gradient substrates for studying mechanotactic cell migration. *Advanced Materials*, *24*(45), 6059–6064. https://doi.org/10.1002/adma.201202520

Kuo, J. C. (2014). Focal adhesions function as a mechanosensor. In *Progress in Molecular Biology and Translational Science* (1st ed., Vol. 126). Elsevier Inc. https://doi.org/10.1016/B978-0-12-394624-9.00003-8

Lab, M. J., Bhargava, A., Wright, P. T. & Gorelik, J. (2013). The scanning ion conductance microscope for cellular physiology. *American Journal of Physiology - Heart and Circulatory Physiology*, *304*(1), 1–11. https://doi.org/10.1152/ajpheart.00499.2012

Lampi, M. C. & Reinhart-King, C. A. (2018). Targeting extracellular matrix stiffness to attenuate disease: From molecular mechanisms to clinical trials. *Science Translational Medicine*, *10*(422), 1–15. https://doi.org/10.1126/scitranslmed.aao0475

Lantoine, J., Grevesse, T., Villers, A., Delhaye, G., Mestdagh, C., Versaevel, M., Mohammed, D., Bruyère, C., Alaimo, L., Lacour, S. P., Ris, L. & Gabriele, S. (2016). Matrix stiffness modulates formation and activity of neuronal networks of controlled architectures. *Biomaterials*, *89*, 14–24. https://doi.org/10.1016/j.biomaterials.2016.02.041

Lau, L. W., Cua, R., Keough, M. B., Haylock-Jacobs, S. & Yong, V. W. (2013). Pathophysiology of the brain extracellular matrix: A new target for remyelination. *Nature Reviews Neuroscience*, *14*(10), 722–729. https://doi.org/10.1038/nrn3550

Lee, J., Ishihara, A., Oxford, G., Johnson, B. & Jacobson, K. (1999). Regulation of cell movement is mediated by stretch-activated calcium channels. *Nature*, *400*(6742), 382–386. https://doi.org/10.1038/22578

Leipzig, N. D. & Shoichet, M. S. (2009). The effect of substrate stiffness on adult neural stem cell behavior. *Biomaterials*, *30*(36), 6867–6878. https://doi.org/10.1016/j.biomaterials.2009.09.002

Levitan, I., Christian, A. E., Tulenko, T. N. & Rothblat, G. H. (2000). *Membrane Cholesterol Content Modulates Activation of Volume-regulated Anion Current in Bovine Endothelial Cells*. *115*(April).

Li, S. W. Æ. X., Liang, Æ. C. C. Æ. Y., David, J. P. Æ. & Ma, G. W. Æ. H. (2007). *Membrane Tension Modulates the Effects of Apical Cholesterol on the Renal Epithelial Sodium Channel*. 21–31. https://doi.org/10.1007/s00232-007-9071-7

Lo, C. M., Wang, H. B., Dembo, M. & Wang, Y. L. (2000). Cell movement is guided by the rigidity of the substrate. *Biophysical Journal*, *79*(1), 144–152. https://doi.org/10.1016/S0006-3495(00)76279-5

Lu, P., Takai, K., Weaver, V. M. & Werb, Z. (2011). Extracellular Matrix degradation and remodeling in development and disease. *Cold Spring Harbor Perspectives in Biology*, *3*(12), 1–24. https://doi.org/10.1101/cshperspect.a005058

Lumpkin, E. A. & Caterina, M. J. (2007). Mechanisms of sensory transduction in the skin. *Nature*, *445*(7130), 858–865. https://doi.org/10.1038/nature05662

Lundbæk, J. A., Birn, P., Hansen, A. J., Søgaard, R., Nielsen, C., Girshman, J., Bruno, M. J., Tape, S. E., Egebjerg, J., Greathouse, D. V., Mattice, G. L., Koeppe, R. E. & Andersen, O. S. (2004). Regulation of Sodium Channel Function by Bilayer Elasticity: The Importance of Hydrophobic Coupling. Effects of Micelle-forming Amphiphiles and Cholesterol. *Journal of General Physiology*, *123*(5), 599–621. https://doi.org/10.1085/jgp.200308996

Lynch, M. A. (2004). Long-term potentiation and memory. *Physiol Rev*, 87–136. https://doi.org/10.1142/9789814366700_0001

Lyubin, E. V. (2012). Cellular viscoelasticity probed by active rheology in optical tweezers. *Journal of Biomedical Optics*, *17*(10), 101510. https://doi.org/10.1117/1.jbo.17.10.101510

MacManus, D. B., Pierrat, B., Murphy, J. G. & Gilchrist, M. D. (2017). Region and species dependent mechanical properties of adolescent and young adult brain tissue. *Scientific Reports*, *7*(1), 1–12. https://doi.org/10.1038/s41598-017-13727-z

Martinac, B. (2014). The ion channels to cytoskeleton connection as potential mechanism of mechanosensitivity. *Biochimica et Biophysica Acta - Biomembranes*, *1838*(2), 682–691. https://doi.org/10.1016/j.bbamem.2013.07.015

Martino, F., Perestrelo, A. R., Vinarský, V., Pagliari, S. & Forte, G. (2018). Cellular mechanotransduction: From tension to function. *Frontiers in Physiology*, *9*(JUL), 1–21. https://doi.org/10.3389/fphys.2018.00824

Matthews, B. D., Overby, D. R., Mannix, R. & Ingber, D. E. (2006). Cellular adaptation to mechanical stress: Role of integrins, Rho, cytoskeletal tension and mechanosensitive ion channels. *Journal of Cell Science*, *119*(3), 508–518. https://doi.org/10.1242/jcs.02760

Mih, J. D., Marinkovic, A., Liu, F., Sharif, A. S. & Tschumperlin, D. J. (2012). Matrix stiffness reverses the effect of actomyosin tension on cell proliferation. *Journal of Cell Science*, *125*(24), 5974–5983. https://doi.org/10.1242/jcs.108886

Mikhaylova, M., Rentsch, J. & Ewers, H. (2020). Actomyosin Contractility in the Generation and Plasticity of Axons and Dendritic Spines. *Cells*, *9*(9), 1–14. https://doi.org/10.3390/cells9092006

Mohammed, D., Versaevel, M., Bruyère, C., Alaimo, L., Luciano, M., Vercruysse, E., Procès, A. & Gabriele, S. (2019). Innovative tools for mechanobiology: Unraveling outside-in and inside-out mechanotransduction. *Frontiers in Bioengineering and Biotechnology*, *7*(JUL). https://doi.org/10.3389/fbioe.2019.00162

Moore, S. W. & Sheetz, M. P. (2012). *Differentiation and Repair*. *71*(11), 1090–1101.

https://doi.org/10.1002/dneu.20947.Biophysics

Mostowy, S. & Cossart, P. (2012). Septins: The fourth component of the cytoskeleton. *Nature Reviews Molecular Cell Biology*, *13*(3), 183–194. https://doi.org/10.1038/nrm3284

Mullender, M., El Haj, A. J., Yang, Y., van Duin, M. A., Burger, E. H. & Klein-Nulend, J. (2004). Mechanotransduction of bone cells in vitro: Mechanobiology of bone tissue. *Medical and Biological Engineering and Computing*, *42*(1), 14–21. https://doi.org/10.1007/BF02351006

Murphy, M. C., Jones, D. T., Jack, C. R., Glaser, K. J., Senjem, M. L., Manduca, A., Felmlee, J. P., Carter, R. E., Ehman, R. L. & Huston, J. (2016). Regional brain stiffness changes across the Alzheimer's disease spectrum. *NeuroImage: Clinical*, *10*, 283–290. https://doi.org/10.1016/j.nicl.2015.12.007

Musah, S., Wrighton, P. J., Zaltsman, Y., Zhong, X., Zorn, S., Parlato, M. B., Hsiao, C., Palecek, S. P., Chang, Q., Murphy, W. L. & Kiessling, L. L. (2014). Substratum-induced differentiation of human pluripotent stem cells reveals the coactivator YAP is a potent regulator of neuronal specification. *Proceedings of the National Academy of Sciences of the United States of America*, *111*(38), 13805–13810. https://doi.org/10.1073/pnas.1415330111

Nardone, G., Oliver-De La Cruz, J., Vrbsky, J., Martini, C., Pribyl, J., Skládal, P., Pešl, M., Caluori, G., Pagliari, S., Martino, F., Maceckova, Z., Hajduch, M., Sanz-Garcia, A., Pugno, N. M., Stokin, G. B. & Forte, G. (2017). YAP regulates cell mechanics by controlling focal adhesion assembly. *Nature Communications*, *8*(May). https://doi.org/10.1038/ncomms15321

Needham, D. & Nunn, R. S. (1990). Elastic deformation and failure of lipid bilayer membranes. *Biophysical Journal*, *58*(October), 997–1009. http://www.ncbi.nlm.nih.gov/pmc/articles/PMC1281045/pdf/biophysj00122-0174.pdf

Nimmerjahn, A., Kirchhoff, F. & Helmchen, F. (2005). Resting microglial cells are highly dynamic surveillants of brain parenchyma in vivo. *Neuroforum*, *11*(3), 95–96. https://doi.org/10.1515/nf-2005-0304

Norman, L. L. & Aranda-Espinoza, H. (2010). Cortical neuron outgrowth is insensitive to substrate stiffness. *Cellular and Molecular Bioengineering*, *3*(4), 398–414. https://doi.org/10.1007/s12195-010-0137-8

O'Keefe, J., Dostrovsky, J. & J. O'Keefe, J. D. (1971). Short Communications The hippocampus as a spatial map . Preliminary evidence from unit activity in the freely-moving rat. *Brain Research*, *34*(1), 171–175. http://www.ncbi.nlm.nih.gov/pubmed/5124915

Pelham, R. J. & Wang, Y. L. (1997). Cell locomotion and focal adhesions are regulated by substrate flexibility. *Proceedings of the National Academy of Sciences of the United States of America*, *94*(25), 13661–13665. https://doi.org/10.1073/pnas.94.25.13661

Pellerin, L., BOUZIER-SORE, A.-K., AUBERT, A., SERRES, S., MICHEL, M., ROBERT, C. & MAGISTRETTI, P. J. (2007). Activity-Dependent Regulation of Energy Metabolism by Astrocytes: An Update. *GLIA*, *55*, 1251–1262. https://doi.org/10.1002/glia

Peyton, S. R. & Putnam, A. J. (2005). Extracellular matrix rigidity governs smooth muscle cell motility in a biphasic fashion. *Journal of Cellular Physiology*, *204*(1), 198–209. https://doi.org/10.1002/jcp.20274

Preilowski, B. (2009). Remembering an amnesic patient (and half a century of memory research). *Fortschr Neurol Psychiatr*, *77*(10), 568–576. https://doi.org/10.1055/s-0028-1109664

Previtera, M. L., Langhammer, C. G. & Firestein, B. L. (2010). Effects of substrate stiffness and cell density on primary hippocampal cultures. *Journal of Bioscience and Bioengineering*, *110*(4), 459–470.

https://doi.org/10.1016/j.jbiosc.2010.04.004

Proia, P., di Liegro, C. M., Schiera, G., Fricano, A. & Di Liegro, I. (2016). Lactate as a metabolite and a regulator in the central nervous system. *International Journal of Molecular Sciences*, *17*(9). https://doi.org/10.3390/ijms17091450

Raposo, C. & Schwartz, M. (2014). Glial scar and immune cell involvement in tissue remodeling and repair following acute CNS injuries. *Glia*, *62*(11), 1895–1904. https://doi.org/10.1002/glia.22676

Reid, S. E. & Zanivan, S. (2017). Tumor stiffness extends its grip on the metastatic microenvironment. *MOLECULAR & CELLULAR ONCOLOGY*, *4*(6). https://doi.org/10.1038/ncb2756

Ricks, C. B., Shin, S. S., Becker, C. & Grandhi, R. (2014). Extracellular matrices, Artificial neural scaffolds and the promise of neural regeneration. *Neural Regeneration Research*, *9*(17), 1573–1577. https://doi.org/10.4103/1673-5374.141778

Riveline, D., Zamir, E., Balaban, N. Q., Schwarz, U. S., Ishizaki, T., Narumiya, S., Kam, Z., Geiger, B. & Bershadsky, A. D. (2001). Focal contacts as mechanosensors: Externally applied local mechanical force induces growth of focal contacts by an mDia1-dependent and ROCK-independent mechanism. *Journal of Cell Biology*, *153*(6), 1175–1185. https://doi.org/10.1083/jcb.153.6.1175

Rochlin, M. W., Itoh, K., Adelstein, R. S. & Bridgman, P. C. (1995). Localization of myosin II A and B isoforms in cultured neurons. *Journal of Cell Science*, *108*(12), 3661–3670. https://doi.org/10.1242/jcs.108.12.3661

Ryu, J., Liu, L., Wong, T. P., Wu, D. C., Burette, A., Weinberg, R., Wang, Y. T. & Sheng, M. (2006). A critical role for myosin IIB in dendritic spine morphology and synaptic function. *Neuron*, *49*(2), 175–182. https://doi.org/10.1016/j.neuron.2005.12.017

Sánchez, D., Johnson, N., Li, C., Novak, P., Rheinlaender, J., Zhang, Y., Anand, U., Anand, P., Gorelik, J., Frolenkov, G. I., Benham, C., Lab, M., Ostanin, V. P., Schäffer, T. E., Klenerman, D. & Korchev, Y. E. (2008). Noncontact measurement of the local mechanical properties of living cells using pressure applied via a pipette. *Biophysical Journal*, *95*(6), 3017–3027. https://doi.org/10.1529/biophysj.108.129551

Schafer, D. P. & Stevens, B. (2015). Microglia Function in Central Nervous System Development and Plasticity. *Cold Spring Harb. Perspect. Biol*, *7*. https://doi.org/10.1016/s1054-3589(08)60887-x

Schmidt, D., Del Mańmol, J. & MacKinnon, R. (2012). Mechanistic basis for low threshold mechanosensitivity in voltage-dependent K+ channels. *Proceedings of the National Academy of Sciences of the United States of America*, *109*(26), 10352–10357. https://doi.org/10.1073/pnas.1204700109

Shahbazian-Yassar, R. (2013). Atomic force microscopy. In *Encyclopedia of Tribology*. https://doi.org/10.1007/978-0-387-92897-5

Simon W. Moore, Roca-Cusachs, P. & Sheetz, M. P. (2010). Stretchy Proteins on Stretchy Substrates: The Important Elements of Integrin-Mediated Rigidity Sensing. *Dev Cell*, *19*(2), 194–206. https://doi.org/10.1016/j.devcel.2010.07.018.Stretchy

Sit, S. T. & Manser, E. (2011). Rho GTPases and their role in organizing the actin cytoskeleton. *Journal of Cell Science*, *124*(5), 679–683. https://doi.org/10.1242/jcs.064964

Smith, S. J. (1988). Neuronal cytomechanics: The actin-based motility of growth cones. *Science*, *242*(4879), 708–715. https://doi.org/10.1126/science.3055292

Snaidero, N. & Simons, M. (2014). Myelination at a glance. *Journal of Cell Science*, *127*(14), 2999–3004.

https://doi.org/10.1242/jcs.151043

Solon, J., Levental, I., Sengupta, K., Georges, P. C. & Janmey, P. A. (2007). Fibroblast adaptation and stiffness matching to soft elastic substrates. *Biophysical Journal*, *93*(12), 4453–4461. https://doi.org/10.1529/biophysj.106.101386

Somjen, G. G. (1988). Nervenkitt: Notes on the history of the concept of neuroglia. *Glia*, *1*(1), 2–9. https://doi.org/10.1002/glia.440010103

Stogsdill, J. A. & Eroglu, C. (2017). The interplay between neurons and glia in synapse development and plasticity. *Current Opinion in Neurobiology*, *42*, 1–8. https://doi.org/10.1016/j.conb.2016.09.016

Tanaka, A., Fujii, Y., Kasai, N., Okajima, T. & Nakashima, H. (2018). Regulation of neuritogenesis in hippocampal neurons using stiffness of extracellular microenvironment. *PLoS ONE*, *13*(2), 1–16. https://doi.org/10.1371/journal.pone.0191928

Tsimbouri, P. (2015). Adult Stem Cell Responses to Nanostimuli. *Journal of Functional Biomaterials*, *6*(3), 598–622. https://doi.org/10.3390/jfb6030598

Tyler, W. J. (2012). The mechanobiology of brain function. *Nature Reviews Neuroscience*, *13*(12), 867–878. https://doi.org/10.1038/nrn3383

Tyler, W. J. (2018). Neuromechanobiology. In *Mechanobiology in Health and Disease*. Elsevier Ltd. https://doi.org/10.1016/B978-0-12-812952-4.00011-8

Urbanczyk, M., Layland, S. L. & Schenke-Layland, K. (2020). The role of extracellular matrix in biomechanics and its impact on bioengineering of cells and 3D tissues. *Matrix Biology*, *85–86*, 1–14. https://doi.org/10.1016/j.matbio.2019.11.005

Urbanski, M. M., Brendel, M. B. & Melendez-Vasquez, C. V. (2019). Acute and chronic demyelinated CNS lesions exhibit opposite elastic properties. *Scientific Reports*, *9*(1), 1–13. https://doi.org/10.1038/s41598-018-37745-7

Van Rossum, D. & Hanisch, U. K. (2004). Microglia. *Metabolic Brain Disease*, *19*(3–4), 393–411. https://doi.org/10.1023/B:MEBR.0000043984.73063.d8

Van Strien, N. M., Cappaert, N. L. M. & Witter, M. P. (2009). The anatomy of memory: An interactive overview of the parahippocampal- hippocampal network. *Nature Reviews Neuroscience*, *10*(4), 272–282. https://doi.org/10.1038/nrn2614

Verma, D., Meng, F., Sachs, F. & Hua, S. Z. (2015). Flow-induced focal adhesion remodeling mediated by local cytoskeletal stresses and reorganization. *Cell Adhesion and Migration*, *9*(6), 432–440. https://doi.org/10.1080/19336918.2015.1089379

Wasser, C. R., Ertunc, M., Liu, X. & Kavalali, E. T. (2007). Cholesterol-dependent balance between evoked and spontaneous synaptic vesicle recycling. *Journal of Physiology*, *579*(2), 413–429. https://doi.org/10.1113/jphysiol.2006.123133

Wells, R. G. (2008). The role of matrix stiffness in regulating cell behavior. *Hepatology*, *47*(4), 1394–1400. https://doi.org/10.1002/hep.22193

Wen, Y. Q., Gao, X., Wang, A., Yang, Y., Liu, S., Yu, Z., Song, G. B. & Zhao, H. C. (2018). Substrate stiffness affects neural network activity in an extracellular matrix proteins dependent manner. *Colloids and Surfaces B: Biointerfaces*, *170*, 729–735. https://doi.org/10.1016/j.colsurfb.2018.03.042

Wiggan, O., Shaw, A. E., DeLuca, J. G. & Bamburg, J. R. (2012). ADF/Cofilin regulates actomyosin assembly

through competitive inhibition of myosin II binding to F-actin. *Bone*, *22*(3), 530–543. https://doi.org/10.1016/j.devcel.2011.12.026.ADF/Cofilin

Yang, S.-T., Kreutzberger, A. J. B., Lee, J., Kiessling, V. & Lukas K. Tamm. (2017). The Role of Cholesterol in Membrane Fusion. *Biophysical Journal*, 136–143. https://doi.org/10.1016/j.bpj.2016.11.078

Yu, Y., Liu, S., Wu, X., Yu, Z., Xu, Y., Zhao, W., Zavodnik, I., Zheng, J., Li, C. & Zhao, H. (2019). Mechanism of Stiff Substrates up-Regulate Cultured Neuronal Network Activity. *ACS Biomaterials Science and Engineering*, *5*(7), 3475–3482. https://doi.org/10.1021/acsbiomaterials.9b00225

Yuste, R. & Bonhoeffer, T. (2001). MORPHOLOGICAL CHANGES IN DENDRITIC SPINES ASSOCIATED WITH LONG-TERM SYNAPTIC PLASTICITY. *Annu. Rev. Neurosci*, *24*, 1071–89.

Zampieri, F., Coen, M. & Gabbiani, G. (2014). The prehistory of the cytoskeleton concept. *Cytoskeleton*, *71*(8), 464–471. https://doi.org/10.1002/cm.21177

Zhang, Q. Y., Zhang, Y. Y., Xie, J., Li, C. X., Chen, W. Y., Liu, B. L., Wu, X. A., Li, S. N., Huo, B., Jiang, L. H. & Zhao, H. C. (2014). Stiff substrates enhance cultured neuronal network activity. *Scientific Reports*, *4*, 12–15. https://doi.org/10.1038/srep06215

Zhao, B., Tumaneng, K. & Guan, K. L. (2011). The Hippo pathway in organ size control, tissue regeneration and stem cell self-renewal. *Nature Cell Biology*, *13*(8), 877–883. https://doi.org/10.1038/ncb2303

Zhou, D. W., Lee, T. T., Weng, S., Fu, J. & García, A. J. (2017). Effects of substrate stiffness and actomyosin contractility on coupling between force transmission and vinculin-paxillin recruitment at single focal adhesions. *Molecular Biology of the Cell*, *28*(14), 1901–1911. https://doi.org/10.1091/mbc.E17-02-0116

Zimmermann, D. R. & Dours-Zimmermann, M. T. (2008). Extracellular matrix of the central nervous system: From neglect to challenge. *Histochemistry and Cell Biology*, *130*(4), 635–653. https://doi.org/10.1007/s00418-008-0485-9